The Application of SOA for Dispersion Management of 2D-WH/TS Codes in Incoherent OCDMA System

By

Md Shakil Ahmed

A thesis submitted for the Degree

Of

Doctor of Philosophy

Centre for Intelligent Dynamic Communications (CIDCOM)

Department of Electronic & Electrical Engineering

University of Strathclyde

Glasgow G1 1XW

United Kingdom

December 2018

Declaration

This thesis is the result of the author's original research. It has been composed by the author and has not been previously submitted for examination, which has led to the award of a degree. The copyright of this thesis belongs to the author under the terms of the United Kingdom Copyright Acts as qualified by University of Strathclyde Regulation 3.50. Due acknowledgement must always be made of the use of any material contained in, or derived from, this thesis.

Signed: Date:

Committee in-charged:

Convenor: Professor Dr Ivan Andonovic

External Examiner: Associate Professor Dr Xu Wang

Internal Examiner: Professor Dr Craig Michie

Preface

This thesis is submitted to the University of Strathclyde for partial fulfilment of the requirements for the degree of Doctor of Philosophy.

This doctoral work has been performed at the Department of Electronic and Electrical Engineering, Centre for Intelligent Dynamic Communications (CIDCOM), with Professor Ivan Glesk as main supervisor and Dr. Vladimir Stankovic, as co-supervisor.

Abstract

In high data rate optical fibre communication networks, dispersion phenomenon plays a pivotal role. It is important to investigate the dispersion effects in a multi-wavelength picosecond optical code division multiple access (OCDMA) system. This research is focused on the analysis of the effects of fibre dispersion on the OCDMA autocorrelation; and how these effects can be resolved in a tuneable way so that the originally recovered OCDMA autocorrelation function at the decoder receiver can be revived without further manual adjustment of fibre (SMF-28) cable lengths. The environmental effects and the subsequent mitigation process are also investigated further in this research. The chirp in OCDMA is examined experimentally and analytically in an initiative to find the more in-depth understanding of finely tuneable chromatic dispersion (CD) compensation technique in a coarsely compensated link by using semiconductor optical amplifier (SOA). A practical investigation was carried over a partially CD compensated 17 km bidirectional testbed between the University of Strathclyde and the University of Glasgow to perform the fine-tuning of CD adjustment using SOA. A 19.5 km SMF-28 fibre spool was also used in an environmental chamber to investigate the temperature induced dispersion effects and subsequent mitigation. The tuneable dispersion compensation measures are vital to ensure the high data rate optical communication using an all-optical approach in future data network end-points where the advantages of ultra-high speed optical communication bandwidth are at present disrupted due to opto-electronic conversions commonly known as ‘electronic bottlenecks’.

Acknowledgements

First and foremost, I pray to Allah for giving me the ability to continue the PhD study.

I am very grateful to my esteem supervisor Professor Ivan Glesk for his continuous guidance and support to teach me how to do research in black and white. His perennial encouragement, not only in terms of knowledge sharing but in also being a good friend (as seen in discussions while taking cup of coffee in the departmental canteen) continued throughout the PhD journey. My deep thanks to him for being by me through thick and thin. Words will not suffice to express my gratitude for his patience. I take the opportunity to thank my second supervisor Dr. Vladimir Stankovic for his motivational boost to endure the stressful phases of this journey.

The numerous facilities and assistance from the staffs of this university also stood me in good stead and helped me utilize the study time with effectiveness and purpose.

I am very lucky to have such a wonderful and gracious wife Mrs. Atiya Najma Nur, who has been a source of never-failing inspiration in all aspects, particularly incurring a deep support and encouragement to continue my research in the academia. Her patience and concern served as the anchor on which I could bank unconditionally throughout the research period. I am grateful to my son, Zayan Umair Ahmed and daughter, Zara Umair Ahmed for putting up with me, despite the fact that I had to devote time and attention to my studies, and be engaged with the research. I must acknowledge my amma Mrs. Shakina Jabber and my ammu Prof.

Najma Shams, uncle Dr. Majid Khan for encouraging me to complete this study. I do appreciate my long-time friend Dr. Abdul Hasib Chowdhury for his academic guidance and faith in me to complete the PhD study. Finally, I would like to dedicate this thesis work to late Doctor Tahammul Haque, my brother-in-law, my only sister Zakia Parvin's husband and a good friend of mine. He left us for his eternal abode at the age of only 50 years. May his soul rest on peace! I lost him during my PhD tenure and I remember him as an inspiring friend who always encouraged me to pursue and continue PhD research from the very beginning.

Example is not the main thing in influencing others, it's the only thing.

— Albert Schweitzer

Table of Contents

List of Figures

List of Abbreviations

OTDM	optical time division multiplexing
WDM	wavelength division multiplexing
OCDM	optical code division multiplexing
2D-WH/TS	Two-Dimensional Wavelength-Hopping Time-Spreading
CD	chromatic dispersion
TD	temperature-induced dispersion
BER	bit error rates
FWHM	full-width at half-maximum
DCF	dispersion compensation fibre
ISI	inter-symbol interference
FBG	fibre Bragg gratings
PLC	planar light-wave circuits
AWG	arrayed waveguide gratings
VIPA	virtually imaged phased arrays
SOA	semiconductor optical amplifier
OLT	optical line terminal
ONU	optical network unit
MAI	multiple access interference
LAN	local area network
OOC	optical orthogonal codes
PC	prime codes
EPC	extended prime codes
MPC	modified prime codes
EQCC	extended quadratic congruence codes
OSCG	optical supercontinuum generator
DDF	dispersion decreasing fibre
ML Laser	Mode Locked Laser
RF	radio frequency
RZ	return to zero
FP	Fabry Perot
DFB Laser	distributed feedback laser

IOR	index of refraction
MFD	mode field diameter
EDFA	erbium doped fibre amplifier
GVD	group velocity dispersion
SMF	single mode fibre
CFBG	chirped fibre Bragg gratings
FBG-DCM	FBG based dispersion compensation modules
IL	insertion loss
DC	dispersion compensation
DWDM	dense wavelength division multiplexing
MEMS	microelectromechanical systems
GTE	Gires-Tournois etalons
NC-FBG	nonlinearly chirped fibre Bragg gratings
SLM	spatial light modulator
CDC	chromatic dispersion compensation
OSG	optical supercontinuum generator
ITU	international telecommunication union
OSA	optical spectrum analyser
OSC	oscilloscope
AWG	Array Waveguide Gratings
CW/HB	continuous-wave holding beam
OP/HB	optical pulse holding beam
BPF	band pass filter
ODL	optical delay line
OC	optical circulator
Att	optical attenuator
SPM	self-phase modulation
ASE	amplified spontaneous emission
KK	Kramers-Kronig
CMOS	complementary metal-oxide semiconductor
SOI	Silicon-On-Insulator
SWG	sub-wavelength waveguide gratings

List of Tables

List of My Works

Journals -

1. **M. S. Ahmed**, I. Glesk, "Application of semiconductor optical amplifier (SOA) in managing chirp of optical code division multiple access (OCDMA) code carriers in temperature affected fibre link", Applied Sciences, vol-8, no-5, pp. 715, May. 2018. DOI:10.3390/app8050715.

2. **M. S. Ahmed**, and I. Glesk, "Management of OCDMA Autocorrelation Width by Chirp Manipulation Using SOA," *IEEE Photonics Technology Letters*. vol-30, no-9, pp. 785-788, May. 2018. DOI:10.1109/lpt.2018.2814788.

3. **M. S. Ahmed**, and I. Glesk, "Mitigation of Temperature Induced Dispersion in Optical Fibre on OCDMA Autocorrelation," *IEEE Photonics Technology Letters*, vol. 29, no. 22, pp. 1979-1982, Nov. 2017. DOI:10.1109/lpt.2017.2758163.

4. **M. S. Ahmed**, M. S. K. Abuhelala, and I. Glesk, "Managing dispersion affected OCDMA autocorrelation based on PS multi-wavelength code carriers using SOA," *IEEE/OSA Journal of Optical Communications and Networking*, vol. 9, no. 8, pp. 693-698, Jul. 2017. DOI: 10.1364/jocn.9.000693.

5. **M. S. Ahmed**, and I. Glesk, "Photonic platform and the impact of optical nonlinearity on communication devices," *Acta Physica Slovaca*, vol. 65, no. 2, pp. 65-152, Apr. 2015.

Conference Papers -

6. **M. S. Ahmed**, and I. Glesk, "Chirp management in communication systems with picosecond data carriers using a single SOA," In *Proc. 20th International Conference on Transparent Optical Networks, ICTON*, 2018. In press.

7. I. Glesk, **M. S. Ahmed**, Z. Wang, L. R. Chen, “Multiplexing Systems Performance Enhancements with All-Optical Signal Processing,” In*Photonics North*, 2018, Centre Mont-Royal.

8. I. Glesk, **M. S. Ahmed**, Z. Wang, L. R. Chen, “Towards integrated devices for ultrafast all-optical signal processing in optical networks,” In *Proc. SPIE Proceeding, 10536-39,* 2018. DOI: 10.1117/12.2296939.

9. M. Abuhelala, **M. S. Ahmed**, M. Ibrahim, and I. Glesk, “Investigation temporal skewing among O-CDMA code carriers under fibre temperature variations," In *Proc. 25th Telecommunications Forum TELFOR*, 2017. DOI:10.1109/telfor.2017.8249490.

10. **M. S. Ahmed**, M. Abuhelala, and I. Glesk, “Management of OCDMA autocorrelation function distorted by dispersion effects,” In *Proc. 19th International Conference on Transparent Optical Networks, ICTON*, 2017. Piscataway, N.J.: IEEE. DOI: 10.1109/ICTON.2017.8024789.

11. **M. S. Ahmed**, and I. Glesk, “Recent advances in all-optical signal processing for performance enhancement of interconnects,” in *Proc. 18th International Conference on Transparent Optical Networks ICTON*, 2016, Trento, Italy. Invited. DOI: 10.1109/ICTON.2016.7550537.

12. **M. S. Ahmed**, and I. Glesk, “Tunable chromatic dispersion management of optical fibre communication link using SOA,” in *Proc. 11th International conference Electro* 2016, Štrbské Pleso, Slovakia. Invited. DOI:10.1109/elektro.2016.7512026.

13. **M. S. Ahmed**, and I. Glesk, 2015, “Towards lasing on a silicon chip: gallium and its alloy or rare earth doped gallium nitride as the solution?” In *Proc. R. Kumar (Ed.), Proceedings of the Third International Conference Advances in Computing, Communication and Information Technology- CCIT 2015. (pp. 25-29),* 2015. DOI:10.15224/978-1-63248-061-3-16.

Poster Presentations -

14. **M. S. Ahmed**, and I. Glesk, “Overview of the second order optical nonlinearity in GaN waveguides for use in devices for optical communication,” Poster session presented at Sixth Annual SU2P Symposium, KY16 9AJ, United Kingdom. 2015.

15. **M. S. Ahmed**, and I. Glesk, “Optical Nonlinearity and Its Uses in Ultrafast All-optical Switching”. Poster presentation in the ‘Faculty Research Presentation Day-2014, 2014.

16. **M. S. Ahmed**, and I. Glesk, “Optical Nonlinearity and Its Uses in Ultrafast All-optical Switching”. Poster presentation in the 'University Research Day -2014', 2014.

Chapter 1

Introduction

1.1 Motivation

Optical Time Division Multiplexing (OTDM) [1], has been developed together with Optical Code Division Multiplexing (OCDMA) [2] for use in fibre optic networks. In recent years, incoherent OCDMA based on two-dimensional wavelength hopping time spreading (2D-WH/TS) family of codes has attracted the attention of researchers [2] including our research group. In order to support and achieve large cardinality and a large number of simultaneous users, the 2D-WH/TS OCDMA uses multi-wavelength picosecond code carriers [3]. However, if not properly addressed, using picosecond code carriers can lead to undesirable dispersion effects [4] during data transmission. The motivation for this PhD research was to investigate the effect of dispersion on 2D-WH/TS OCDMA fibre transmission and find ways for its mitigation.

To mitigate the dispersion impairments, a number of compensation techniques have been demonstrated using dispersion shifting fibres [5], fibre Bragg gratings (FBGs) [6], planar light-wave circuits (PLCs) [7], virtually imaged phased arrays (VIPAs) [8], and arrayed waveguide gratings (AWGs) [9].

The conventional method of CD compensation is often accomplished by using matching lengths of DCF modules. This method is time consuming and tedious and becomes difficult to implement if the fibre lengths are not known before hand or dispersion is changing due to environmental changing conditions particularly for the cases of multi-wavelength picosecond incoherent OCDMA system. There are several vexing issues, which may necessitate that the dispersion compensation mechanisms are tuneable in nature. For example, in almost all 40+ Gb/s systems, dispersion management with high accuracy is a necessity, preferably using tuneable dispersion compensators as discussed in [10].

In OCDMA systems, the multi-wavelength picosecond pulses are distributed within a data bit-width to form an OCDMA code. Due to CD or temperature-induced dispersion (TD), these short multi-wavelength pulses propagating in the optical fibre will be broadened and affected by a so-called time-skewing effect. As a result, at the receiver side, the recovered OCDMA autocorrelation function becomes distorted, as it changes its shape, notably its width. This can drastically influence the OCDMA system performance in terms of bit error rate (BER) and the total number of simultaneous users [11, 12]. Therefore, dispersion management is critical to maintain the system performance.

1.2 Research Aims and Contributions

The aim of this thesis was to investigate the use of SOA to mitigate the dispersion effects on 2D-WH/TS incoherent OCDMA autocorrelation and code carriers based on multi-wavelength picosecond pulses after traveling on optical fibre.

In addition, the effect of optical chirp on multi-wavelength code carriers was also investigated.

In the investigation of CD, a fibre optic testbed connecting the University of Strathclyde and the University of Glasgow was used. To investigate the temperature induced fibre dispersion in optical fibre, an environmental chamber was used to set different temperatures for the optical fibre link under the test.

The research contributions are:

(1) To investigate for the first time, the use of SOA to mitigate the 2D-WH/TS incoherent OCDMA autocorrelation broadening and skewing due to residual CD.

(2) To investigate the temperature induced fibre dispersion, the experimental setup based on the 2D-WH/TS incoherent OCDMA and a 19.5 km long CD compensated fibre link represented by a spool of fibre placed in an environmental chamber were built.

(3) It was experimentally demonstrated that, the fibre link when exposed to an increase in temperature, would alter the FWHM value of the recovered 2D-WH/TS OCDMA autocorrelation based on picosecond multi-wavelength carriers. It was shown for the first time that the SOA could mitigate the observed amount of OCDMA autocorrelation broadening. Also shown that a dispersion compensated (DC) spool of fibre, when under an increase in temperature would make the link ‘over-compensated’ and a decrease in temperature would make it ‘under-compensated’.

(4) It was demonstrated for the first time the use of an SOA at the transmission side to control a recovered OCDMA autocorrelation function and its width at the receiver side by controlling the chirp of multi-wavelength ps OCDMA code carriers. The formula incorporating the chirp parameter *C* into mathematical description of the recovered OCDMA autocorrelation envelope composed of multi-wavelength code carriers were also developed.

(5) The effect of changing chirp value on the 2D-WH/TS OCDMA autocorrelation envelope and its width changes imposed by the SOA was investigated experimentally and by calculation.

(6) It was investigated for the first time the use of an SOA for both, pre- and post- CD compensation, in order to mitigate CD effects in a fibre transmission link used by an incoherent OCDMA system based on multi-wavelength picosecond 2D-WH/TS codes.

1.3 Organization of the Thesis

The thesis comprises of a number of Chapters with diversified issues all linked together coherently and cohesively. As for example, **Chapter-1** deals with the main objective or aim of the thesis and emphasizes on the need for tuneable dispersion compensation in case of 2D-WH/TS OCDMA based on multi-wavelength picosecond code carriers. **Chapter-2** describes the basic elements of configuring an incoherent OCDMA system much related to the research for later Chapters. **Chapter-3** describes the basic theory of dispersion in optical fibre communication; and how this detrimental dispersion effect is manageable in a conventional manner.

Analysis of dispersion effect on 2D-WH/TS OCDMA based on multi-wavelength picosecond carriers is also highlighted. **Chapter-4** reports for the first time an experimental investigation of using SOA to mitigate the CD effect on 2D-WH/TS OCDMA autocorrelation width, based on *multi-wavelength* picosecond carriers. **Chapter-5** depicts for the first time an experimental demonstration of fibre temperature induced effects on the said system and the mitigation of these effects by SOA as an application. **Chapter-6** investigates a technique to adjust the recovered OCDMA autocorrelation function FWHM width via a chirp control by using an SOA applied on carriers before the code transmission through the link. **Chapter-7** concludes the thesis with in-depth discussion about the future works in the areas of tuneable dispersion compensation for an incoherent OCDMA system.

Chapter 2

Incoherent OCDMA System

2.1 Introduction

Advances in optics led to the development of optical fibre communication systems that support multiple types of traffic for the usage of mobile phones, cable TV, internet etc. Supporting all these devices as a baseband system requires the data to be sent by simple ways of turning the transmitter on and off [13]. However, this baseband system or in other word, the 'access network' faces tremendous challenges to handle the ever-increasing demand for capacity and speed in communication systems. Some of the challenges are the multi-service capability, protocols and cost issues. Fibre optics technology has a number of advantages in addressing the above issues with the implementation of different types of multiplexing techniques. In this Chapter, the need for data multiplexing, coherent and incoherent OCDMA, generation of 2D-WH/TS incoherent OCDMA coding, the OCDMA autocorrelation function, the requirement of multi-wavelength picosecond pulse as the code carriers will be discussed.

2.2 Need for Data Multiplexing

To transmit large amount of data is very important for many applications. Due to the limitations of opto-electronic signal processing (known as electronic-

bottleneck) at the transmission and receiving ends of the network, multiplexing low speed data streams onto an optical fibre were developed to increase the data throughput [14]. Fibre optic communication systems use different multiplexing techniques e.g., optical time division multiplexing (OTDM), wavelength division multiplexing (WDM) and optical code division multiplexing (OCDM) to carry the data. WDM or OTDM techniques use wavelength or time-slots, respectively to perform the data multiplexing. The investigation mentioned in this thesis is focused on incoherent OCDMA using 2D-WH/TS with picosecond code carriers.

2.3 Evolution of OCDMA

CDMA technique originated in the context of radio frequency communication and it was applied first to optical domains in 1980s [15]. Researchers wanted to use the excess bandwidth in single-mode fibres towards the random asynchronous operation, where the centralized network controller would not be required. This technology enables multiple users to share the same transmission medium and media access control is greatly simplified. This system consists of optical source modulated incoherently (power) or coherently (field) with the user data [16]. The OCDMA system can be categorised broadly into two types, basing on the way a user's code is applied to the optical signal.

2.3.1 Coherent OCDMA

In a 'coherent OCDMA' approach, users' codes are created via optical signal's phase coding. Some examples of this scheme are spectral phase encoding (SPE-OCDMA) [17] and temporal phase encoding [18]. SPE-OCDMA is achieved

by spectral encoding of broadband spectrum of an optical pulse. Here, the code is generated by applying different phase shift patterns to each spectral component. In case of temporal phase coding, the code is generated by a sequence of pulses which are relatively phase shifted depending on the sequence of the optical code. The light pulses are required to have a coherence length greater than the chip length for coherent summation in the correlation process for a coherent OCDMA system [19]. The term ‘coherence’ means, the degree to which electromagnetic radiation maintains a near-constant phase relationship, both temporally and spatially. In case of light sources such as lasers, the waves are identical and in phase, thereby produce a beam of coherent light [20]. The time over which the phase relationship remains nearly constant is called the coherence time. The path length corresponding to the coherence time is known as coherence length [21]. The role of coherence on OCDMA system and its impact will be further discussed in Section 2.4 and 2.5.

2.3.2 Incoherent OCDMA

On the other hand, in ‘incoherent OCDMA’, amplitude-modulated approach is deployed to generate OCDMA codes. Here, the intensity modulation and direct detection processes are involved. To adhere to the focus of this thesis, only incoherent OCDMA will be further discussed. The initial works related to the incoherent OCDMA system were reported in [22, 23, 24]. In [22], Hui proposed a model, based on a broadcast network, where the tapped delay lines were used for the generation and detection of optical patterns. Hui’s work also indicated the use of amplifiers and hard-limiters for the regenerations of weak coded optical pulses. Prucnal et al. demonstrated spread spectrum local area network (LAN) in [24], where

the foundation was laid for incoherent OCDMA system using different devices such as mode-locked laser, modulators, encoders /decoders and fibre. This type of system utilized optical fibres as delay lines for incoherent signal processing. The simplest mature optical encoders or decoders utilizing time spreading indicate the power splitter, fibre delay lines and power combiners for coding as shown in Fig. 2.1. Here, a bit interval T_b is divided into equal time-slots T_c also known as chips. As soon as the data bit, '1' is sent to the encoder, the incoming signal is split into an optical pulse series with identical energy by the power splitter (1 × W).

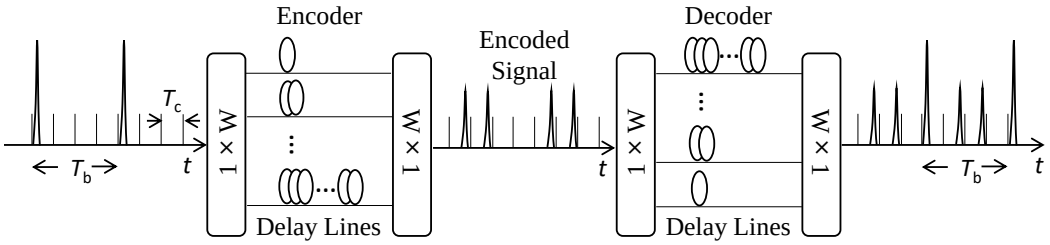

Fig. 2.1: Encoders / Decoders based on optical delay lines.

The split number of pulses is equal to the code weight. These pulses are then, selectively delayed through the process of fibre optic delay lines, where the pulse positions pre-determined by a unipolar 'code sequence' spread through the assigned delay lines. Finally, with the help of power combiner (W× 1), the delayed pulses are combined to generate the encoded burst of optical pulses.

2.4 1D and 2D Incoherent OCDMA Codes

In the early development of incoherent OCDMA system, the focus was on getting unipolar codes having auto- and cross-correlation functions. For example, the optical orthogonal codes (OOC) [23, 25], prime codes (PC) and quadratic

congruence codes [26] were investigated. Later, the extended prime codes (EPC) [27], modified prime codes (MPC) [28] and extended quadratic congruence codes (EQCC) [29] were studied. These are 'one dimensional' codes and OOC has the best performance. OOCs are a family of (0, 1) sequences with desired autocorrelation and cross-correlation properties providing asynchronous multiple-access communications with easy synchronization and good performance in OCDMA communication networks [30]. From the functional point of view, an OOC (N, w, λ_a, λ_c) is a family C of (0, 1) sequences of length N and weight w and satisfies the following properties [31]:

(1) Autocorrelation Property: $\sum_{t=0}^{N-1} x_t\, x_{t+\tau} \leq \lambda_a$

for any x $\in C$ and any integer τ, $0 < \tau < N$.

(2) Cross-correlation Property: $\sum_{t=0}^{N-1} x_t\, y_{t+\tau} \leq \lambda_c$

for any x $\neq$ y $\in C$ and any integer τ.

Here the numbers λ_a and λ_c are the auto- and cross-correlation constraints and (0, 1) sequences of an OOC are known as the code words. The size of the OOC is the number of code words. A one-dimensional (1D) code has inherent restriction on code length and weight. On the other hand, the two-dimensional codes (2D) operate in time and wavelengths domains and could overcome the limitations imposed by a 1D coding. Tancevski and Andonovic proposed a 2D time spreading integrated with wavelength hopping pattern [32]. In [32], the author showed that the codes constructed had an autocorrelation function with zero side-lobes and a cross-

correlation of at most one by using prime codes. This improved the orthogonality condition compared to 1D prime sequences [33]. In general, a family of 2D OOC codes can be represented by five important parameters ($N \times M$, w, λ_a, λ_c), where N is the code length in time domain, M is the number of available wavelengths, w represents code weight, and λ_a and λ_c correspond to autocorrelation and cross-correlation values, respectively [33]. The above 2D family of OOC codes increases the cardinality with a smaller reduction in the user's data rate, and at the expense of increased transmitter and receiver complexity [33]. A 2D-WH/TS coding approach can spread the codes in both time and wavelength domains simultaneously. This approach achieves high code design flexibility and code performance by placing the optical pulses at different chips across the bit period where each chip possesses different wavelengths and thereby makes a wavelength-hopping pattern [34]. Additionally, the obtained zero autocorrelation side-lobes in 2D-WH/TS system allow easy synchronization in between the transmitter and the intended receiver [34]. This is an approach using prime codes for both spreading and hopping results in a perfect needle-shaped autocorrelation function [32]. In this system, the sequence of codes is created by locating the pulses of varied wavelengths in different time chips by a hopping pattern [35]. As such, this type of codes can be represented by a 2D code matrix in the dimensions of wavelength and time where, the wavelength domain is divided into N_λ channels of wavelengths and the time domain is divided into N_T chips [34]. As for the illustration, two code sequences of 2D-WH/TS matrix are shown in Fig. 2.2.

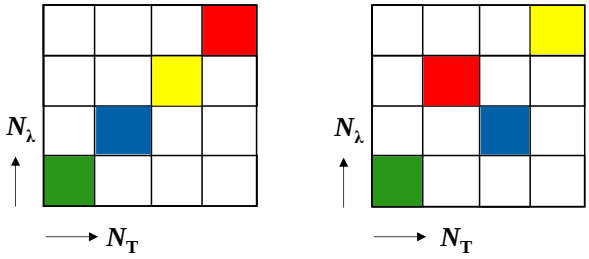

Fig. 2.2: Two code sequences for 2D-WH/TS OCDMA. Bit period is divided into N_T chips and code sequences are formed by placing w pulses of different wavelengths N_λ in them.

In case of incoherent OCDMA systems, MAI is the dominant noise and the effect of beat noise is minimal [33]. Because, the impact of beat noise in incoherent OCDMA system is gradually eliminated with increasing coherence ratio, where the coherence ratio is defined as the ratio of the chip duration to the coherence time of the light source [36]. Beat noise is also known as interferometric noise (IN) and the classes of IN and their impact on the OCDMA system performance is discussed in [37]. How the IN introduces significant system power penalties is shown in [38] as an example. It is also mentioned in [38] that this IN must be taken into consideration in any OCDMA network designs and implementations. Incoherent OCDMA systems use unipolar codes. Because, in these systems, the optical encoding /decoding operation is performed based on the signal power as such it works in unipolar manner (1, 0), where, '1' means the presence of a signal and '0' means no signal at all.

2.5 2D-WH/TS Incoherent OCDMA Coding

An incoherent OCDMA system requires very narrow optical pulses as code carriers to achieve large cardinality [39]. The generation of 2D-WH/TS incoherent OCDMA codes was demonstrated by utilising the multi-wavelength lasers thereby

providing short pulses at varied wavelengths [40]. However, the multi-wavelength sources using array of lasers are limited having higher complexity mainly for controlling a large number of lasers [41]. As a result, the system cost rises for using multi-wavelength laser sources at each node. A broadband optical source (broad optical bandwidth) spectrally sliced for achieving a multi-wavelength output was also demonstrated in [42]. In 2D-WH/TS incoherent coding scheme, the optical source should be high speed for temporal spreading and spectrally broadband for spectral coding [43, 44, 45]. Moreover, the source should have a relatively short coherence time compared with the pulse duration to achieve incoherent superposition of the decoded optical pulses [46]. The impact of laser source coherence time on bit error rate (BER) and autocorrelation function performances of a direct sequence OCDMA system was studied in [47]. An OCDMA system can use either coherent (Laser, Super-Continuum Laser and Mode Locked Laser, etc.) or incoherent (LED, ASE from EDFA and SOA, etc.) optical sources [48]. As for example, a variety of wideband incoherent sources such as amplified broadband spontaneous emission was used for incoherent OCDMA architecture [49, 50]. Some other architecture of incoherent 2D-WH/TS OCDMA deployed an erbium doped fibre mode locked laser in combination with an optical supercontinuum generator to generate optical supercontinuum. As such a supercontinuum source consists of a pulsed laser and a non-linear element where a combination of non-linear effects broadens the narrow-band laser radiation into a continuous spectrum without destroying the spatial coherence of the laser light [51]. The optical supercontinuum generator (OSCG) consisting of a high-power erbium doped fibre amplifier and dispersion decreasing fibre (DDF) can generate short optical pulse over a broad spectral range. Earlier, self-

phase modulation following self-focusing and optical breakdown as well as four wave mixing were thought to be the main mechanism for supercontinuum (SC) generation [52]. SC generation is now believed to be a result of the complex interplay of diverse phenomena due to the third-order nonlinear susceptibility, as well as ionization and plasma generation for the anomalous dispersion regime [53]. A number of multi-wavelength picosecond pulses can thus be produced simultaneously by spectral slicing (filtering out the wavelengths of interests) by using 2D-WH/TS FBG encoders [54, 55]. As for example, a ps ML Laser centred at 1545 nm can generate the SC wave beyond 1551 nm and then be spectrally sliced to required wavelengths by the FBG encoder. The following Fig. 2.3 shows a schematic demonstrating a FBG-based WH/TS encoder. An optical pulse from a broadband source like OSCG passes to a series of FBGs via an optical circulator to produce 2D-WH/TS codes. This is the approach used in the experimental investigations described in this thesis [40].

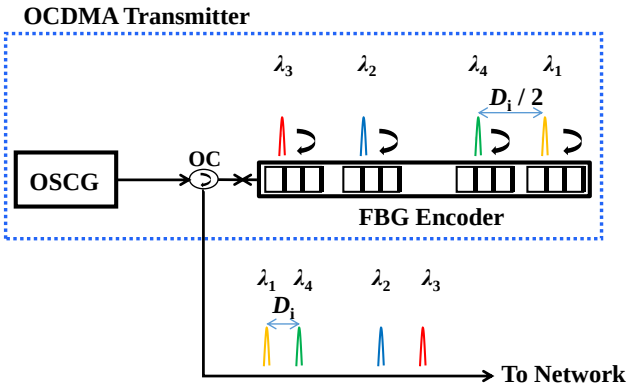

Fig. 2.3: 2D-WH/TS Encoder with four wavelengths λ_i in the code using FBG technology; OC – optical circulator, D_i – optical delay.

The WH/TS encoders have also been implemented using some other technologies as narrated in [34]. As for example, the use of arrayed waveguide

gratings (AWGs) or thin-film filters (TFFs) was demonstrated for the wavelength-hopping processes, while set of fixed or tuneable delay lines was used for the control of time-spreading process [56, 57]. Figure 2.4 shows a simple implementation of a WH/TS en/decoder using two AWGs: (1 × N wavelength de-multiplexer and N × 1

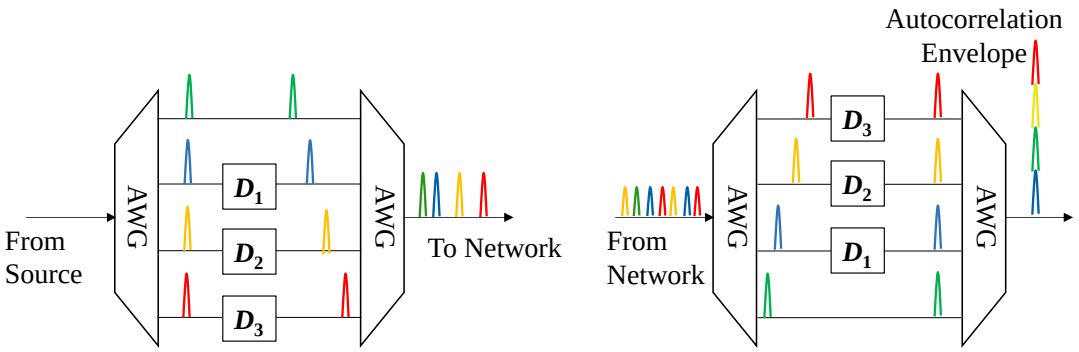

Fig. 2.4: 2D-WH/TS Encoder and Decoder with four wavelengths in the code using AWG technology.

wavelength multiplexer) with fixed or tuneable delay lines in between them [34]. As described in [42], the encoder made of AWG was used for de-multiplexing the input spectrum, which was followed by different lengths of fibre loops. The delays and spectral components' amplitude were utilised to define the WH/TS codes by recombining the same waveguide gratings in a feedback configuration [58]. The switched delay lengths enable to program the encoder to have varied prime-hop codes. After transmission through dispersion shifted (DS) fibre link, the received signal was passed through a decoder just identical to the encoder with conjugate delay loops where the time-spread and spectral coded data was collapsed and the original data was recovered. In another example, en/decoders based on chirped Moire gratings (CMGs) and holographic Bragg reflectors (HBGs) combine wavelength hopping and time spreading into a single process [34]. Table 2.1 shows a comparison of advantages /disadvantages of different types of OCDMA en/decoders.

Table 2.1: Comparison of Advantages /Disadvantages for Different Types of OCDMA Encoders /Decoders [41]:

FBG	**CMG**	**AWG**	**Integrated Holographic En/Decoder**	**Thin-Film Filters**
All-fibre en/decoding.	Composed of superposed linearly chirped FBGs.	Low insertion loss. Consists of a phased array of optical waveguides.	Basic building block is holographic Bragg reflector (HBR).	Can be considered as Fabry-Perot (FB) etalons with multiple reflective dielectric thin-film layers to form the mirrors surrounding the FB cavity.
Support reconfigurable systems using tuneable devices.	The number of codes are limited. Independent control and delay of each wavelength is forbidden.	Entire en/decoder is waveguide integratable resulting in a smaller footprint.	Provides excellent channel specific pass-band control like thin film filters and FBGs.	Flexible, low loss, passive temperature compensation, provide lowest-loss solution at low channel count. Insensitive to polarization and stable to temperature variations.
Can generate WH/TS codes.	Enable use of a single passive grating structure to implement WH/TS codes.	Can generate WH/TS codes. More mature technology than FBG.	Ability to provide both spectral slicing and temporal delay simultaneously implies that HBR-based WH/TS en/decoders can be made very small.	Can be used for WH/TS en/decoders. Increased code matrix size can be used for better system performance.

2.6 2D-WH/TS Incoherent OCDMA Autocorrelation Function

In a broadcast network, the signals transmitted from all the transmitters are received back by the 2D-WH/TS OCDMA decoder. The decoder correlates the received signal with the code sequence assigned to that receiver and in this process; it will undo the time spreading by aligning the wavelength carriers back in time on top of each other, thereby producing the autocorrelation function. Here, the decoder removes all delays that are imposed on individual code carriers by the encoder [59]. Autocorrelation envelope's height as shown in Fig. 2.5 is equal to combined power of all individual wavelength pulses (code weight - *w*) that formed the autocorrelation envelope or function. In the investigations, the autocorrelation function S_T^L(t) was used to describe 2D-WH/TS OCDMA autocorrelation envelope as

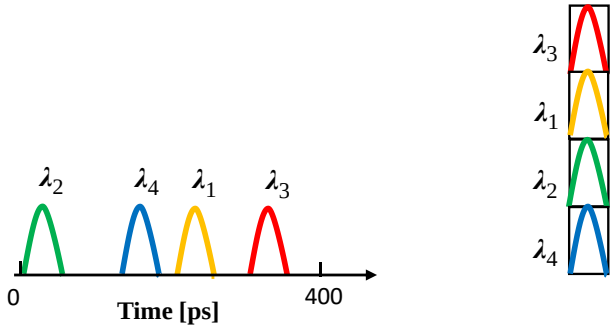

Fig. 2.5: Illustration of the recovered OCDMA autocorrelation function at the decoder. (a) Two-dimensional wavelength-hopping time-spreading (2D-WH/TS) transmitted OCDMA code; (b) Recovered OCDMA autocorrelation - ideal case.

mentioned in [12] to further analyse the varied effects on it which will be elaborately described in subsequent Chapters 3 to 6.

2.7 Why Use Picosecond Multi-Colour Pulses as Code Carriers?

2.7.1 Generation of Ultra-Short Pulses

Lasers as the light source are used for their very short spectral widths in most single mode fibre system [60]. The short optical pulses can be generated by several methods such as Q switching [61], mode locking [62], gating of Continuous Wave (CW) light by an external modulator [63] and gain switching [64]. Generation of ultra-short pulses required for incoherent OCDMA system under investigation in this thesis uses mode locked laser. The laser output occurs at discrete numbers of wavelengths corresponding to different modes (resonant frequencies) of the resonator. The various frequencies will interfere with each other if there is no fixed phase relationship between these modes resulting in fluctuations at the output over time. However, the laser will emit a train of narrow light pulses due to constructive and destructive interference by fixing the relative phases of these modes, which is the basic principle of mode locking [65]. The shorter the duration of the mode-locked generated pulses will be for larger the band of frequencies (the gain bandwidth) over which the laser oscillates. Active, passive and hybrid mode locking techniques are further described in [65]. How the ps ML Lasers can generate shorter pulse widths by mode locking a laser can be understood from [66, 67, 68].

2.7.2 Spectral Efficiency in OCDMA System

The basic definition of ‘spectral efficiency’ is a fundamental performance measure for an optical communication system and specifies the overall throughput per unit of optical bandwidth associated with a fixed bit error rate (BER) [69].

$$\sum_{\text{BER}} = \frac{N_U R}{B_0} \quad (1)$$

Here, N_U is the number of simultaneous users emitting at a bit rate R and B_0 is the optical bandwidth occupied by the system. The highest performance systems are generally those that achieve the largest spectral efficiency at identical BER. In an investigation as mentioned in [69], it was shown that the maximum spectral efficiency of OCDMA systems with coherent sources is at least a factor of 5 higher than OCDMA systems with incoherent sources. In [70], the spectral efficiency of direct detection OCDMA system using both coherent and incoherent optical sources were evaluated. It was found that the DS-OCDMA system had the highest spectral efficiency in the coherent configuration. However, for incoherent case, the maximal spectral efficiency was obtained with SAC-OCDMA system. However, a careful code design may increase spectral efficiency, as for example, in [71], a multi-dimensional OCDMA scheme was proposed to obtain both higher spectral efficiency and lower bit error probability (BEP).

2.7.3 Requirement of Ultra-Short Pulses in OCDMA

For an incoherent OCDMA system, each user is assigned a unique signature, i.e., a code of length '*N*' selected from optical orthogonal code (OOC) set [33]. At the receiver site, each user is distinguished by its own signature from the encoded data of all users because of appropriate auto- and cross-correlation properties of these codes. The bit-time T_b is divided equally into '*N*' smaller chip times, expressed as T_c. Now a user's signature code specifies ω out of *N* chips to contain an optical pulse with duration of T_c. Here, ω is the code weight. The data of different users in OOC-

OCDMA system cannot be completely orthogonal for the unipolar characteristics of optical intensity based OCDMA system. As such, a new concept of threshold known as maximum collision parameter is defined for OOC. The parameter κ is the maximum allowed number of chip collisions of any code word with the circularly shifted version of itself or other code words [72]. The code length must increase in order to increase the number of code words available to support more network users. Nevertheless, to increase the code length and at the same time maintain the unchanged bit rate, it requires the use of shorter duration optical pulses, which means, the reduced chip time. Consequently, it is required to choose the temporal width of laser pulse equal to or shorter than the chip width. However, the use of shorter laser pulse is preferable to achieve better system performance, because the unwanted overlap of these shorter pulses by OCDMA codes will decrease [35].

It is important to consider the spectral widths. Since the pulses get narrower, the corresponding spectral widths also increase. In fact, for each pulse width there is corresponding minimum spectral width. As such, transform limited pulses are required. Otherwise, the dispersive effects will be much greater causing the pulse to spread out in time domain, thereby reducing the transmission length of the signal if the spectral width is wider than its minimum value [65]. Another important reason for choosing the short multi-colour pulses as the coding scheme can be explained as follows:

In comparison to the electronic bipolar codes (conventional), such as Gold codes [73], the cross-correlation function for the unipolar codes is high and the number of codes in the family is very low. As such, long sparse codes having very

few ones with narrow pulses help to achieve greater number of users and high transmission capacities [74]. As mentioned in [75] that the wavelength numbers' combination, code weight, the time-chips number and the **optical pulse widths** determine the code performance metrics. Also highlighted in [76, 39] that, to increase the number of chips within the 2D-WH/TS code, the chip width must be reduced. However, in practice, this will require to reduce the code carrier wavelength's pulse duration or width, which might be rather broadened due to dispersion effects if not properly compensated. At this point, it is required to know how the chromatic and temperature related dispersions affect the 'optical code widths' (one important parameter for the code performance metrics) for the cases of incoherent OCDMA transmission, which will be studied in the subsequent Chapters of this thesis.

2.8 Discussion

Incoherent OCDMA is a promising multiplexing technique, which is suited for future access networks. It has some inherent advantages such as: asynchronous transmission, flexibility, scalability, quality of services etc. In this Chapter, the basic concept of an incoherent 2D-WH/TS OCDMA system including the various system components for its operations was discussed. A simplified code generation concept using the encoder-decoder pairs, as the very important part of this system, was also enumerated. The literature reviews also mentioned about the categories of OCDMA system and different code types. Different en/decoding methods were also denoted. Finally, the importance of maintaining the short multi-wavelength picosecond OCDMA code carriers to maintain the code performance metrics was highlighted.

How the effect of dispersion plays an important role in fibre optic communication in general and then on 2D-WH/TS incoherent OCDMA based on multi-wavelength picosecond carriers will be discussed next as the control of dispersion is very important for the systems performance metrics.

Chapter 3

Fibre Dispersion and Its Effect on Picosecond 2D-WH/TS OCDMA

3.1 Introduction

The information encoded in optical signal transmits over long distances via fibre optic communication system. While a non-monochromatic impulse of light transmits through a fibre line, its shape changes because of light wave speed dependence on multiple factors producing transmission impairments in the network. In case of transmission speeds greater than 3 Gb/s, the transmission impairment such as dispersion plays a vital role for larger distances and as such, the system becomes dispersion-limited [77]. Dispersion is in fact the spreading out of light pulses while they travel along a fibre line. Like attenuation, dispersion can limit the distance a signal can travel through an optical fibre, but it does so in a different way. Dispersion does not weaken a signal, rather it 'blurs' it. If one sends one pulse every nanosecond but the pulses spread to 10 ns at the end of the fibre, they blur together. The signal is present, but it is so blurred in time that it becomes unintelligible. In systems that carry multiple wavelengths, dealing with CD is more complex. As for example, WDM systems require the management of dispersion over the entire range of wavelengths that are transmitting optical channels. For multi-wavelength picosecond OCDMA system, the code carriers are formed of varied wavelengths spectrally

separated from each other. Hence, dispersion management on this type of system is also important to ensure optimum BER performance. This Chapter discusses the causes of fibre dispersion, different types of it, fibre characteristics changes because of temperature, some important parameters, common techniques of dispersion compensation, tuneable dispersion compensation, chirp effects on fibre and a short mathematical analysis of effects of chromatic dispersion (CD) on 2D-WH/TS OCDMA based on multi-wavelength picosecond code carriers.

3.2 Chromatic Dispersion as Transmission Impairment

When a pulse of light passes through a fibre optic cable, the aperture, core diameter, wavelength, refractive index profile, laser linewidth properties etc. cause the optical pulse broadening [78]. This is a well-known effect and is one of the main impairments limiting optical fibre systems performance. Optical fibres are optimized for their operation for particular wavelength of use. As the optical pulse moves down the fibre, longer wavelengths travel faster in comparison to those of shorter wavelengths and as a result, the spreading of optical pulse occurs as shown in Fig. 3.1.

Fig. 3.1: Optical pulse broadening.

The refractive index of a material is defined as the ratio of light speed in a medium to that in a vacuum. The effective refractive index for fibre is about 1.45.

However, the refractive index and hence the light speed in fibre is wavelength dependent [79]. The graph for refraction index changes vs the change in wavelength for a fused silica can be represented as in Fig. 3.2. Optical pulses propagating at shorter wavelengths have an effect of larger refraction indices on the silica fibre than for the cases of longer wavelengths. Hence, the lights for different wavelengths

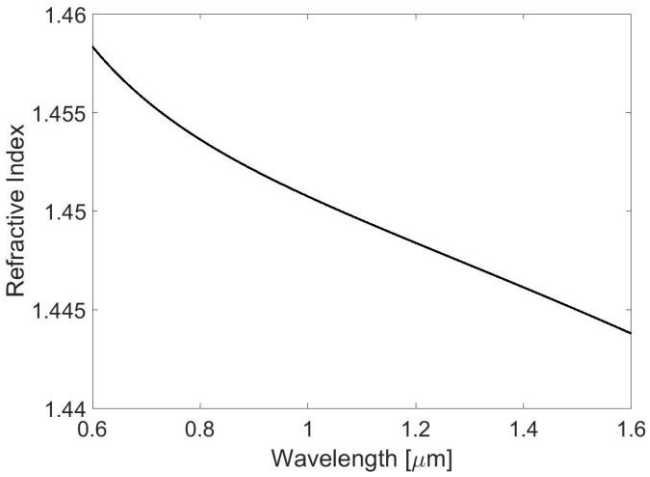

Fig. 3.2: Graph for refractive index vs wavelength for a fused silica.

travel at different speeds. The less the monochromatic light from the transmitter, the more the velocity difference will be among the wavelength components of longest and the shortest ones propagating through the fibre [77]. The light sources such as LED diode and diode lasers are characterized by the 'spectral width'. As for example, a Fabry Perot (FP) laser has 2 nm, a single-mode laser has 0.1 nm, and a DFB Bragg laser has 0.05 nm spectral width [77]. It can be said that, the smaller the bandwidth for a light source, the smaller will be the dispersion effects. As such, the DFB lasers produce the smallest CD in a fibre optic propagation. Typically, the CD is expressed in nanoseconds or picoseconds per (km-nm). CD consists of two parts namely waveguide dispersion and material dispersion. The refractive index of a medium is related to the speed of light with the following expression:

$$n = c / v \tag{3.1}$$

Here, n is the refractive index, c is the light speed in vacuum and v is the speed for the same wavelength as seen in the material. The refractive index changes in accordance with the wavelength, since the value of v as seen in Eq. (3.1) changes for each wavelength. As such, dispersion from this kind of phenomenon is known as material dispersion as it arises from the material fibre properties [80]. Material dispersion deals with 'wavelength' dependence on the 'index of refraction (IOR)' of the glass. On the other hand, 'waveguide dispersion' deals with the 'waveguide's physical structure'. The wavelength of the light is not much bigger than the fibre core in a single mode fibre. As a result, when the light travels down the fibre, it travels beyond the areas of core diameter known as "mode field diameter (MFD)". MFD is related to the light wavelength where the longer wavelengths travel in a larger mode field diameter (Fig. 3.3). As a result, a part of light travels in the fibre geometric core

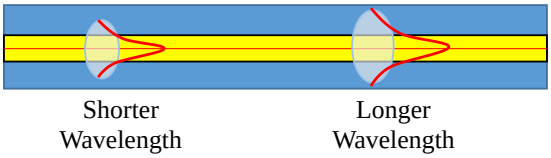

Fig. 3.3: Mode field diameter for different wavelengths.

and the other part travels in the cladding. As the glass core has a higher refractive index than the cladding, the light travels faster in the cladding than the light in the core. Since longer wavelengths have larger MFD, they suffer more material dispersion [79]. The waveguide dispersion depends on the following parameters [81]:

(1) Refractive index difference Δn, between the core and the cladding.

(2) Core diameter - since with the decrease in core diameter, the dispersion increases in general.

(3) Fabrication of the optical fibre.

It is possible to change substantially the waveguide dispersion by the alteration of the internal fibre structures thereby changing the overall dispersion parameter of the fibre [80]. Depending on the wavelengths of transmission, the ‘material’ and ‘waveguide’ dispersions can be opposite in signs. These two cancel each other at 1310 nm showing zero-dispersion and makes possible the transmission of very high-data communication at this wavelength [78]. However, fibre glasses exhibit minimum attenuation at 1550 nm which is also the operating range for EDFA. As such, zero-dispersion-shifted fibres are developed where the zero-dispersion property of 1310 nm has been shifted to the telecommunication window of 1550 nm ensuring high bandwidth long distance communication. This shift is possible by changing the waveguide design i.e., increasing the magnitude of waveguide dispersion [78].

The important characteristics for silica-based fibre are: the refractive index, dispersion and temperature induced dispersion which are important for the transmission system design. The fibre optic cables can be exposed to various environmental situations, such as: temperature, humidity and wind, which might be laid out as underground, aerial or inter-city ducts. The temperature variations as seen in Table-3.1 [82], can change the index of refraction of the fibre. The increase in fibre temperature does not remain uniform for all the wavelengths which results in varied wavelength speeds while propagation. As such, the refractive index change due to variations in temperature will modify the CD amount that the optical pulse

Table 3.1: Environmental Conditions of Aerial Fibre [82].

Location	Average Minimum Temperature	Average Maximum Temperature
New York	-8 ºC	25 ºC
Arizona	5 ºC	39 ºC
Florida	10 ºC	30 ºC
Wisconsin	-33 ºC	39 ºC

experiences. The temperature dependant chromatic dispersion for silica fibre was computed to be -1.5 ps /nm /km / ^{0}K by calculating the Sellmeier coefficient as mentioned in [83]. In the same paper, the temperature dependence for zero-dispersion wavelength was found linear and computed as, $d\lambda_0/dT$ = 0.025 nm / ^{0}K. The analysis also reports that $d\lambda_0/dT$ is dominant for core-glass material of fibre instead of its design.

3.3 Dispersion Parameters and Group Velocity Dispersion

It is required to know some definitions such as ‘phase velocity’, ‘group velocity’, ‘group velocity dispersion (GVD)’ related to the phenomena of material dispersion [77].

3.3.1 Phase Velocity

Let us consider a plane wave (monochromatic) propagates along the z-axis in an infinite medium as represented in Fig. 3.4 and expressed as [84]:

$$E(z, t) = E_0 \cos(kz - \omega t) \tag{3.2}$$

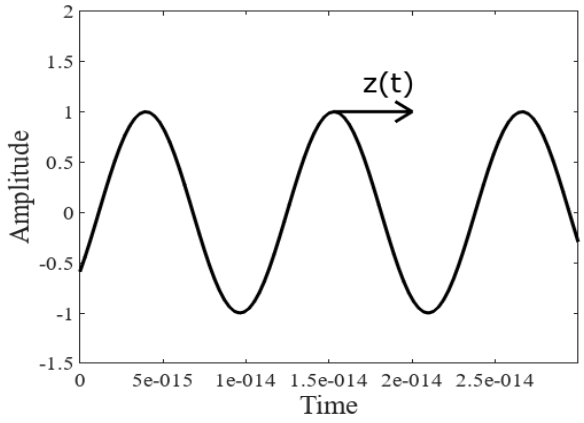

Fig. 3.4: Representation of Phase Velocity.

Now, selecting a point (at the amplitude crest) and analysing its movement, it is assumed that this point keeps a constant phase:

$$kz - \omega t = \text{const} \tag{3.3}$$

from where, the velocity of this point can be found:

$$k\frac{dz}{dt} - \omega = 0 \tag{3.4}$$

$$\text{or } v = \frac{dz}{dt} = \frac{\omega}{k} \tag{3.5}$$

Hence, the 'phase velocity' is defined as the velocity of the wave of the constant phase for a given mode and from Eq. (3.1) and (3.5):

$$v = \frac{c}{n} = \frac{\omega}{k} \tag{3.6}$$

3.3.2 Group Velocity

Group velocity is defined as the propagation speed of a pulse in a medium. If two plane waves are considered with varied parameters but equal amplitude propagating through the medium, the following expressions can be found [84]:

$$E_1(z, t) = E_0 \cos(k_1 z - \omega_1 t),$$

$$E_2(z, t) = E_0 \cos(k_2 z - \omega_2 t) \tag{3.7}$$

Considering the variations of frequencies and wavenumbers by $2\Delta\omega$ and $2\Delta k$, the following expressions can be found:

$$\omega_1 = \omega + \Delta\omega,\ \omega_2 = \omega - \Delta\omega \tag{3.8}$$

$$k_1 = k + \Delta k,\ k_2 = k - \Delta k \tag{3.9}$$

Now, performing the superposition of these waves results in:

$$E(z, t) = E_1(z, t) + E_2(z, t)$$

$$= E_0\{\cos[(k + \Delta k)z - (\omega + \Delta\omega)t] + \cos[(k - \Delta k)z - (\omega - \Delta\omega)t]\}$$

$$= 2E_0 \cos(kz - \omega t)\cos(\Delta kz - \Delta\omega t) \tag{3.10}$$

The Eq. (3.10) is a representation of a wave, the carrier frequency of which is ω and

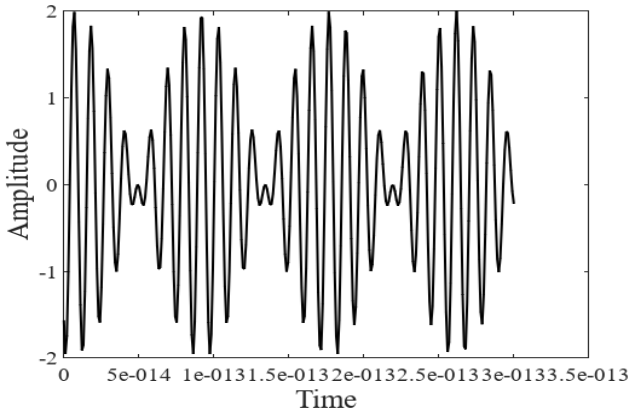

Fig. 3.5: Representation of Group Velocity.

it is modulated by a sinusoidal envelope at beat frequency $\Delta\omega$ (Fig. 3.5). The phase velocity of this carrier wave is, $v = \frac{\omega}{k}$ and the envelope moves at a velocity:

$$v_g = \frac{\Delta\omega}{\Delta\beta} \rightarrow \frac{d\omega}{dk} \tag{3.11}$$

In free space, $\omega = kc$ (known as dispersion relation), the group velocity is $v_g = \frac{d\omega}{dk} = c$. Important to note that, in case of a free space (vacuum), the phase (v) and group velocities (v_g) are identical. However, in a medium, the dispersion relation, i.e. $\omega = \omega(k)$ dependence is a complicated function. For the propagation of light in fibre optic medium, the group velocity in fibre takes the form as [77]:

$$v_g = \frac{d\omega}{d\beta} \tag{3.12}$$

where, β is the propagation constant.

3.3.3 Group Velocity Dispersion

From Fig. 3.2, the dependence of fibre refractive index on wavelength suggests that the shorter waves (blue) which are characterized by larger refractive index, move slower (supported by Eq. 3.6) than the longer waves (red). This is a simplified statement for the cases of ideally monochromatic planar waves. It is important to consider the phase $\Phi(\omega)$ of the wave propagating on the optical path L through a fibre characterized by refractive index $n(\omega)$ mainly to analyse the group velocity, the group velocity dispersion (GVD) and the dispersion coefficient D_{CD}.

Now, from further analysis as mentioned in [77], the electric field intensity in the frequency domain $\hat{E}\ (r, \omega - \omega_0)$ can be represented by the following expression:

$$\tilde{E}(r, \omega - \omega_0) = F\ (x, y)\ \tilde{A}\ (z, \omega - \omega_0)\ exp(i\beta z) \tag{3.13}$$

Here, $F\ (x, y)$ defines the field distribution in the plane, which is perpendicular to the z-axis, $\tilde{A}\ (z, \omega - \omega_0)$ defines the slowly varying electric field along the direction (z-axis) of optical signal propagation and β is the propagation constant, which corresponds to the wave vector for the planar wave in vacuum. β is one of the most important parameters for the wave propagation through an optical fibre and can be represented as:

$$v = \frac{c}{n} = \frac{\omega}{\beta} \tag{3.14}$$

The term $exp\ (i\beta z)$ as mentioned in Eq (3.13) defines the changes of phase $\Phi(\omega)$ and for the optical signal moving a distance L, using Eq. (3.14), the phase change can be expressed as:

$$\Phi(\omega) = \frac{\omega n(\omega)}{c} L \tag{3.15}$$

To know more about $\Phi(\omega)$, it can be expanded in Taylor series around the central frequency ω_0 as [77]:

$$\Phi(\omega) = \Phi_0 + \left(\frac{d\Phi}{d\omega}\right)(\omega - \omega_0) + \frac{1}{2}\left(\frac{d^2\Phi}{d\omega^2}\right)(\omega - \omega_0)^2 + \frac{1}{6}\left(\frac{d^3\Phi}{d\omega^3}\right)(\omega - \omega_0)^3 \tag{3.16}$$

The optical pulse $A(z,t)$ in time domain is related to the frequency domain spectrum $\tilde{A}_z(z, \omega - \omega_0)$ by the following expression (Inverse Fourier Transform):

$$\hat{E}(r, \omega - \omega_0) = \frac{1}{2\pi} \int_{-\infty}^{\infty} A(z, \omega - \omega_0) e^{i\Phi(\omega)} e^{-i\Phi(\omega - \omega_0)t} d\omega \tag{3.17}$$

Now, by substituting Eq. (3.16) into Eq. (3.17), as discussed in [77] that, the first term Φ_0 has no influence on the propagated pulse's temporal shape and has an influence only on the phase shift. The second term does not have any effect on the pulse's temporal shape; rather it generates the time delay of the propagated pulse through the medium. This can be obvious by comparing the first derivative of Eq. (3.15) with the group velocity, v_g as mentioned in Eq. (3.12):

$$\frac{d\Phi}{d\omega} = \frac{n}{c}\left(1 + \frac{\omega}{n}\frac{dn}{d\omega}\right) L = \frac{d\beta}{d\omega} L = \frac{L}{v_g} = t_g \tag{3.18}$$

Here, t_g is the time required by the spectral component moving at the group velocity v_g to cover the distance L. The third term $\left[\frac{1}{2}\left(\frac{d^2\Phi}{d\omega^2}\right)(\omega - \omega_0)^2\right]$ in Eq. (3.16), has an influence on the temporal shape of the optical pulse. Now, assuming $\delta = \frac{d^2\Phi}{d\omega^2} =$

constant and substituting this value to Eq. (3.17), the following expression can be obtained [77]:

$$E'(t) = \frac{E_0}{\sqrt{\tau^2 + i\,\delta}}\, e^{-t^2/2\tau'^2}\; e^{i\frac{\delta}{\tau^2}\frac{t^2}{2\tau'^2}} \tag{3.19}$$

Here, the modified pulse duration in time-domain is:

$$\tau_c = \tau_0 \sqrt{1 + \frac{\tau_c^4}{\tau_0^4}} \tag{3.20}$$

Where, $\tau_c = \sqrt{|\delta|} = \sqrt{\left(\frac{d^2\Phi}{d\omega^2}\right) L} = \sqrt{\beta_2 L}$ (3.21)

From the above analysis, it is understandable that the nonlinear term $\left[\frac{1}{2}\left(\frac{d^2\Phi}{d\omega^2}\right)(\omega - \omega_0)^2\right]$ results the temporal broadening and this broadening happens due to different group velocities for different wavelength components of an optical pulse which cover the optical path *L* in different times. This effect is known as GVD [77]. It is also summarized in [77] that, the GVD effect becomes important for pulses of picosecond time scale or shorter. The nonlinear effects of the refraction index begin to play an important role in fast optical transmission speeds > 100Gb/s. It was also mentioned that, fast transmission requires fast modulation and this fast modulation generates pulses in the form of quasi-monochromatic wave packet in a given spectral range. As because the refraction index $n(\omega)$ of every material depends on the radiation frequency, every frequency component in the pulse propagate with a bit different group velocity v_g. The wider spectral range, the larger would be the GVD.

3.4 Dispersion Management Techniques

In high bit rate digital communication, it requires short optical pulses as data carriers. However, effective management of optical pulse broadening of these shorter and shorter pulses and the subsequent inter-symbol-interference due to dispersion effects becomes increasingly challenging. The conventional way to reduce the chromatic dispersion is to apply optical fibres with high negative CD coefficient known as 'dispersion compensation fibre (DCF)' [85]. DCF becomes the part of the total fibre length, which is usually one sixth of the total length. DCF in fact compensates the delays of the individual light impulses at varied wavelengths. Normally the dispersion coefficient of DCF is equal to 'four to eight times' compared to that of SMF fibre. To get this higher dispersion level, the diameter of the DCF fibre core is reduced which produces the transmission loss and limits the optical power; that can be transmitted effectively through the optical fibre [86]. These DCF fibres have higher attenuation, which are about 0.5 dB/km (roughly 2~3 times that of SMF) and susceptible to nonlinear effects [87]. Another commonly used cost-effective method of dispersion compensation is the usage of fibre Bragg gratings (FBGs). However, the control of FBG chirp is the key to achieve very fine dispersion compensation [88]. In case of the chirped fibre Bragg grating (CFBG), a grating is written near to the fibre core where the index of refraction varies periodically along the grating length [89]. The spectral signal components, which propagate faster, are reflected later by the grating producing a longer delay; on the other hand, the spectral components propagating slower are reflected earlier. As an outcome, the optical pulses are compressed and dispersion compensated, which are reflected from the CFBG and using the optical circulator, these can be subtracted. One important

advantage of FBG based dispersion compensation modules (FBG-DCM) is lower insertion loss (IL). As for example, a FBG-DCM has IL in the range of 2 to 4 dB, while an equivalent DCF has IL of 10 dB or higher [86]. IL originates in DCF mainly due to the attenuation of the DCF fibre itself as the core diameter is reduced to get the desired dispersion compensation (DC) as mentioned earlier resulting in linear increase of IL with the span length. On the other hand, as the length of FBG is very short, it has only a fraction of the total loss. This is because the IL of FBG-DCM is governed mainly by the other design components such as circulators, tilt filters etc. Some other approaches are the usage of new modulation schemes, chirp pre-compensation methods, electronic dispersion compensation, digital filters [88, 90, 91] etc. The use of equalization circuits are commonly used to compensate dispersion by electronic dispersion compensation (EDC) [90].

3.4.1 Need for Tuneable Dispersion Compensation

Dispersion management using the conventional method (DCF) is not a very practical approach if a short length of SMF-28 has to be added requiring compensation by matching the length of the DCF fibres. The use of ultra-short optical carriers demands a high (sub-picosecond) dispersion compensation accuracy [92]. Here, the main disadvantage of DCF for fine CD tuning is the bulky nature of this approach. There is, therefore, a widely recognized need for tuneable dispersion compensation techniques. Tuneable dispersion compensators are required for the following reasons [89]:

(1) In case of the DWDM system, the channels at the extreme transmission bands are seen over or under compensated while a fixed CD compensation is used for the centre channel of the band.

(2) Due to the rerouting or for the optical add/drop multiplexing, in case of reconfigurable networks, the residual CD can always change.

(3) Very fine CD compensation is necessary for upgrading the 10 Gb/s link to 40 Gb/s as the tolerable threshold for dispersion becomes smaller.

Many types of tuneable dispersion compensators such as chirped fibre Bragg gratings (CFBG), adaptive tuneable dispersion control, dispersion equalization by monitoring extracted-clock power level, virtually imaged phase arrays (VIPA), microelectromechanical systems (MEMS), tuning (thermal) of free space or FBG coupled-cavities Gires-Tournois etalons (GTE's) and other methods were demonstrated [93, 94, 95, 96, 97, 98, 99]. In [93], the devices such as fibre Bragg gratings with on-fibre integrated heaters are used to get the tuneable chirp and dispersion compensation. The disadvantages of this technique are, they are suitable for per channel operation and require optical circulators to get back the reflected signals. In [95], variable dispersion compensation method utilizing the virtually imaged phase array (VIPA) was shown to mitigate the dispersion tolerances in 40 Gb/s DWDM system. Compared to FBG and PLC devices, the periodical characteristics of VIPA based compensators were found advantageous because a few modules were required to cover the whole C or L bands. In [6], the tuneable dispersion compensation was shown for a single and for a multichannel 40 Gb/s systems and the devices known as nonlinearly chirped fibre Gratings (NC-FBGs)

were used. The advantages of the technique are wide tuning ranges, negligible intra-channel third-order dispersion and obtaining both positive and negative dispersion values. In [7], a planer light-wave circuit (PLC) based dispersion equalizer formed of numbers of asymmetric Mach-Zehnder interferometers in cascade were used and the equalization was suitable for both the values of positive and negative dispersions by adjusting the phase-shift differences of the interferometric arms. In [94], an adaptive tuneable dispersion compensation technique was demonstrated where an error was calculated first from time-domain waveform of the output signal and the dispersion compensation was achieved by a tuneable dispersion compensator controlled by minimizing the errors through steepest-descent method. In [8], a virtually imaged phased-array (VIPA) and spatial light modulator (SLM) based tuneable dispersion compensator was demonstrated. This system provided an accurate CD compensation of -4080 to +850 ps/nm and was independent of the polarization state at the input for its operation.

3.4.2 System Performance

As studied in Chapter-2, to increase the bitrate for 2D-WH/TS OCDMA systems, the bit-width and consequently the related chip size must be shortened [11]. As a result, the performance of the system will be severely affected by dispersion effects [40] even though the data rate is only 2.5 Gb/s (400 ps bit-width), the chip size can be just a few picosecond which will be investigated further in this research. The main factor that limits the system performance is autocorrelation time skewing [40]. For the multi-wavelength ultra-short (picosecond) optical code carriers, such as incoherent OCDMA system, dispersion related broadening with time-skewing has

been studied in [11, 100, 101, 102, 103, 104]. In [11], it was mentioned as an example that for a 3-wavelength and 7-chiptime optimized code, a 10-Gchip/sec 2D-WH/TS OCDMA system is limited to just under 4 km due to time skew effect but could operate up to 80 km mainly due to pulse spreading. As shown in [100], it has been investigated that even a meagre 50 m SMF-28 fibre mismatch from the fully dispersion compensation state would lead to 1 dB power penalty. The performance degradation of 2D-WH/TS system due to GVD effects including pulse broadening, peak power reduction and time skewing is also studied in [105]. An impact of fibre CD on the BER performance of an optical CDMA IM/DD transmission system was analysed in [103]. The calculated results obtained in [12] also indicated that dispersion due to fibre temperature changes can affect the recovered OCDMA autocorrelation function and BER. As shown in [106], the OCDMA system transmission quality and the BER are affected by the pulse shape. As such, a skewed pulse profile of the recovered OCDMA auto-correlation will also impact the system BER and the overall system performance. In the research works mentioned in later Chapters (4-6), the consequence of fibre dispersion resulting in received optical pulse broadening and the subsequent mitigation technique to restore its widths will be discussed. However, the BER characterization of system performance used in the investigation of this thesis was not carried out because the related analysis has already been done in various studies as mentioned above. In this Chapter, as for example, the Section-3.5 describes the consequence of fibre dispersion for incoherent OCDMA. It is required to find a suitable method to perform the tuneable dispersion compensation for this type of multi-wavelength picosecond OCDMA system. This

will be investigated and exploited further in subsequent Chapters. Before that, some short pre-ambles on this methodology are explained in the next paragraphs:

3.4.3 Chirp and Its Relation to Fibre Dispersion

The effect of fibre dispersion was observed on an optical pulse propagating through a fibre medium. It is required to explore more about other influential effects such as chirp on the propagated optical pulse. Subsequently, the main goal would be to find a way to fine-tune the dispersion affected optical pulse broadening. A signal is chirped if its frequency increases or decreases with time. The presence of chirp in an optical pulse is distinguishable by the time dependence of the pulse's instantaneous frequency. For a chirped optical pulse, its carrier frequency changes with time and this 'frequency change' is related to the phase derivative. A parameter '*C*' governs the linear frequency chirp imposed on an optical pulse. The spectrum of an optical pulse is broadened considerably because of the frequency chirp imposed on it. The pulse broadening is undesirable as mentioned in the previous sections of this Chapter. The frequency chirp can limit the performance of a fibre optic communication system. This is because a directly modulated semiconductor laser always accompany phase modulation caused by the carrier-induced change in the refractive index of the waveguide [107]. In [108], for a high bit-rate transmission system, the fibre CD penalty was measured as a function of modulation chirp parameter using a Ti:$LiNbO_3$ based optical modulator. With proper optimization or adjustment of the frequency chirp the impairments due to dispersion were minimized for the given transmission links. It was also observed that, the positive value of chirp *C* led to additional dispersion penalty. On the contrary, with the controlled

implementations of negative chirp *C* could mitigate the pulse broadening resulting in reduced dispersion penalties [108]. Now the question is, “Is it possible to control the chirp parameter to overcome the dispersion related impairments in some other tuneable ways?” The next paragraph will focus on this issue.

3.4.4 SOA and Chirp Control

The SOA based chirp control was first demonstrated in [109] where the single wavelength system comprised with an electro-absorption (EA) modulator producing a positive chirp. An SOA was used to control the generated chirp by utilizing the phase modulation via the SOA [110]. An SOA is in fact a gain medium. The gain is a result of carrier injection into the active region of the SOA. The injected carriers occupy energy states in the conduction band of the active material and leave holes in the valence band. In this case, electrons and holes recombine radiatively or non-radiatively and release the recombination energy in the form of photons [111]. Now, the change in phase $\Delta\varphi$ at the SOA output depends on a number of factors such as: (1) confinement factor Γ, (2) the net power gain change Δg, (3) the device length L and *alpha-factor* α of SOA as expressed mathematically as follows: [111]:

$$\Delta\varphi(N) = \alpha\,\Gamma\,\Delta g\,L\,/2 \tag{3.22}$$

In case of bulk or QW structures, high confinement factor Γ and α values of 2-8 are observed. The *alpha-factor* relates the ‘change in refractive index’ with the ‘change in gain’ that happens while an optical signal is introduced into a medium or an electrical bias applied to a diode changes. Although the refractive index and the

material gain or absorption are related by the more complex Kramers-Kronig (KK) integral expression [112], the *alpha-factor* relates the two quantities with a simple constant. In an SOA, the expression for *alpha-factor* is defined as the ratio of change in refractive index and the change in gain with respect to a change in carrier density N [113].

$$\alpha = -\frac{4\pi}{\lambda}\frac{\partial n_{\mathrm{r}}/\partial N}{\partial g/\partial N} \approx -\frac{4\pi}{\lambda}\frac{\Delta n_{\mathrm{r}}}{\Delta g} \tag{3.23}$$

Here, Δn_{r} is the change of the real part of effective refractive index n, Δg is the change of modal gain g in the medium of SOA, and λ is the wavelength in vacuum. Further description for the origin of chirp in SOAs with a summary of a typical SOA including gain profiles with drive current, linear, non-linear operations can be found in [65]. SOA is also suitable for multi-wavelength communication systems. In the investigation for SOA based chirp control for multi-wavelength OCDMA system, the salient features of SOA, which will be used, are as follows [114]:

(1) Kamelian OPA-20-N-C, having wide optical bandwidth exhibiting a ~80 nm optical gain bandwidth at the 3dB drop from the peak.

(2) The SOA used can operate in single and multi-wavelength environments.

(3) In multi-wavelength scenarios, the level of chirp produced is proportional to the amount of gain compression the signals are subject to and all multi-wavelength ps 2D-WH/TS code carriers will be subject to chirp.

At this point, from section 3.4.2, it is known that the chirp is nothing but the change on phase of an optical pulse with time. It is also known that the Eq. (3.22) is

the expression for the phase changes $\Delta\varphi$. How this phase change or chirp via the usage of SOA can be exploited to overcome the dispersion in the multi-wavelength picosecond incoherent OCDMA system will be demonstrated in the rest of the Chapters of this thesis.

The impact of SOAs on fibre dispersion compensation was initially demonstrated with theoretical foundations in [115]. In [115], the phase compensation mechanism using optical amplifiers was studied to overcome the pulse broadening in optical transmission system. The chirping parameters for light sources and semiconductor laser amplifiers (SLA) were analysed which clearly showed their opposite phase characteristics that determine the chirping cancellation conditions. Similar solutions based on SOA associated with electro-absorption modulated laser (EML), have also been proposed in [109, 116].

First and foremost, the consequence of fibre dispersion on an incoherent OCDMA system will be analysed in the next Section and then in further up the Chapters, the chirp control methodology will be exploited in more detail both experimentally and analytically in an initiative to fine-tune the chromatic and temperature induced dispersion on this system.

3.5 Analysis of Dispersion Effects on 2D-WH/TS OCDMA Based on PS Multi-Wavelength Carriers

The chromatic dispersion (CD) in multi-wavelength picosecond OCDMA code carrier becomes very serious issue. The consequences are severe even for a few meters length of fibre mismatch from full CD compensation [11, 103, 117, 118].

It is known that, the index of refraction for the fibre optics core is a wavelength dependent quantity. As such, different wavelengths of light propagate at different speeds. Consequently, the propagating data pulse widens as the transmission distance increases, defined as CD. The mathematical expression for total CD is:

$$\sigma = D_{CD} \times \Delta\lambda \times L \tag{3.24}$$

Here, σ is the total broadening of an optical pulse, D_{CD} is the dispersion coefficient for the optical fibre in ps/nm•km, $\Delta\lambda$ is spectral linewidth in nm, and L is the total fibre length in km. The relative pulse broadening due to CD effect is therefore more significant when the optical pulses are shorter because they occupy more optical spectrum $\Delta\lambda$. After propagation through the fibre, pulse will spread into adjacent chips causing an inter symbol interference (ISI). The ISI effect becomes a serious issue with ultra-short data pulses [119]. Here the communication can completely stop for excessive dispersion of signals [78]. As for example, at 40 Gb/s, the signals are 16 times more sensitive to CD than that at 10 Gb/s [120]. In 2D-WH/TS OCDMA based on picosecond multi-wavelength carriers, different wavelengths will travel at different velocities through the fibre link and produce skewing effect. It is, therefore, necessary to fully understand the dispersion effects affecting 2D-WH/TS incoherent OCDMA system and find the control mechanism to overcome dispersion related impairments.

Before going for in-depth analysis for the 2D-WH/TS OCDMA based on multi-wavelength picosecond code carriers affected with slight fibre mismatch or CD effects, it is required to understand the dispersion effects of a single wavelength

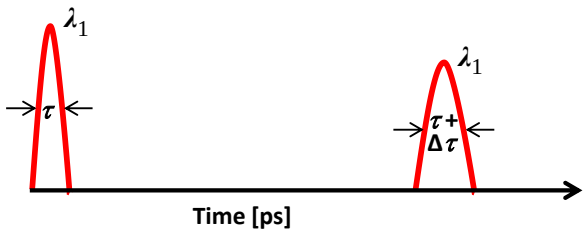

Fig. 3.6: Illustration of a single wavelength optical pulse broadened due to dispersion.

optical pulse moving a distance L of SMF-28 fibre. The graphical representation for this single wavelength optical pulse and the link residual dispersion effect on it is illustrated in Fig. 3.6. It has been observed that the initial optical pulse of FWHM width τ has been broadened by $\Delta\tau$ due to fibre dispersion effects after its propagation through a link length L. The theoretical bases are:

(1) To obtain a single wavelength Gaussian optical pulse, the expression is:

$$S\,(\mathrm{t}) = P_0 exp\{-2.77\left[\frac{t}{\tau}\right]^2\} \tag{3.25}$$

Where, $P_0 = 1$ is the single wavelength normalized peak power.

(2) To obtain the CD effects on a single wavelength Gaussian optical pulse due to fibre re-location by small amount of SMF-28 fibre, the expression is:

$$S\,(\mathrm{t}) = P_0 exp\{-2.77\left[\frac{t}{\tau+\Delta\tau}\right]^2\} \tag{3.26}$$

Where,

$$\Delta\tau = D_{\mathrm{CD}} \times \Delta\lambda \times \Delta L \tag{3.27}$$

$\Delta\tau$ is the FWHM width changes due to chromatic dispersion for SMF-28 fibre mismatch away from full CD compensation state. The spectral line-width for a single wavelength carrier is $\Delta\lambda$, the chromatic dispersion coefficient, D_{CD} = 17 ps/nm.km and ΔL is the fibre mismatch.

As for example, the Gaussian optical pulse can be represented as in Fig. 3.7a. Here, the overall fibre link's residual dispersion (CD) is zero for a particular length of fibre, which has been fully compensated by using equivalent amount of DCF. However, for only a few meters of mismatch say for 50m or 100m

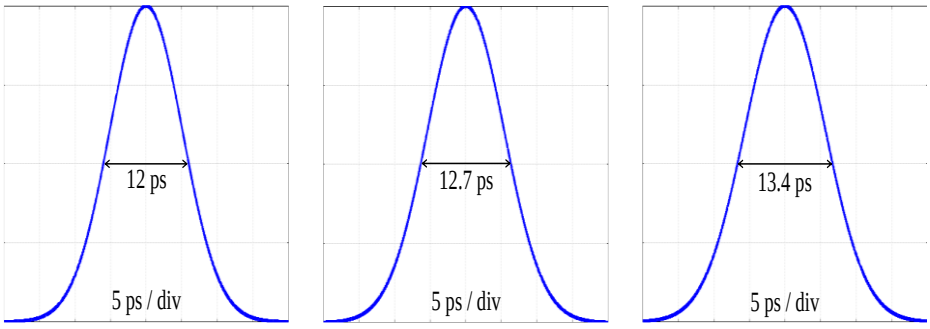

(a) (b) (c)

Fig. 3.7: Gaussian shape for a single wavelength optical pulse; (a) Single-wavelength Gaussian pulse with full CD compensation; (b) Single-wavelength Gaussian pulse with 50 m fibre mismatch away from full compensation; (c) Single-wavelength Gaussian pulse with 100 m fibre mismatch away from full compensation.

(SMF-28 fibre mismatch from the full-compensation point), the Gaussian optical pulse shape will be broadened by 0.7 ps and 1.4 ps respectively. That means, the new FWHM value of the received optical pulse for fibre re-location or mismatch by 50 m or 100 m from the chromatic dispersion compensation (CDC) point, would be 12.7 ps and 13.4 ps respectively and this is for single wavelength Gaussian optical pulse (Fig. 3.7b and 3.7c respectively).

(3) In 2D-WH/TS family of codes, the number of multi-wavelength picosecond pulses is arranged in both, wavelength and time domain to form a family of codes for use by a varied number of network users. At a receiver site, the incoming data are recovered for each user by a decoding process, which produces a so-called OCDMA autocorrelation function. During data transmission, it is very important to preserve its undistorted shape in order to maintain the highest performance of OCDMA systems [121]. To obtain the multi-wavelength picosecond OCDMA autocorrelation function and the distortion due to fibre re-location, the following expression is used:

$$S\,(\mathrm{t}) = \sum_{k=0}^{w-1} P_0 exp\{-2.77\left[\frac{t-k\Delta t}{\tau+\Delta\tau}\right]^2\} \tag{3.29}$$

Where, the expression for $\Delta\tau$ is as same as that in Eq. (3.27) and the temporal skew Δt due to fibre re-location is given by:

$$\Delta t = D_{\mathrm{CD}} \times \Delta\Lambda \times \Delta L \tag{3.30}$$

$\Delta\Lambda$ is the spectral spacing of OCDMA code carriers. As mentioned before, ΔL is the fibre mismatch by small amounts of SMF-28 fibres. As in the experiment, the 2D-WH/TS OCDMA code consists of four wavelength code carriers (λ_1 = 1551.72 nm, λ_2 = 1550.92 nm, λ_3 = 1552.52 nm, and λ_4 = 1550.12 nm). The spectral linewidth for each wavelength carrier is $\Delta\lambda$ = 0.8 nm and the code carriers' spectral separation is also $\Delta\Lambda$ = 0.8 nm. The recovered OCDMA autocorrelation function at the decoder receiver after propagation of code carriers for a particular fibre length with full CD compensation will be calculated as shown in Fig. 3.8. For the OCDMA autocorrelation envelope for four wavelength code carriers, the FWHM value τ =

12 ps may be represented as in Fig. 3.8 (blue shape). Here, the overall fibre dispersion (CD) is zero as the fibre link has been fully compensated by using equivalent amount of DCF. However, for only a few meters of mismatch (say for 50m or 100m SMF-28 fibre mismatch from the full-compensation point), the OCDMA autocorrelation function will be broadened by 0.8 ps and 1.8ps respectively. That means, the new FWHM value of OCDMA autocorrelation function for fibre re-location or mismatch by 50 m or 100 m, would be 12.8 ps (red envelope as in Fig. 3.8) and 13.8 ps (magenta envelope as in Fig. 3.8) respectively. It is seen that the CD effect on OCDMA autocorrelation for relocation of fibre link by

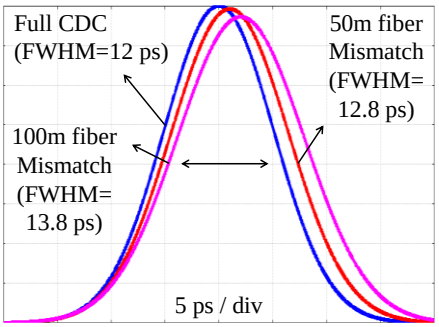

Fig. 3.8: OCDMA autocorrelation at room temperature (blue shape for full CD compensation, red shape for 50 m fibre mismatch away from full compensation, magenta shape for 100 m fibre mismatch away from full compensation).

small amount of SMF-28 is more severe compared to the single wavelength optical pulse (compare Fig. 3.7 and Fig. 3.8) propagation through a particular fibre link.

3.6 Discussion

In this Chapter, the basic concept of fibre dispersion related to a fibre optic communication system have been discussed. The common causes and effects of fibre dispersion for a single mode fibre (SMF-28) link was enumerated clearly. The

different types of CD as transmission impairments were stated. The important parameter such as GVD was analytically deducted and how the optical pulse is broadened for a Gaussian optical pulse propagated through a transparent medium was stated. The importance of conventional dispersion compensation techniques was also described. The urgent need for the 'management of tuneable dispersion compensation' for ultra-short pulse communication system was established in the study. In the later part of this Chapter, the basic relation of chirp with dispersion was explained and the SOA based chirp control technique was depicted clearly. Then the analysis of dispersion effects on multi-wavelength picosecond 2D-WH/TS OCDMA autocorrelation function was mentioned. The following Chapters will deal with the tuneable ways to mitigate the dispersion related broadening on 2D-WH/TS OCDMA autocorrelation based on picosecond multi-wavelength carriers.

Chapter 4

Investigation of SOA Use as Tuneable Dispersion Compensator

4.1 Introduction

CD management is important for high data rate incoherent fibre-optic communication [122] but is essential for incoherent OCDMA transmission based on schemes using multi-wavelength picosecond code carriers [102, 123]. As these code carrier pulses are short, transmitted codes will be strongly affected by CD, even if the transmission distance changes by a few meters. One example is the addition of an optical fibre in order to relocate the OCDMA transmitter or receiver [123]. If CD is not properly implemented, the recovered OCDMA autocorrelation by an OCDMA decoder will show temporal skewing among individual wavelength code carriers, thereby severely influencing OCDMA system performance [102]. The impact of CD on 2-D WH/TS codes was analysed in [118] and also investigated in the previous Chapter. It has been shown that the CD related pulse distortion and related time skewing will cause undesirable broadening of recovered OCDMA autocorrelation. The autocorrelation surrounding cross-correlation will also be impacted by CD, leading to a reduced auto-to-cross-correlation ratio. This in turn will increase the multi-access interference noise and cross talk leading to performance degradation and a drastic reduction in the number of simultaneous users [118]. To mitigate fully

the CD impact on the OCDMA system would therefore require addressing both auto- and cross-correlation compensations.

In this Chapter, the use of an SOA for chromatic dispersion compensation (CDC) of a data transmission that uses a *single wavelength* as the data carrier [124] and then on a multi-wavelength PS OCDMA system was investigated. The advantage of using an SOA is that it offers a convenient tuneable approach to CD compensation [124, 125, 126, 127]. The concept behind using an SOA for distorted OCDMA autocorrelation width adjustment is based on exploiting refractive index and gain changes in a biased SOA [110, 124, 128]. Such changes can be introduced in a variety of ways:

- varying the SOA bias current,
- through an SOA gain depletion,
- injecting an optical continuous wave (cw) called a continuous-wave holding beam (CW/HB) together with a data signal at the SOA input, or
- using an optical pulse stream called an optical pulse holding beam (for short OP/HB).

The above will result in the SOA's refractive index changes [128]. Now, the interaction between the chirp triggered by these SOA changes and the incoming data pulses affected by CD can be exploited for managing CD effects [109].

The common picture of the experimental setup in a lab is shown in Fig. 4.1.

Fig. 4.1: Picture of the setup in a lab.

4.2 The Investigation of SOA for Dispersion Compensation in Single Wavelength System

4.2.1 SOA Control by Bias Current

The experimental setup used for the investigation is shown in Figure 4.2. Here, the ps ML Laser produces a 1.8 ps single wavelength (1545 nm) optical clock at OC-48 rate (bit-width equal to ~400ps), which is then passed through an optical supercontinuum generator (OSG) by PriTel, Inc. (Naperville, IL, USA). The OSG consists of a high-power erbium doped fibre amplifier and dispersion decreasing fibre (DDF). The optical clock from the ps ML Laser that was cantered at 1545 nm after the amplification by an 18 dBm erbium doped fibre amplifier (EDFA) is injected into approximately a 1 km long DDF. This way, a 3.2 nm wide optical supercontinuum is generated in a spectral region of 1550–1553.2 nm. The supercontinuum is then spectrally sliced by an OCDMA encoder (OKI Industries, Irving, TX, USA), which is based on four FBGs (central frequencies are: λ_1 = 1551.72 nm, λ_2 = 1550.92 nm, λ_3 = 1552.52 nm, λ_4 = 1550.12 nm) matching the 100

GHz ITU grid. An add/drop AWG module is used after the encoder to select a single wavelength λ_2 which is then transmitted down the optical fibre. Optical Spectrum Analyser (OSA) Agilent 86146B and Sampling Oscilloscope (OSC) Agilent Infiniium DCA-J 86100C with 64 GHz optical sampling head are used to monitor the optical data at various system test points A-F.

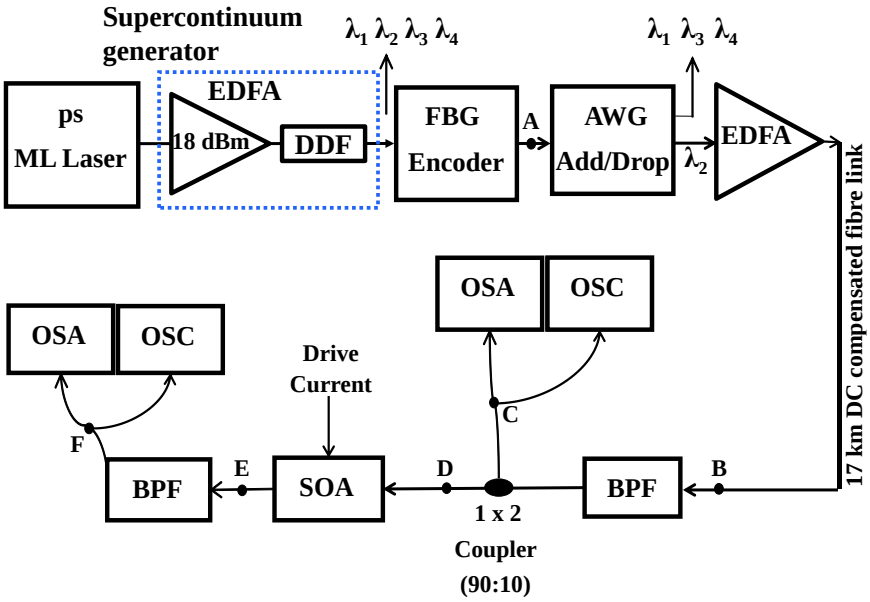

Fig. 4.2: Experimental setup for a chromatic dispersion compensation in optical fibre by use of SOA.

Before proceeding further, the accuracy of pulse-width measurements by the OSC was first validated by an optical autocorrelator (Femtochrome Research Inc FR-103XL) as indicated in Fig. 4.3. Typically, autocorrelators are used to measure ultrashort pulses in the time domain [129, 130]. The basic principle using an autocorrelator is that, the pulse is used to measure itself and its operation is similar to an interferometer. The incoming optical pulse generated by an optical source is split into two beams of equal intensity. An adjustable optical delay is inserted into one of the arms. These two optical pulses are then recombined within a nonlinear material

such as a second harmonic generation (SHG) crystal. The emitted SHG signal is then photo-detected and observed by the "slow" oscilloscope [40].

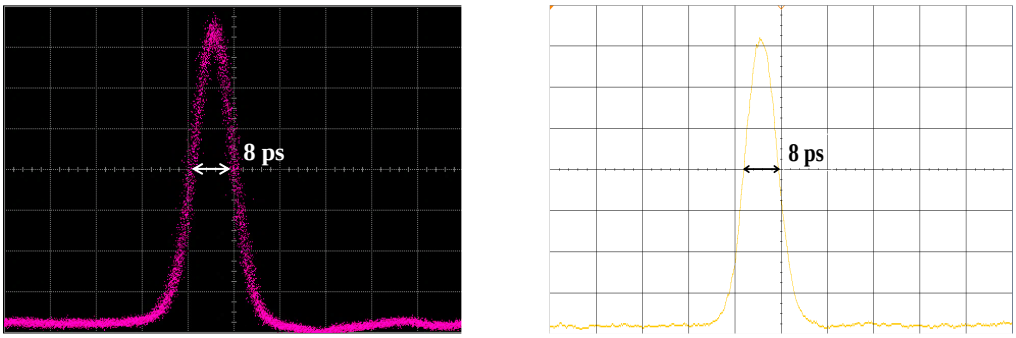

(a) (b)

Fig. 4.3: (a) 8 ps pulse using Agilent Infiniium DCA-J 86100C; (b) validated 8 ps pulse at the output of Femtochrome Research Inc FR-103XL.

Now, coming back to the experiment, as seen from Fig. 4.2, the compensated optical data pulses having FWHM = 23 ps first pass through a band-pass filter (BPF) and then enter an SOA for a final fine dispersion tuning. By varying the SOA drive current, the chromatic dispersion compensation i.e., optical pulse compression or expansion was controlled. At the input of SOA (point D), the measured pulse-width of the data pulse was 23 ps (Fig. 4.4). By adjusting the SOA drive current, it was

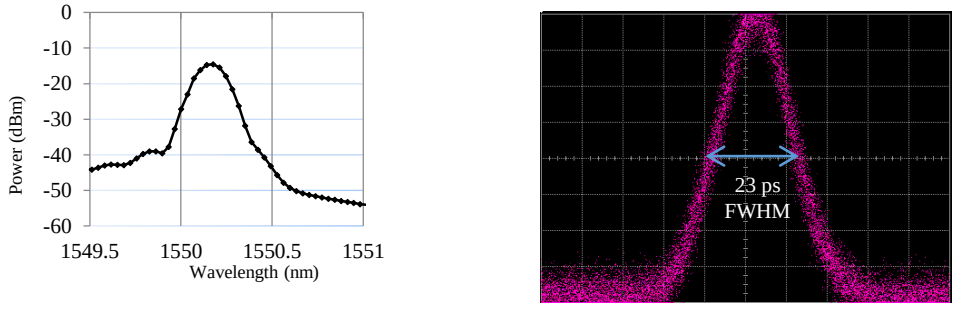

(a) (b)

Fig. 4.4: (a) Frequency Domain representation of returned data at the SOA input; (b) Time Domain representation of returned data at the SOA input.

found that the pulse-width could be compressed to 20 ps for the SOA drive current of 29 mA (Fig. 4.5). After changing the SOA drive current to 70 mA (Fig. 4.6), the pulse-width of the data signal has reached again to 23 ps (the same value of input data). But at this condition, the input signal has been amplified to -10 dBm peak

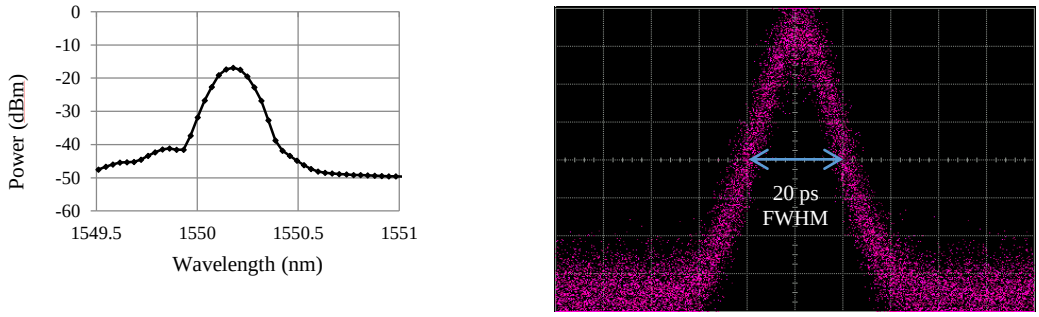

`(a) (b)

Fig. 4.5: (a) Frequency Domain representation of the compressed data pulse at the output for 29 mA SOA drive current; (b) Time Domain representation of the compressed data at the output for 29 mA SOA drive current.

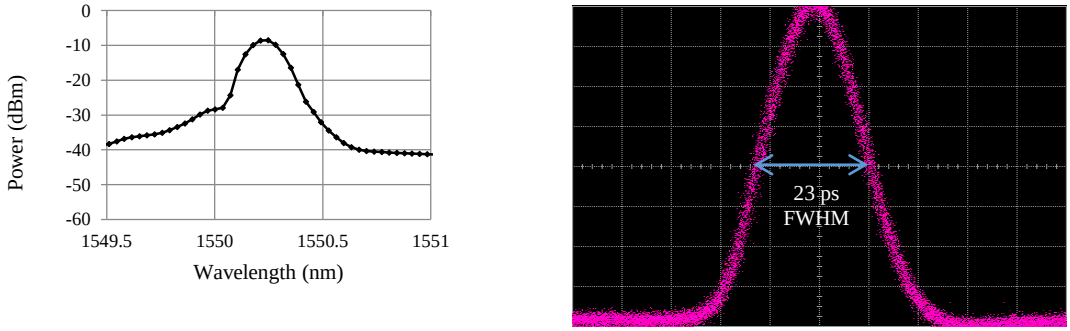

(a) (b)

Fig. 4.6: (a) Frequency Domain representation of the data pulse at the output for 70 mA SOA drive current; (b) Time Domain representation of the data at the output for 70 mA SOA drive current.

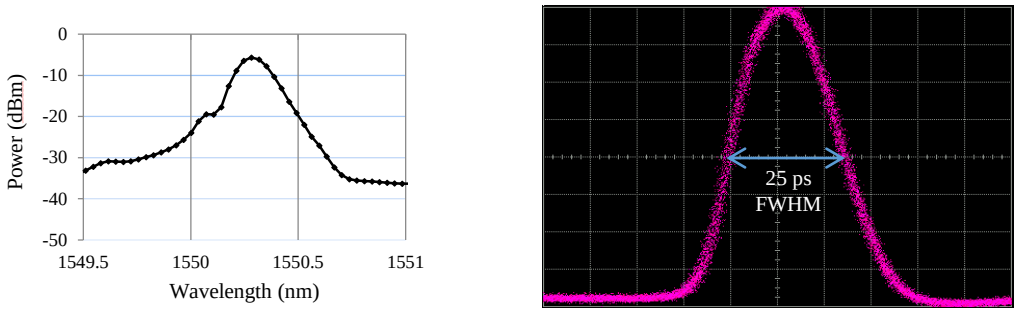

(a) (b)

Fig. 4.7: (a) Frequency Domain representation of the broadened data pulse at the output for 150 mA SOA drive current; (b) Time Domain Representation of the broadened data pulse at the output for 150 mA SOA drive current.

level. This is an added advantage of this technique since it can also alter the received signal power level to compensate for the insertion loss in optical network [109].

At the SOA drive current of 70 mA there was no compression or expansion, but just a gain change of the passing signal. After further increase in SOA drive current to 150 mA, the pulse-width expanded to 25 ps (Fig. 4.7). It is important to note that, both pulse compression and expansion are possible by varying the SOA drive current. This is an important feature for fine-tuning of optical fibre dispersion and achieving compensation or expansion of optical pulses traveling in optical networks. This will enable us to fine-tune chromatically dispersion compensated fibre optic networks for sudden small changes of dispersion. This simple approach demonstrates that by controlling the SOA drive current, a pulse compression or expansion can be achieved. This gives a great operational flexibility to network operators for managing high-speed optical communication systems to mitigate detrimental effects of dispersion.

In this experiment, the SOA drive current of 70 mA may be considered as the "neutral" setting point where there is neither compensation nor expansion of optical signal data pulses. By increasing or decreasing the drive current around this value, the signal pulse-width can be expanded or compressed. In such a way, the practical requirement of CD fine tuning needs in high speed communication networks can be fulfilled.

4.2.2 SOA Control by OP/HB

The setup for the chirp control in SOA by varying the locally generated optical clock power is shown in Fig. 4.8. The experimental setup was described in the last section. The amplified signal from EDFA is passed through an SOA with an intention to control and fine tune the residual dispersion of the coarsely CD compensated 17 km long fibre optic transmission link. At the same time, an optical clock signal locally generated by the picosecond mode locked laser was introduced at the SOA input using a 2×1 coupler.

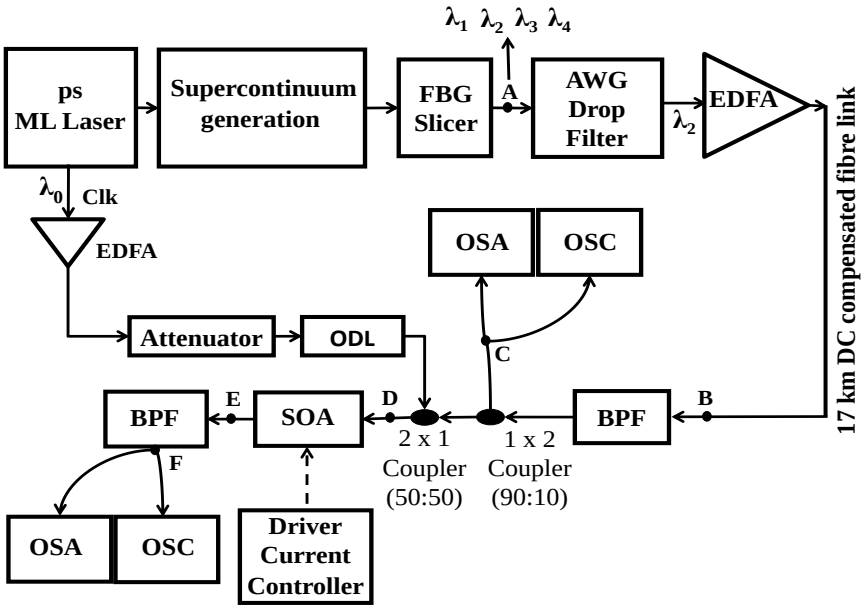

Fig. 4.8: Experimental setup for automatic dispersion compensation using clock power where ps is picosecond, ML Laser-Mode Locked Laser, OSA-Optical Spectrum Analyser, OSC-Sampling Oscilloscope, BPF-Band Pass Filter, FBG-Fibre Bragg Gratings, AWG-Array Waveguide Grating, EDFA-Erbium Doped Fibre Amplifier, ODL-Optical Delay Line, SOA-Semiconductor Optical Amplifier).

An optical attenuator was used to set different clock power levels during the experiment. Optical Spectrum Analyser (OSA) Agilent 86146B and Sampling Oscilloscope (OSC) Agilent Infiniium DCA-J 86100C with 64 GHz optical sampling head were used to monitor the optical data at various system test points A-F. During the experiment, the optical clock power was varied from 0 to 12.5 mW. The full width at half maximum (FWHM) of the incoming data pulses at the input of SOA (point D) was measured as 23 ps [125]. Here, an optical delay line (ODL) is used to synchronize the data signal with the clock to affect the gain in active region of SOA. As a result, the desired compression of the data signal pulses is achieved. The different pulse-width ratios between output and input optical data pulses vs clock power for varied SOA drive currents are shown in Fig. 4.9.

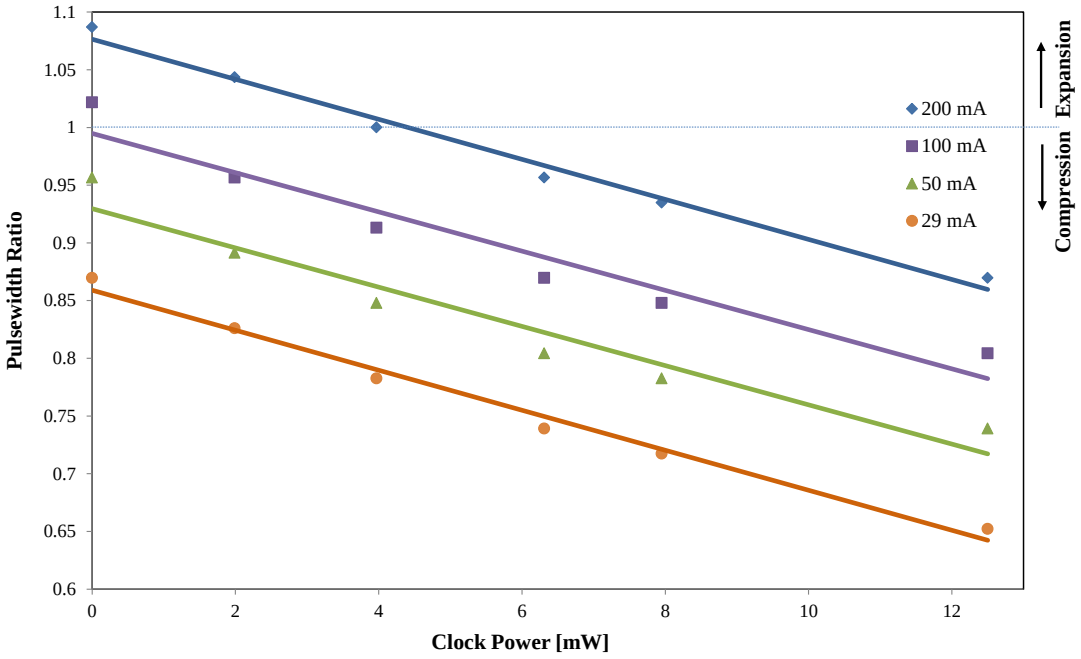

Fig. 4.9: Data output /input pulse width ratio vs clock power for different SOA drive currents.

From the experiment, it is seen that below the SOA drive current of 100 mA and for different clock power settings, only the pulse compression happens. But at above the SOA drive current of 100 mA such as 200 mA, both pulse compression and expansion can be achieved for different settings of optical clock powers. Mentionable here that SOA gain becomes saturated at a drive current of ~150 mA [125]. This means that the pulse compression occurs bellow the SOA saturation point. Above the SOA saturation conditions, only expansion of data pulses occurs. It is found that input data pulse-width of 23 ps FWHM can be compressed up to 15 ps FWHM at SOA drive current of 29 mA with clock power setting of 12.5 mW. The maximum pulse expansion observed was 25 ps FWHM at SOA drive current of 200 mA with the optical clock disabled condition. The holding beam (HB) effect on SOA is further analysed in [131]. This technique is used as a versatile approach to improve saturation characteristic, to reduce pattern fluctuation, and to shorten carrier recovery

time in SOA. It is also applicable for any types of SOA for ultrahigh bit-rates and the gain is easily tuneable by varying the HB power or changing the applied current into the SOA.

Managing CD in fibre optic networks is a necessity because a fine readjustment of dispersion compensated fibre links for ultra-high speed incoherent communication is always required. This is becoming even more desirable as the serial signal data are approaching Tbit/s rates. This can be accomplished by using SOA via its chirp control by varying the locally generated optical clock power and SOA's pump current in the harmony with the incoming data when passing through this SOA. By choosing the clock power levels between 0 to 12.5 mW for a different SOA gain levels, the inbound data pulse-width can be efficiently manipulated. It has been demonstrated that the pulse compression can be achieved for the SOA pump currents up to 100 mA with a varied optical clock powers. On the other hand, if SOA pump current is set above 100 mA, a data pulse expansion (broadening) is observed. Using this technique, both pulse compression and expansion are possible.

4.3 The Use of SOA in Multi-Wavelength OCDMA

In this section, an experimental investigation was shown using SOA to mitigate the effect of CD on 2D-WH/TS OCDMA autocorrelation width based on *multi-wavelength* picosecond carriers. The approach was applied to the recovered OCDMA autocorrelation of an incoherent OCDMA system based on two dimensional wavelength-hopping time spreading codes, with 8 ps multi-wavelength pulses as code carriers.

A 17 km long OCDMA testbed, as shown in Fig. 4.10 was used to study the effectiveness of an SOA for simultaneous multi-wavelength CD compensation. This was for the transmission of an incoherent OCDMA system based on short multi-wavelength code carriers (four wavelengths, each pulse featuring 8 ps FWHM). The data traffic was generated by User-1 OCDMA encoder. After propagation in the testbed, it was presented to a User-1 OCDMA decoder, which was matched to the USER-1 encoder, producing a code weight four OCDMA autocorrelation peak. The

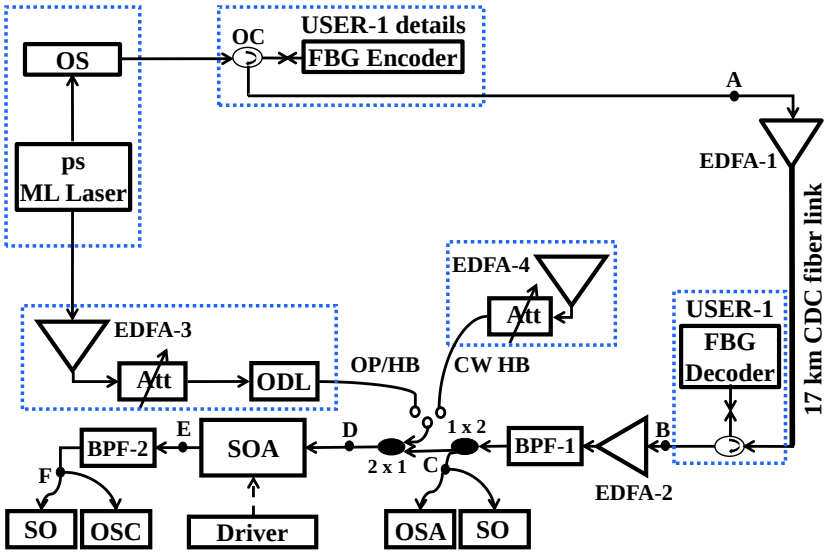

Fig. 4.10: OCDMA testbed to evaluate SOA CDC capabilities. OS, optical supercontinuum; OC, optical circulator; EDFA, erbium-doped fibre amplifier; BPF, tuneable band pass filter; SOA, semiconductor optical amplifier; OSA, optical spectrum analyser; SO, sampling oscilloscope; ODL, optical delay line; Att, optical attenuator; ps ML Laser, picosecond erbium-doped fibre mode-locked laser; CW HB, continuous-wave holding beam; OP/BH, optical pulse holding beam.

OCDMA used 2D-(4,47) WH/TS prime codes [35]. WH/TS prime codes are a class of two-dimensional (2D: wavelength–time) incoherent (direct detection), asynchronous codes that support wavelength hopping within time-spreading codes over a Galois field of prime numbers with zero autocorrelation side lobes (for ease of

self-synchronization) and periodic cross-correlation functions of at most one (for minimal multiple-access interference) [35].

Each code consisted of four wavelength carriers with a 100 GHz (i.e., a 0.8 nm) separation: λ_1 = 1551.72 nm, λ_2 = 1550.92 nm, λ_3=1552.52nm, and λ_4 = 1550.12 nm. These were positioned into 47 time chips (each of 8 ps duration) to create 2D-(4,47) WH/TS USER-1 code. Wavelength carriers were generated by spectral slicing of a 3.2 nm wide optical supercontinuum (OS). The OS resulted from a compression of a 1.8 ps FWHM laser pulse generated by an erbium-doped fibre mode-locked laser (PriTel Inc.) running at 2.5 Gb/s. The OS was supplied into a User-1 OCDMA code generator based on FBG encoder (OKI Industries, Japan), producing a unique 2D-(4,47) WH/TS OCDMA code. User-1 code uses all four wavelengths by positioning them accordingly into chips. The chips occupied by the User-1 code is (1-λ_2, 21-λ_4, 24-λ_1, 39-λ_3). This output from the User-1 was then re-amplified by an 18 dBm EDFA-1 and launched into a 17 km long bidirectional fibre link connecting the University of Strathclyde and the University of Glasgow. The link was then compensated for CD by using a commercially available dispersion-compensating fibre module (DCM). The matching DCM was selected based on the testbed link length determined from OTDR measurements. Both BPF-1 and BPF-2 are 3.2 nm wide tuneable band-pass filters with the central wavelength set to 1551.32 nm to ensure all four 2D-WH/TS OCDMA code wavelength carriers are passed and block amplified spontaneous emission (ASE) from EDFA-2 and the SOA, respectively.

4.3.1 Management of Multi-Wavelength Dispersion Compensation

First, the operation of SOA-based compensation will be discussed. The SOA used was Kamelian OPA-20-N-C with a gain recovery time of τ_G = 75 ps. At 2.5 Gb⁄s data rate, the User-1 autocorrelation peaks are separated by $\tau_{ACsepar}$ = 400 ps. The decoding of User-1's own 2D-WH/TS code produces a User-1 autocorrelation with the code weight w (no autocorrelation side lobes) and the cross-correlation bound to one (if also simultaneous users are transmitting) [35]. If User-2 to User-4 were also transmitting (i.e., the number of simultaneous users was N = 4), due to the User-1 decoding process, the cross-correlation surrounding the decoded User-1 autocorrelation peak would be represented by 12 [$w \times (N - 1)$] code carrier pulses separated from each other by $\tau_{CCsepar} \sim T / 12$ = 33 ps (assuming an even cross-correlation spreading). Note that $\tau_{CCsepar}$ is much smaller than the SOA recovery time (τ_G = 75 ps). Now, when the autocorrelation peak surrounded by the cross-correlation enters the SOA compensator, only the highest intensity autocorrelation peak can significantly influence the SOA gain dynamics via full or partial depletion of its gain. Because the autocorrelation peak separation $\tau_{ACsepar}$ = 400 ps is greater than τ_G = 75 ps, there is enough time for the SOA to fully recover its gain before the next one arrives, and the compensation can take place each time the autocorrelation passes the fully recovered SOA.

As indicated earlier, the separation between adjacent cross-correlation pulses $\tau_{CCsepar} \sim$ 33 ps is much less than the SOA gain recovery τ_G = 75 ps. Therefore, to simultaneously compensate both, the auto- and cross-correlation, an SOA with a

recovery time shorter than $\tau_{CCsepar}$ is needed. Ideally, an SOA with $\tau_G < \tau_{chip}$, where τ_{chip} is the chip width, would be desired.

Before starting the experimental investigation, to mimic the receiver relocation, first the "residual level" of CD into the fibre-optic testbed was introduced by adding a few meters of SMF-28 optical fibre. Since no commercial equipment was available, the "residual" level of CD was determined as follows:

First, the FWHM value Δ_{BB} of the OCDMA autocorrelation peak produced by the OCDMA USER-1 FBG decoder was determined from back-to-back

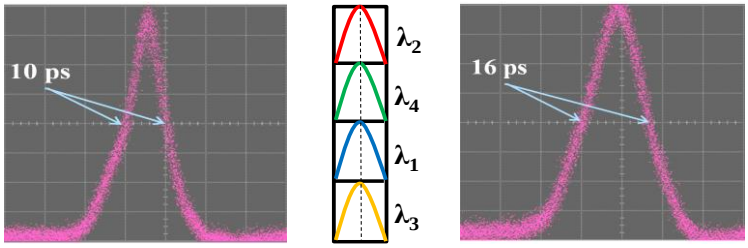

(a) (b) (c)

Fig. 4.11: (a) OCDMA autocorrelation as seen at the OCDMA User-1 decoder output for back-to-back measurements. FWHM value is ΔBB = 10 ps. (b) Illustration of the OCDMA autocorrelation. (c) OCDMA autocorrelation after 17 km of propagation in a partially CD-compensated fibre link. The FWHM value is Δ = 16 ps. [Data were recorded by a sampling oscilloscope, Agilent Infiniium DCA-J 86100C, with a 64 GHz optical sampling head].

measurements (the case when CD does not affect OCDMA autocorrelation). The results are shown in Fig. 4.11(a). Figure 4.11(b) illustrates that the OCDMA auto-correlation consists of all four wavelength pulses aligned by the FBG decoder to 'sit' on top of each other. It is noted here that the polarization is not considered in any

detail with the research. It is an important parameter, which influences system performance owing to the polarization sensitivity of the SOA [132].

Second, the FWHM value of the autocorrelation was measured after a 17 km long OCDMA data transmission to point C (see Fig. 4.10) with the CD compensation implemented. Prior to taking this measurement, the signal was amplified by EDFA-2 and the recovered USER-1 OCDMA autocorrelation (spectral width 4 × 100 GHz) was then passed through a 3.2 nm band pass filter (BPF-1) with its centre wavelength set to 1551.32 nm. The results obtained are shown in Fig. 4.11(c). All FWHM measurements were carried out using an Agilent Infiniium DCA-J 86100C equipped with a 64 GHz optical sampling head. By comparing the results shown in Fig. 4.11(a) and 4.11(c), it was found a 6 ps under-compensation of the transmission link. This value was then compared with results published in [123]. It was concluded that the 6 ps broadening of the USER-1 OCDMA autocorrelation observed is due to the CD compensation mismatch, which is equivalent in length to 66 m of SMF-28 fibre. To make the testbed "fully" CD compensated, this length would need to be deducted from the existing testbed length. Therefore, to account for this, it was decided to determine if an SOA could be utilised for such compensation instead. This investigation was then performed for incoherent OCDMA transmission based on 2D-WH/TS codes with 8 ps multi-wavelength pulses as the code carriers.

4.3.2 Dispersion Compensation by Changing the SOA Bias Current (SOA Gain) and by Varying the Optical Power of the CW/HB

In this investigation, the OCDMA autocorrelation produced by the USER-1 decoder after a 17 km propagation in the partially CD-compensated fibre link was

first amplified by EDFA-2. The OCDMA autocorrelation was then passed through a band pass filter (BPF-1). It was then injected into an SOA (Kamelian OPA-20-N-C with a gain recovery time τ_G = 75 ps), which was kept at a constant temperature of 20°C by a current-temperature controller. BPF-1 was used to reject the out-of-band ASE noise [133] produced by EDFA-2.

It was determined that an SOA bias current of I = 30 mA corresponds to an SOA gain G = 1 (0 dB), while I = 125 mA led to SOA gain saturation [124]. Figure 4.12(a) shows a parameter R as a function of the SOA bias current I, where $R = \Delta_I / \Delta_{BB}$. Here Δ_{BB} = 10 ps is the measured FWHM value of the *back-to-back* OCDMA autocorrelation produced by the USER-1 OCDMA decoder [see Fig. 4.11(a)] and Δ_I is its value measured at point E after 17 km long transmission in the testbed with a 6 ps CD mismatch and the SOA bias current set to value I.

The meaning of parameter R is analysed as:

- When $\Delta_I = \Delta_{BB}$, the parameter R = 1, which means that the OCDMA autocorrelation width after passing the biased SOA has the same value as for the *back-to-back* measurements. This indicates that the effect of transmission link CD on the OCDMA autocorrelation has been compensated for by the SOA.

- When $R < 1$, $\Delta_I < \Delta_{BB}$ at the SOA output and the compression will be observed as shown in Fig. 4.13.

- When $R > 1$, $\Delta_I > \Delta_{BB}$ at the SOA output indicates autocorrelation broadening by the SOA, as shown in Fig. 4.12.

In Fig. 4.12(a), it is seen that $R \in (1.8 - 2.15)$. The value $R = 1.8$ corresponds to $I = 30$ mA and $\Delta_{I=30} = 18$ ps, while $R = 2.15$ corresponding to $I = 100$ mA (SOA's saturation point) leads to $\Delta_{I=100} = 21.5$ ps.

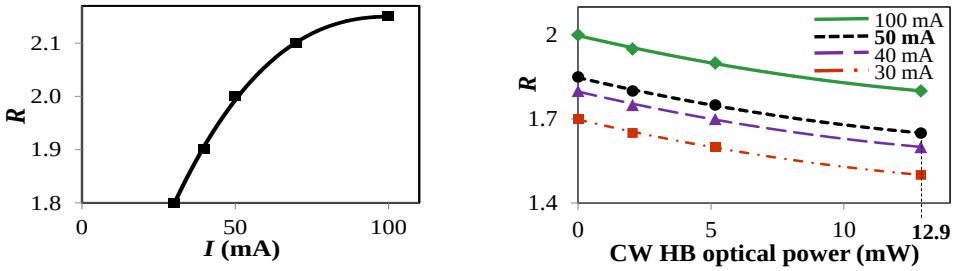

(a) (b)

Fig. 4.12: (a) Coefficient *R* versus SOA bias current *I* – no ASE from EDFA-2. (b) Coefficient *R* versus CW/HB optical power for the case of four different SOA bias currents *I* when ASE from EDFA-2 was not present. (Point *I* = 50 mA and CW/HB optical power of 12.9 mW is indicated for cross referencing).

The experimental results are in line with the theory presented in [134], where the pulse spectrum changes due to self-phase modulation (SPM) via nonlinear refractive index changes introduced by the SOA bias current variations, i.e., SOA gain and in turn the SPM-induced chirp affects the SOA traversing USER-1 OCDMA autocorrelation. Results shown in Fig. 4.12(a) clearly show the autocorrelation FWHM broadening with an increasing SOA drive current, i.e., gain.

Next, a CW/HB generated by an 18 dBm EDFA (EDFA-4 in Fig. 4.10) was introduced to investigate how the coefficient *R* changes with different values of SOA bias current *I* in the presence of different optical power levels of the CW/HB. The results are shown in Fig. 4.12(b). Greater compression, smaller *R* values, $R \in (1.5 - 2.0)$, are observed with the presence of increasing CW/HB optical power than without CW/HB, $R \in (1.8 - 2.15)$.

4.3.3 Dispersion Compensation by Varying the Optical Power of OP/HB at SOA Input

To exploit the gain dynamics of the SOA, it has been investigated how the presence of a short optical pulse as the holding beam (OP/HB*)* affects the SOA's ability to modify CD. Based on availability, for OP/HB, optical pulses ($\lambda_{OP/HB}$ = 1545 nm, 2 ps FWHM) generated by the ML laser was used (see Fig. 4.10). Both BPF-1 and BPF-2 are 3.2 nm wide tuneable band-pass filters with the central wavelength set to 1551.32 nm to ensure that all four 2D-WH/TS code wavelength carriers are passed, but ASE from EDFA-2 and $\lambda_{OP/HB}$ on the SOA output are blocked. OP/HB was injected into the SOA in line with the USER-1 OCDMA autocorrelation via an optical delay line (ODL) set to produce a 0 ps relative delay between them. The varying OP/HB optical power via an optical attenuator, Att (Agilent 8156A, Fig. 4.10), changes the value of *R*. The results are shown in Fig. 4.13. The full CD compensation by the SOA (R = 1) was observed for one of the following settings:

- OP/HB optical power 1.3 mW and I = 30 mA;
- OP/HB optical power 5.16 mW and I = 40 mA;
- OP/HB optical power 8.19 mW and I = 50 mA.

A maximum achieved compression by the SOA (R_{min} = 0.8) resulted in FWHM Δ_I = 8 ps for the following setting:

- OP/HB power level 12.9 mW and I = 30 mA.

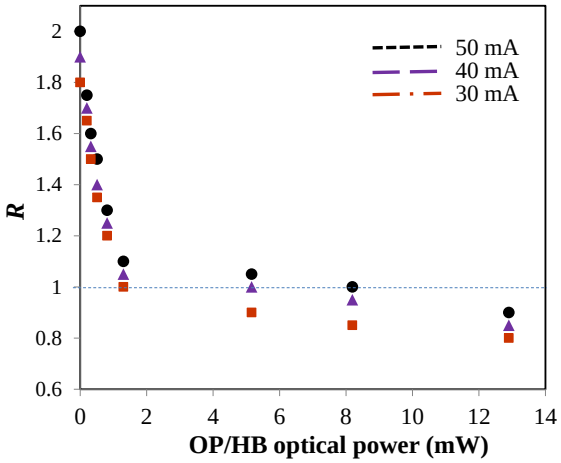

Fig. 4.13: Coefficient *R* versus OP/HB optical power for four different SOA bias currents for the case when ASE from EDFA-2 is not present.

4.3.4 Dispersion Compensation by Varying the Optical Power of the OP/HB at SOA Input in the Presence of ASE

Next, it was investigated how the presence of ASE at the SOA input affects the ability of the OP/HB to vary CDC. Again, 2 ps FWHM optical pulses from the ML laser as OP/HB (see Fig. 4.10) were combined with ASE from EDFA-2 (BPF-1

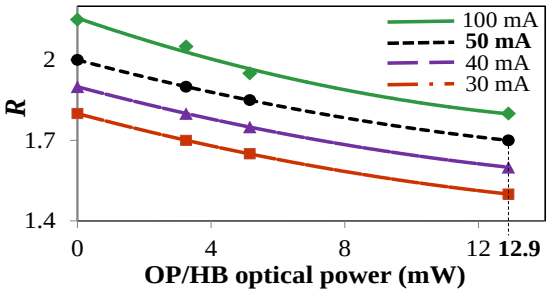

Fig. 4.14: Coefficient *R* versus OP/HB optical power for four different SOA bias currents *I* when ASE from EDFA-2 was present. (Point *I* = 50 mA and OP/HB optical power of 12.9 mW is indicated for cross-referencing).

was removed at the EDFA-2 output, Fig. 4.10) and then injected into the SOA together with the USER-1 OCDMA autocorrelation via the ODL. The values of *R*

obtained versus the OP/HB optical power for different SOA bias currents *I* are shown in Fig. 4.14. It can be seen that, for a given OP/HB optical power, lower *R* values are achieved for lower SOA bias currents, i.e. lower gain. By comparing the results obtained, $R \in (0.8, 2.1)$ in Fig. 4.13 with $R \in (1.5, 2.1)$ in Fig. 4.14, it can be concluded that the presence of ASE limits the ability of the OP/HB to achieve the OCDMA autocorrelation compression (values $R < 1$) observed without ASE.

In the absence of ASE, the SOA traversing OCDMA autocorrelation experiences a red-shift of its leading edge (negative chirp), while a negligible blue-shift (positive chirp) is imposed over its trailing edge. This leads to a stronger-in-average negative chirp if compared to the case when ASE is present. In other words, compression will increase with increasing negative chirp [109]. The presence of ASE slightly reduces the amount of red-shift (negative chirp) at the leading edge but significantly increases the blue-shift (positive chirp) of its trailing edge due to the ASE-induced SOA recovery speed-up. The net result is a predominantly linear chirp across the central part of the OCDMA autocorrelation. All of the above indicate that the SOA produces a more negative chirp in the "absence of ASE" at its input than in the "presence of ASE" and therefore more compensation (smaller *R*) is possible. In addition, the narrower the OP/HB pulses are (steeper the leading edge) the more "instantaneous" the SOA gain change becomes and as such, a larger value of compression can be achieved. The use of an SOA for CDC will also positively mitigate the influence of multi-access interference from the other encoders as was shown in [135].

4.3.5 The Role of Relative Delay between OP/HB and OCDMA Autocorrelation

The position of OP/HB relative to the USER-1 OCDMA autocorrelation peak at the entry point of the SOA was investigated in the presence of ASE. The ODL (Fig. 4.10) was used for delay adjustments. The results obtained are shown in Fig. 4.15. It can be seen that more compression (i.e. smallest *R*) was achieved when

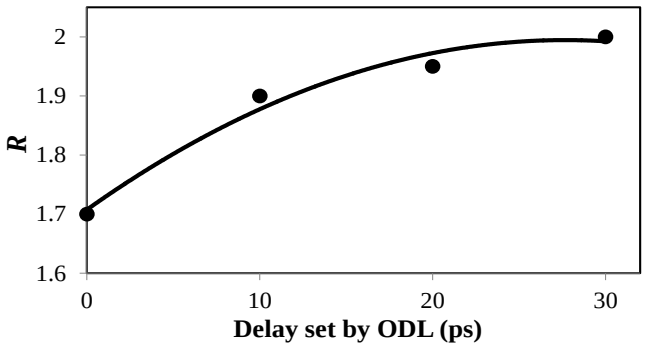

Fig. 4.15: Coefficient *R* vs relative delay between OP/HB and the USER-1 OCDMA autocorrelation for the case when *I* = 50 mA, OP/HB optical power was 12.9 mW, and ASE from EDFA-2 was present (no BPF-1 present).

OP/HB entering the SOA was overlapped with the USER-1 OCDMA autocorrelation peak (0 ps delay). This is because the combined optical peak power from both overlapping pulses (relative delay equal to zero) maximizes the SOA gain depletion and thus creates preferred conditions for the compression by the SOA.

In addition, instead of using a locally generated OP/HB for controlling the SOA gain dynamics, an all-optical clock recovery from the incoming OCDMA traffic [136] can be implemented for OP/HB generation. This will also help to eliminate a possible timing jitter between the locally generated OP/HB and the recovered OCDMA autocorrelation.

4.4 Discussion

The SOA was investigated for its use to compensate the OCDMA autocorrelation broadening/skewing due to the fibre link CD. The investigation was applied to an incoherent OCDMA transmission system based on 2D-(4, 47) WH/TS OCDMA codes with *multi-wavelength picosecond pulses* as code carriers. The results were obtained for different SOA control parameters such as: (1) varying drive current, (2) changing the power of CW and optical pulses used as holding beams (CW/HB and OP/HB), (3) the presence of ASE from EDFA at the SOA input, and (4) the role of a relative delay between OP/HB and the OCDMA autocorrelation at the SOA input. Also shown that if the compensation was applied directly to the recovered OCDMA autocorrelation, only a single control pulse per the data bit was needed to simultaneously affect all four wavelength code carriers. To conduct the investigations, a 17 km long fibre-optic testbed connecting the University of Strathclyde and the University of Glasgow was used. It was shown that the *back-to-back* 10 ps FWHM OCDMA autocorrelation *composed of multi-wavelength* picosecond code carriers, when distorted by a 17 km long propagation in the partially compensated fibre-optic testbed, could be either compressed down or further broadened to values between 8 and 21 ps by controlling the SOA chirp. This makes the demonstrated SOA approach to OCDMA autocorrelation compensation an attractive option for implementation in incoherent OCDMA systems based on picosecond multi-wavelength code carriers. To fully mitigate the impact of CD on the OCDMA system performance would also require addressing cross-correlation compensation by using an SOA with its gain recovery time shorter than the chip width.

Chapter 5

Mitigation of Temperature Induced Dispersion by SOA

5.1 Introduction

Fibre optic cables are buried at least 2-4 feet beneath the ground facing an average of 20 °C temperature variations [137]. In a number of countries, fibre optic cables are carried on pools above the ground where they are exposed to even higher temperature fluctuations [138]. As of today, there has been a very limited number of studies [10, 11, 137, 138, 139, 140] investigating the effects of temperature induced dispersion variations in optical fibres and how a high speed data communication and/or OCDMA based on picosecond multi-wavelengths data carriers will be affected. In [10], it has been reported that ON/OFF keying 40-Gb/s systems will require mitigation of temperature induced dispersion. In [11, 141], it has been predicted that CD induced temporal skewing (consequently leading to autocorrelation broadening) has a strong detrimental effect on bit-error-rate (BER) of OCDMA systems with 2D-WH/TS codes using multi-wavelength picosecond pulses as their carriers. In [103] it is shown that a CD imposed pulse broadening and resulted power penalty will limit the number of simultaneous users and degrade the OCDMA system BER. Uncontrolled CD results in pulse-broadening, inter-symbol interference and can lead to a complete collapse of data transmission [10, 142]. The calculated results obtained in [12] indicate that fibre temperature changes can similarly affect the recovered OCDMA autocorrelation function and BER but no

experiments were performed. Various methods have been investigated for chromatic dispersion compensation (CDC). Manual and automatic /tuneable ways of realizing CDC have been considered [10, 143, 144]. For example, tuneable dispersion compensation can be implemented by varying the chirp on fibre Bragg gratings with external perturbation [143]. In [124] and [125] were reported that SOA can be used to mitigate optical pulse-width changes inflicted by the anomalous CD in optical fibre. In [125], a study of using SOA for CD mitigation in case of a single wavelength data carrier was demonstrated in a 17 km long SMF-28 based fibre optic testbed. By varying the SOA bias current, both pulse compression and expansion between 20 ps to 25 ps of the original 23 ps optical pulse was achieved. In [124], combination of SOA bias current changes and injection of the optical holding beam at various power levels into SOA synchronously with a single wavelength data carrier were investigated to control the data carrier pulse width. This Chapter incorporates the issue of temperature effects on fibre link transmission and the resulting distortions on optical pulses. It is also discussed the need for mitigating the temperature induced dispersion on fibre cable lines, distortion due to transmission link temperature changes and its effect on OCDMA system.

5.2 Distortion of OCDMA Autocorrelation due to Transmission Link Temperature Changes

The temperature induced dispersion (TD) for SMF-28 has been determined to be -0.0015 ps /nm /km /ºC [83]. This value seems to be negligible compared to a CD value of +17 ps /nm /km for SMF-28. However, this small value of TD can affect OCDMA systems based on multi-wavelength picosecond code carriers even when

the fibre CD is fully compensated. This varying temperature induced dispersion will affect the propagating 2D-WH/TS OCDMA codes by producing the time-skewing among code carriers, which will then lead to the OCDMA autocorrelation function distortion [12].

In order to investigate how the 2D-WH/TS OCDMA autocorrelation function can be affected by an improper CD compensation, the transmission link was first fully CD compensated with a sub-picosecond accuracy using DCF. Then its length was 'slightly' varied from its full CD compensation during the measurements. In this investigation, the 19.5 km fibre link was kept at the room temperature of 25 ºC and the transmission link's length was varied from its full CD compensation by adding /removing 50 m of SMF-28. At the receiving end, the signal was then decoded by a matched OCDMA decoder. Figure 5.1c and 5.1d are the examples of a distorted OCDMA autocorrelation function when the transmission link was not properly CD compensated due to subtracting (which resulted in over-compensation) or adding (resulted in under-compensation) about a 50 m of SMF-28. For the better clarity, Fig. 5.1a illustrates an undistorted OCDMA autocorrelation function, which in the experiment was composed of four multi-wavelength code carriers: λ_1 to λ_4. Figure 5.1b shows its distortion due to skewing resulted from the incomplete CD compensation of the transmission link. The time-skewing among wavelength code carriers λ_1 to λ_4 is a result of group velocity changes induced by the incomplete CDC.

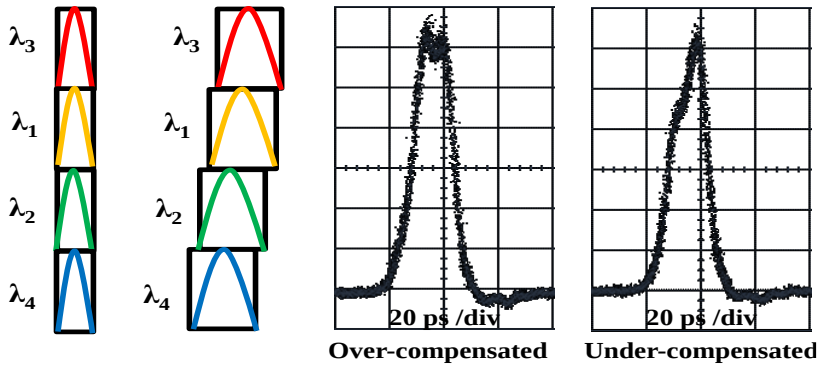

Fig. 5.1: (a) Illustration of OCDMA autocorrelation function; (b) Illustration of its distorted shape by skewing due to CD mismatches; (c) and (d) Obtained result. (Measurements were taken at a room temperature of 25 ºC).

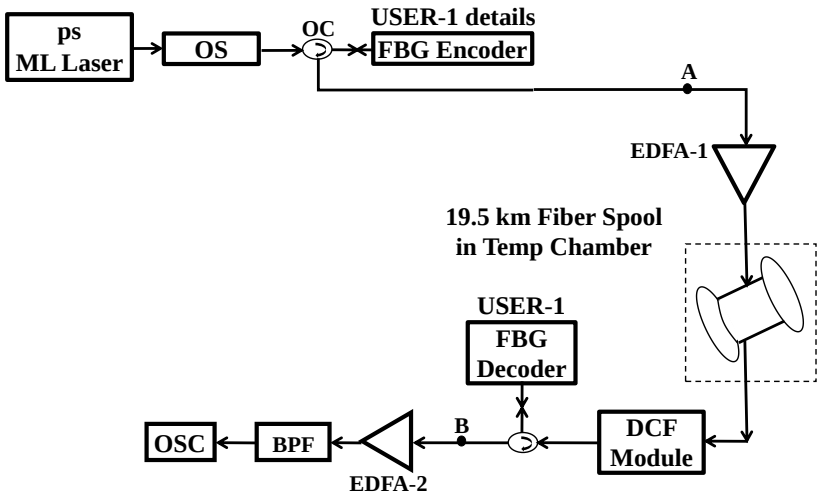

Fig. 5.2: Experimental setup for investigating OCDMA autocorrelation distorted by temperature induced dispersion in optical fibre.

In order to investigate the sole effect of the temperature-induced dispersion on OCDMA systems using 2D-WH/TS codes based on multi-colour picosecond pulses, a 19.5 km fibre link (a spool of SMF-28) was placed inside of the temperature control chamber (shown in Fig. 5.3).

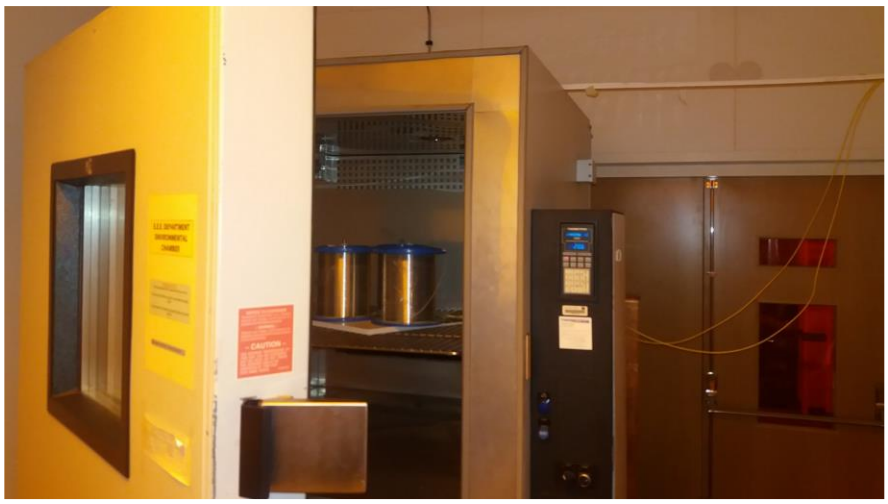

Fig. 5.3: Fibre spools placed in the temperature control chamber.

The DCF module used to fully compensate for the link CD was kept at the room temperature outside of the chamber (see Fig. 5.2). The recovered OCDMA autocorrelation function on the receiver side was observed by an oscilloscope, OSC. As OSC a Digital Communication Analyser Agilent Infiniium DCA-J 86100C with a 64 GHz optical sampling head was used. The measurements are in Fig. 5.4a and Fig. 5.4b and show the received OCDMA autocorrelation functions affected by the transmission in optical fibre kept at 5 °C and 45°C, respectively.

Then the results in Fig. 5.1 were compared with those in Fig. 5.4. It is found that at the fibre temperature of 45 ^{0}C (Fig. 5.4b) the autocorrelation function's shape becomes similar to the shape seen in Fig. 5.1c. Similarly, for the fibre temperature 5 ^{0}C (Fig. 5.4a), the autocorrelation function's shape becomes similar to the one seen in Fig. 5.1d. This means that, increase in the fibre temperature makes the originally fully CD compensated fibre link 'over-compensated' and decrease in the fibre temperature will make it 'under-compensated'. In this particular case, in order to make the fibre link fully dispersion compensated again at 5 ^{0}C /(45 ^{0}C), it would

require removing /(adding) approximately ~80 m of SMF-28 to its original length, respectively.

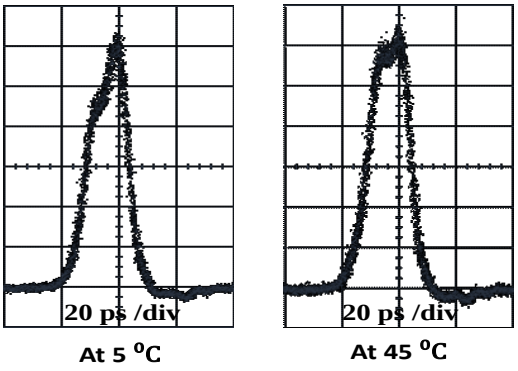

(a) (b)

Fig. 5.4: Temperature induced autocorrelation distortion due to different fibre temperatures: (a) 5 °C; (b) 45 °C.

5.3 Another Effect of Fibre Temperature on OCDMA Autocorrelation

In this section, experimental demonstration of fibre temperature induced effects on 2D-WH/TS OCDMA autocorrelation based on multi-wavelength picosecond pulses as code carriers and the mitigation of these effects by deploying an SOA in the OCDMA receiver were reported. The performed calculations are in good agreement with experimental observations.

There is a number of codes [35] developed to support a coherent OCDMA. The coding is done by manipulating the code carrier phase. An example would be Hadamard codes often referred to as Walsh codes, Gold codes, and Kasami codes. Codes developed to support an incoherent OCDMA do not use the code carrier phase for coding. They are one-dimensional unipolar codes known as optical orthogonal codes, prime codes including 2D-WH/TS code. A 2D-WH/TS prime code is a class

of two dimensional (2D: wavelength-time), incoherent (direct-detection), asynchronous codes that support wavelength-hopping within time-spreading over Galois field of prime numbers with zero autocorrelation side-lobes (for ease of self-synchronization) and periodic cross-correlation functions of at most one (for minimal

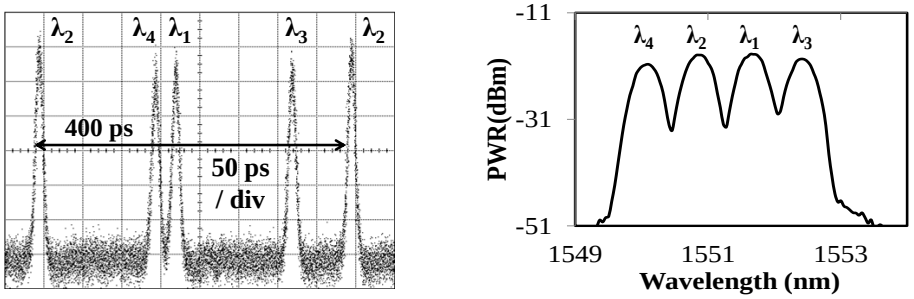

(a) (b)

Fig. 5.5: (a) 2D-WH/TS OCDMA User-1 code 1-λ_2, 21-λ_4, 24-λ_1, 39-λ_3; where, λ_1 = 1551.72 nm, λ_2 = 1550.92 nm, λ_3 = 1552.52 nm, and λ_4 = 1550.12 nm. The code length is 400 ps; (b) optical spectrum occupied by the code.

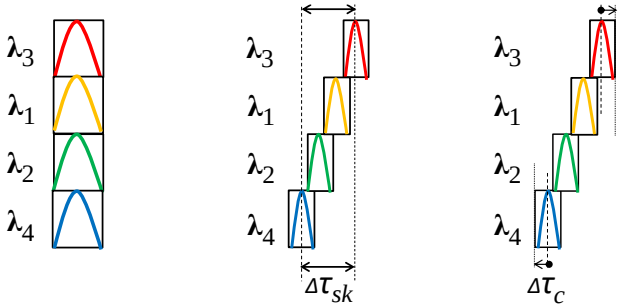

(a) (b) (c)

Fig. 5.6: (a) Unaffected 2D-WH/TS OCDMA autocorrelation (λ_i are code carrier, $\lambda_4 < \lambda_2 < \lambda_1 < \lambda_3$); (b) Illustration how the code carriers skewing influences the autocorrelation width; (c) Illustration how changed carriers' width also contributes to already skewed OCDMA autocorrelation width.

multiple-access interference). They offer good cardinality and can support a large number of simultaneous users. 2D-WH/TS OCDMA codes usually occupy only a small portion of the fibre spectrum. They usually use a set of few picoseconds wide

multi-wavelength pulses as the code carriers. In this investigation, four different wavelength carriers are used that occupied 3.2 nm of spectrum (see Fig. 5.5). Their temporal width will be affected by both, fibre chromatic dispersion and temperature induced dispersion. As a consequence, the recovered OCDMA autocorrelation will be broadened by changes in code carriers' temporal width and by their temporal skewing as is illustrated in Fig. 5.6. This effectively reduces the originally designed number of chips/bit i.e., a maximum number of simultaneous users with error-free BER [35, 103].

The temporal pulse width change of each code carrier λ_i due to the fibre CD can be expressed as $\Delta\tau = D_{CD} \times \Delta\lambda_i \times L$ [11, 102]. D_{CD} is the chromatic dispersion coefficient of the optical fibre link (D_{CD} = 17 ps/nm•km for SMF-28), $\Delta\lambda_i$ is the code carrier's spectral width and L is the propagation distance. When the transmission link is fully CD compensated, it is assumed that $\Delta\tau = 0$ and therefore no code carrier's broadening due to fibre chromatic dispersion is observed and no OCDMA autocorrelation distortion due to temporal skewing will take place. However, if the temperature of the CD compensated transmission link changes by ΔT, the temperature induced fibre link dispersion D_T will come into play and will induce a pulse width change $\Delta\tau_{Ti}$ on each wavelength code carrier λ_i.

$$\begin{aligned} \Delta\tau_{Ti} &= D_T \times L \times \Delta\lambda_i \times \Delta T \\ &= (D_{T\text{-}SMF} \times L_{SMF} + D_{T\text{-}DCF} \times L_{DCF}) \times \Delta\lambda_i \times \Delta T \end{aligned} \quad (5.1)$$

For the SMF-28 fibre the temperature induced dispersion coefficient $D_{T\text{-}SMF}$ = -0.0016 ps/nm•km/°C, for DCF fibre $D_{T\text{-}DCF}$ = +0.004 ps/nm•km/°C [145] and L_{SMF}

(L_{DCF}) is the corresponding fibre length, respectively. It is worth noting that the temperature induced dispersion coefficient for SMF-28 has an opposite sign when compared to D_{CD}.

In the investigations, the four code carriers are spectrally adjacent (see Fig. 5.5(b)) and also have the same spectral width $\Delta\lambda_i$ = 0.8 nm. Therefore, the total spectrum the 2D-WH/TS OCDMA code and related autocorrelation occupy is

$$\Delta\Lambda = \Delta\lambda_i \times w = 0.8 \times 4 = 3.2 \text{ nm} \tag{5.2}$$

where w = 4 is the number of wavelengths (code carriers) used by the 2D-WH/TS code; w is also known as the code weight.

Due to a temperature induced dispersion, each code carrier travels at a different speed v_i. When resulting fibre link $D_T < 0$ and $\lambda_4 < \lambda_2 < \lambda_1 < \lambda_3$ (see Fig. 5.5(b)) then $v_{\lambda 4} < v_{\lambda 2} < v_{\lambda 1} < v_{\lambda 3}$. Because of differences in carriers' arrival times, at the fibre receiving end, the recovered OCDMA autocorrelation width will be affected firstly, by the temporal skewing $\Delta\tau_{sk}$ between code carriers. This is illustrated in Fig. 5.6(b). The amount of $\Delta\tau_{sk}$ is decided by skewing between code carriers with the lowest and the highest speed (i.e., λ_4 and λ_3, respectively - see Fig. 5.6(b)). Secondly, because the code carriers' linewidth $\Delta\lambda_i$ is not infinitely narrow, their temporal width will also change thus additionally contribute to the width change of the already skewed OCDMA autocorrelation. This contribution can be estimated as $\Delta\tau_c$ (see Fig. 5.6(c)). The contribution from both these effects can be expressed as:

$$\Delta\tau_T = \Delta\tau_{sk} + 2 \times \Delta\tau_c \tag{5.3}$$

If the code carriers' temporal shapes approximate as being rectangular and following illustrations in Fig. 5.6,

$$\Delta\tau_{sk} = D_T \times \Delta\lambda_i \times (w-1) \times L \times \Delta T \tag{5.4}$$

For $\Delta\tau_c$ the following expression can be derived,

$$\Delta\tau_c = D_T \times L \times \Delta T \times \Delta\lambda_i /2 \tag{5.5}$$

and by substituting Eq. (5.2), Eq. (5.4), and Eq. (5.5) into Eq. (5.3),

$$\Delta\tau_T = D_T \times \Delta\Lambda \times L \times \Delta T \tag{5.6}$$

This simplified approximation would allow to estimate a scenario when DCF is kept at a constant temperature ($D_{T\text{-}DCF}$ = 0) and only SMF-28 is exposed to a temperature change. After considering values $D_T = D_{T\text{-}SMF}$ = -0.0016 ps/nm•km/°C, $\Delta\Lambda$ = 3.2 nm, transmission distance L = 19.5 km, and the fibre transmission link temperature change ΔT = 30 °C, the estimated numerical value for the OCDMA autocorrelation broadening using this simplified rectangular temporal code carriers envelope shape is $\Delta\tau_T$ ~ 3 ps. It would be seen later that the experimentally measured $\Delta\tau_T$ value was ~1 ps.

A more accurate approximation for $\Delta\tau_T$ can be obtained by assuming a Gaussian shape of the OCDMA multi-wavelength code carrier pulses. Based on [12] and by realizing that in this investigation a $\Delta\lambda_i$ linewidth of each wavelength code

carrier is equal to a code carrier's spectral separation $\Delta\Lambda_i$, the temperature dependent OCDMA autocorrelation envelope S_T^L(t) can be represented by:

$$S_T^L(t) = \sum_{k=0}^{w-1} P_0 exp\ \{-2.77 \left[\frac{t-k\,\Delta\tau_{Ti}}{\tau-\Delta\tau_{Ti}}\right]^2\} \tag{5.7}$$

where $P_0 = P(L = 0, \Delta T = 0) = 1$ is the wavelength code carrier's normalized peak power and $\Delta\tau_{Ti}$ is given by Eq. (5.1). By using a measured temporal width of each wavelength code carrier at 20 °C τ = 12 ps, $D_{T\text{-}SMF}$ = -0.0016 ps/nm•km/°C, $D_{T\text{-}DCF}$ = +0.004 ps/nm•km/°C, temperature change ΔT = 30 °C, L_{SMF} = 19.5 km, L_{DCF} = 3.32 km, $\Delta\Lambda_i$ = 0.8 nm, $\Delta\lambda_i$ = 0.8 nm, three scenarios were investigated. Results for $S_T^L(t)$ were plotted in Fig. 5.7: (a) the fully CD compensated link (i.e., SMF-28 + DCF) at T = 20°C; (b) SMF-28 + DCF at T = 50 °C; (c) SMF-28 at T = 50 °C but DCF at T = 20 °C.

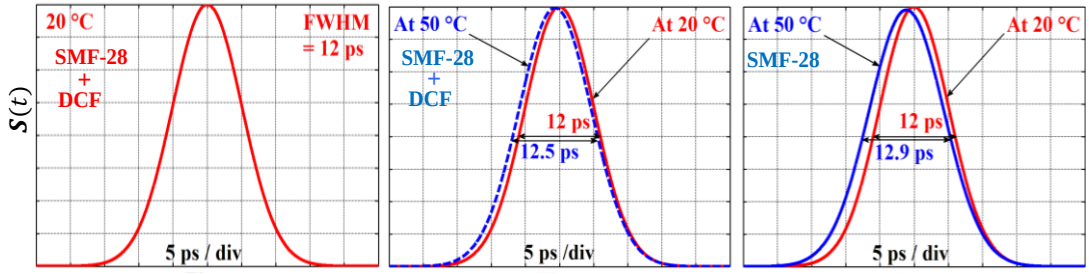

(a) (b) (c)

Fig. 5.7: (a) Unaffected OCDMA autocorrelation envelope $S(t)$ after code transmission in the CD compensated fibre link at 20 °C; (b) after raising link temperature to 50 °C; (c) when only SMF-28 section is heated to 50 °C and DSF section is kept at 20 °C.

By analysing the calculated results of the OCDMA autocorrelation FWHM change, one can conclude: (a) There is no autocorrelation width change for a CD compensated link kept at the constant temperature. (b) A 0.5 ps width broadening

from 12 ps to 12.5 ps for a 30°C temperature increase of an entire transmission link. (c) A 0.9 ps width broadening from 12 ps to 12.9 ps for a 30°C temperature increase of the SMF-28 fibre section only (DCF is kept at a room temperature).

5.3.1 Experimental Setup for the Investigation of Fibre Link Temperature Effect on OCDMA Autocorrelation

The experimental setup used for this investigation is shown in Fig. 5.8. It consists of an OCDMA transmitter, OCDMA receiver, environmental chamber, 19.5 km of SMF-28 optical fibre on a spool, chromatic dispersion compensating fibre (DCF), and diagnostic equipment. Both OCDMA transmitter and receiver are based

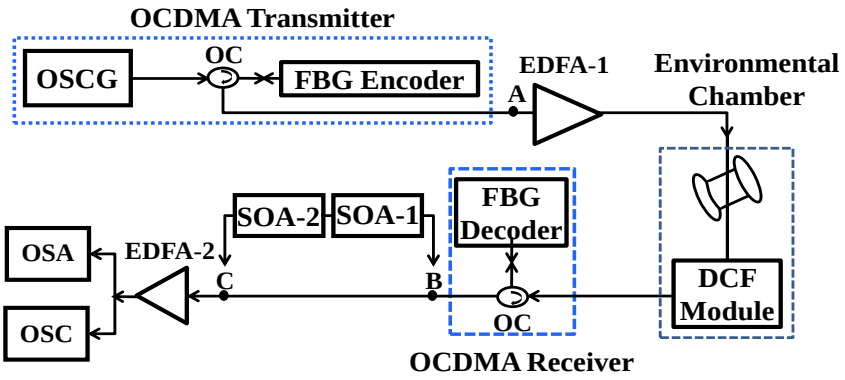

Fig. 5.8: Experimental setup; OSCG - Optical Supercontinuum Generation, OC - Optical Circulator, EDFA - Erbium Doped Fibre Amplifier, DCF - Dispersion Compensating Fibre, SOA - Semiconductor Optical Amplifier, OSC - Oscilloscope, OSA - Optical Spectrum Analyser.

on FBG technology. An integral part of the OCDMA transmitter was an optical supercontinuum generator (OSCG) producing a 3.2 nm wide optical supercontinuum. The supercontinuum was fed into an FBG OCDMA encoder (OKI Industries, Japan) for generation of a 2D-WH/TS OCDMA code. The code consisted of four wavelength code carriers (λ_1 = 1551.72 nm, λ_2 = 1550.92 nm, λ_3 = 1552.52 nm, and

λ_4 = 1550.12 nm). After its amplification by a 15 dBm EDFA-1, the code was launched into a fibre transmission link represented by a 19.5 km long SMF-28 fibre followed by a 3.32 km long DCF fibre for the link DC compensation. During the investigations, the temperature of the link (or its portion) was varied between 20 °C (room temperature) and 50 °C using temperature control chamber (SM-32C from Thermatron Industries).

In order to separate CD effects from the temperature induced dispersion effects, the transmission link was fully CD compensated with the sub-picosecond accuracy by using a matching DCF Module.

On the receiving site, the received OCDMA signal was decoded by a matched FBG-based OCDMA decoder. This produced an OCDMA autocorrelation, which was amplified by EDFA-2. An Oscilloscope, OSC (Agilent Infiniium DCA-J 86100C with an optical sampling head) and Optical Spectrum Analyser (OSA) then evaluated the autocorrelation.

5.3.2 Investigation of Fibre Transmission Link Temperature Effects on OCDMA Autocorrelation and Its Mitigation by SOA

First the environmental chamber holding transmission fibre was set to match the room temperature (20 °C). For future reference, the OCDMA autocorrelation $S_T^L(t)$ was then recorded by OSC using the experimental setup shown in Fig. 5.8, no SOAs were present. The experimental result is shown in Fig. 5.9(a) in black. For a comparison, the calculated result from Fig. 5.7(a) is overlaid (red line). Then the chamber temperature was increased to 50 °C with SMF-28 section only, DCF section

was kept at 20 °C. After reaching a steady state (after ~ 4 hours), the OCDMA autocorrelation was recorded. The experimental result is shown in black in Fig. 5.9(b). For a comparison, the calculated result from Fig. 5.7(c) is overlaid (blue line). It is seen that the amount of autocorrelation broadening $\Delta\tau_T$ = 1 ps

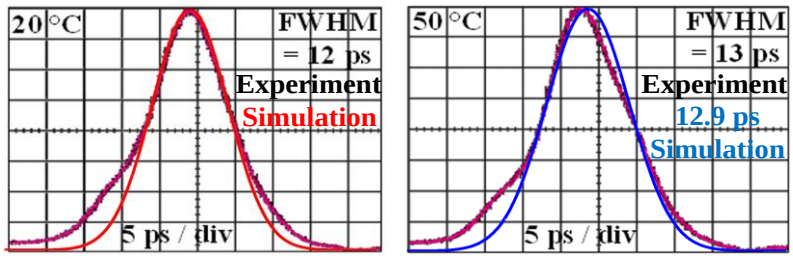

(a) (b)

Fig. 5.9: (a) OCDMA autocorrelation when CD compensated transmission link is at 20 °C: black - experiment, red - calculation; (b) when SMF-28 section is at 50 °C and DCF at 20 °C: black - experiment, blue - calculation.

agrees with a 0.9 ps value predicted by the calculations. Misalignments observed at the pulses base are due to a minor FBG encoder/decoder miss-match resulted from manufacturing imperfections. Because of the setup resolution, it was not possible to experimentally confirm the calculation results shown in Fig. 5.7(b) predicting the $\Delta\tau_T$ = 0.5 ps autocorrelation broadening.

The effect of the temperature can be explained as follows. The SMF-28 fibre produces the anomalous chromatic dispersion ($D_{CD} > 0$) leading to the negative chirp $C < 0$. By adding a matching length of the dispersion compensating fibre (DCF has a normal chromatic dispersion, $D < 0$), the fibre transmission link becomes CD compensated. From this point on, a fibre temperature change (introduces $D_T < 0$) will "flip" the overall transmission link dispersion balance towards the normal dispersion.

The normal dispersion leads to a positive chirp $C > 0$, and a lower group velocity for higher-frequency components. This means the leading edge components of optical pulses travel slower than the rest of the pulse, the trailing edge components travel faster and as a whole, the temporal width of each optical pulse becomes narrower. This way all four multi-wavelength code carriers λ_i are affected. In addition, code carriers with the longer wavelength will travel faster than those with the shorter wavelength. This causes their temporal skewing leading to OCDMA autocorrelation temporal broadening with any fibre temperature increase.

To experimentally study a possibility of using an SOA to mitigate the effects of temperature induced dispersion ($D_T < 0$), an SOA (Kamelian OPA-20-N-C) was inserted between points B and C in the experimental setup (see SOA1 in Fig. 5.8). It is then investigated if by changing the SOA1 gain/bias current it would be possible to eliminate the observed temporal change of the OCDMA autocorrelation width caused by the temperature-induced dispersion. The investigation was started by setting the temperature of the chamber to 50 °C. At this temperature the recorded OCDMA autocorrelation FWHM was found to be 13 ps (see Fig. 5.10(a)). Now, by changing the bias current of SOA1 it was tried to restore the OCDMA autocorrelation FWHM back to the value previously recorded at a room temperature of 20 °C (see Fig. 5.9(a)). By manipulating the bias current I, it was observed that the autocorrelation width would broaden for $I > 23$ mA. For $I < 23$ mA, the autocorrelation was compressed. To allow for a better visualization, the resulting signal was then amplified by SOA2. The result is shown in Fig. 5.10(b). By comparing it with the recorded OCDMA autocorrelation taken at 20 °C shown in

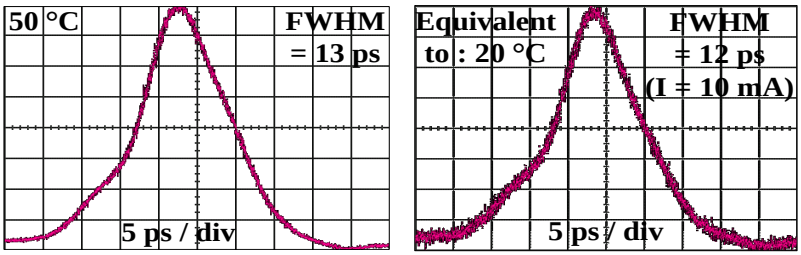

(a) (b)

Fig. 5.10: (a) OCDMA autocorrelation observed at 50 °C; (b) Adjusted OCDMA autocorrelation seen at 50 °C to its value measured at 20 °C; I = 10 mA is the bias current of SOA1.

Fig. 5.9(a), one can conclude that both autocorrelations have a very similar shape and the measured FWHM value of 12 ps.

The above can be explained as follows: a pulse broadening by SOA will occur for pulses positively chirped ($C > 0$) when transiting the SOA1 [146]. As discussed earlier, the temperature induced dispersion D_T in the fibre transmission link imposes a positive chirp ($C > 0$) on optical pulses (OCDMA code carriers). This causes the additional skewing, therefore more broadening of the OCDMA autocorrelation when transiting the SOA1 at bias currents $I > 23$ mA. At low SOA bias currents, $I << 23$ mA (unsaturated gain), compression by the SOA is observed. Reducing the SOA bias current I to 10 mA changed the chirp value in the opposite direction leading to compression observed at the SOA-1 output [146]. SOA2 had no measurable effect on the passing autocorrelation other than amplifying the signal for its better detection.

So far, SOA was used by placing it at the receiver site of the incoherent OCDMA link to see its usage to overcome the dispersion-induced impairments as investigated in Chapter-4 and including this Chapter-5. In the next Chapter-6, it will

be investigated how SOA can perform if it is located at the transmission site of the link to overcome the dispersion related distortions for an optical fibre link.

5.4 Discussion

The effect of fibre temperature on the OCDMA autocorrelation when the temperature of a 22.8 km long CD compensated link or its SMF portion increases from 20 °C to 50 °C is studied in this Chapter. The OCDMA system under investigation used 2D-WH/TS codes based on multi-wavelength picosecond optical pulses as the code carriers. It has been shown by calculations that the link's 30 °C temperature increase would broaden the recovered OCDMA autocorrelation FWHM by a 0.5 ps from 12 ps to 12.5 ps. It has also experimentally demonstrated and then confirmed by calculations that if this 30 °C temperature change applied to its 19.5 km long SMF section, this would alter the FWHM value of the recovered OCDMA autocorrelation from 12 ps to 13 ps (12.9 ps when calculated). The measured 1 ps autocorrelation broadening is in a very good agreement with a 0.9 ps prediction, which assumed a Gaussian temporal shape of code carriers. Also demonstrated that the SOA could be used to mitigate the observed amount of the broadening.

Chapter 6

SOA as a Chirp Manipulator

6.1 Introduction

The deployment of incoherent OCDMA systems that use picosecond pulses as code carriers requires a CD compensated transmission link. If the link is not properly CD compensated, then the distortion due to pulse broadening and time-skewing would cause OCDMA autocorrelation function distortion at the receiving end. This would affect optical communication at chip level, cause inter chip interference resulting in bit-error-rate (BER) degradation, [11, 103, 102]. It is therefore important to ensure that any deviations from the link's CD compensation are under control preferably via tuneable means.

One approach to achieve tuneable CD control is to exploit the signal's chirp before its transmission in the optical fibre. In [147], a laser pulse with a positive chirp was passed through SMF-28 fibre producing a negative chirp (due to fibre anomalous dispersion) leading to pulse compression. At the same time, due to GVD, pulses have experienced broadening while propagating in optical fibre. At a distance known as the dispersion length (L_D), the pulse-width becomes equal to its initial value, seen at the fibre input due to the action of both of these simultaneous effects. After passing a distance L_D, the propagated pulse will start to expand again until reaching the end of the fibre [134]. It is known that, either the initial positive chirp of

a laser pulse or the resulting negative chirp due to fibre anomalous dispersion can be adjusted further to compress the optical pulse. The initial positive chirp of the generated laser pulse can be reduced, or the length of SMF-28 fibre can be changed to vary the resulted chirp from laser pulse propagation in an optical fibre with anomalous dispersion.

It has been reported that, an SOA can also change the chirp of the optical laser pulse passing through the SOA by changing its bias current [148]. In Chapter-5, the effect of temperature-induced fibre dispersion on the OCDMA autocorrelation was mitigated by changing the gain of an SOA placed on the receiver side of the link. Through changes of the SOA gain dynamics and by introducing an optical holding beam (cw and/or optical pulse synchronized with OCDMA autocorrelation at SOA input), the effect of fibre CD was investigated in Chapter-4 by placing SOA at the receiver site. These control mechanisms affect the refractive index inside the SOA via gain changes (as predicted by Kramers-Kronig relations) resulting in a varied amount of chirp being imposed by the SOA on optical pulses passing through the SOA.

In this Chapter, the use of an SOA placed on the transmitter site was investigated to compensate OCDMA autocorrelation broadening on the receiver side caused by fibre CD. This is achieved by controlling the chirp of multi-wavelength OCDMA code carriers before the code is launched into a 16~17 km testbed. A developed equation allows theoretical and experimental investigation of chirp changes imposed by the SOA on the OCDMA autocorrelation. The calculations are in a good agreement with experimental results.

6.2 Experimental Setup for the Investigation of SOA as Chirp Manipulator for Multi-Wavelength OCDMA Code Carriers

Figure 6.1 represents the experimental setup used for the investigations. The OCDMA transmitter Tx produces a 2D-WH/TS OCDMA code based on four wavelengths (λ_1 = 1551.72 nm, λ_2 = 1550.92 nm, λ_3 = 1552.52 nm, λ_4 = 1550.12 nm) with 10 ps FWHM pulses as the code carriers. All pulse carriers have a positive chirp resulted from spectral slicing of the optical supercontinuum by a FBG based 2D-WH/TS OCDMA encoder.

A 2D-WH/TS prime code is a class of two dimensional (2D: wavelength-time), incoherent asynchronous codes that support wavelength-hopping within time-spreading over the Galois field of prime numbers with zero autocorrelation side-lobes and periodic cross-correlation functions of at most one [35].

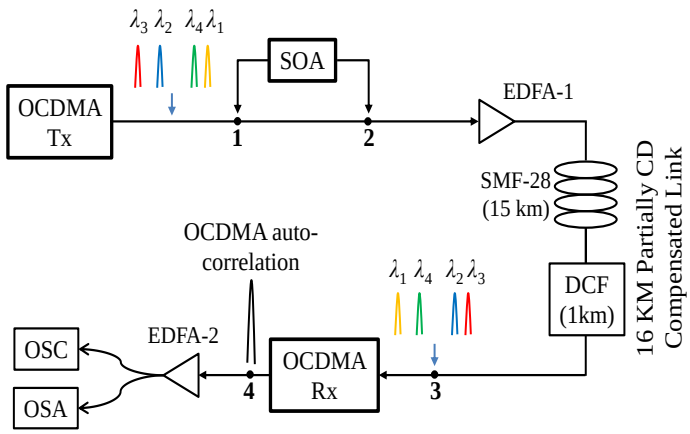

Fig. 6.1: Experimental setup. Tx – OCDMA transmitter, SOA – Semiconductor Optical Amplifier, EDFA – Erbium Doped Fibre Amplifier, DCF – Dispersion Compensating Fibre, SMF – Single Mode Fibre, Rx – OCDMA receiver, OSC – Oscilloscope, OSA – Optical Spectrum Analyser.

This transmitted code (2D-WH/TS OCDMA code, 1-λ_2, 21-λ_4, 24-λ_1, 39-λ_3) then propagates through a 16 km long CD compensated testbed. A related OCDMA autocorrelation signal is then recovered by an OCDMA decoder (Rx) matched to the OCDMA encoder (Tx) at the fibre-receiving end (point-4). For signal amplification, the EDFA-2 amplifier is used and the output is analysed using an Optical Spectrum Analyser (OSA - Agilent 86146B) and a Digitizing Oscilloscope, OSC (Agilent Infiniium DCA-J 86100C with an optical sampling head).

The transmission link (Fig. 6.1) was first CD compensated by using the commercially available DCF module selected to match the 15 km SMF-28 fibre link. After its installation, it was found that there was a small CD mismatch and the link was narrowly over-compensated. That means the overall link is in the normal dispersion region ($\beta_2 > 0$) having its equivalent link GVD parameter $\beta_2 = 0.2$ ps^2/km. To achieve tuneability in CD compensation, and to make the link fully compensated without further adjustment of the DCF length, the use of SOA to fine-tune the compensation was investigated.

First, by performing '*back-to-back*' measurements the OCDMA autocorrelation temporal width in the absence of SOA was obtained at the Tx side (point-1). Then the autocorrelation was obtained after 16 km propagation at the Rx receiver side (point-4). The results measured using the digitizing oscilloscope (OSC) are shown in Fig. 6.2(a) and 6.2(b), respectively.

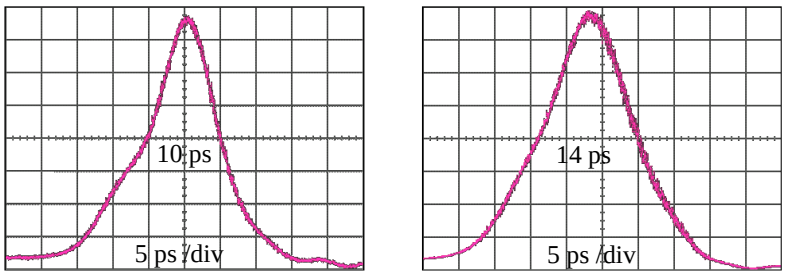

(a) (b)

Fig. 6.2: Measured recovered OCDMA autocorrelation: (a) back-to-back at point-1; (b) after 16 km long fibre transmission at point-4.

From Fig. 6.2(b), it is seen that, as the multi-wavelength picosecond OCDMA pulses (code carriers) propagate through this 16 km long fibre testbed, the FWHM width of the recovered OCDMA autocorrelation function by the decoder Rx (point-4) has broadened from 10 ps to 14 ps when compared to the '*back-to-back*' measurement shown in Fig. 6.2(a).

For $\beta_2 = 0.2$ ps^2/km, the CD value D_{CD} [149] can be calculated as:

$$D_{CD} = -(2\pi c/\lambda^2) \times \beta_2 \qquad (6.1)$$

Here, c is the velocity of light in a vacuum. From Eq. (6.1), the obtained value of D_{CD} is:

$D_{CD} = -0.157$ ps/(nm•km) for the $\lambda = 1550$ nm region.

Now, to investigate the possibility of adjusting the FWHM temporal width of the recovered OCDMA autocorrelation function at the receiver end via controlling chirp of code carriers at the transmitting end by using SOA, an SOA (Kamelian OPA-20-N-C) was inserted between the points 1 and 2 (see Fig. 6.1).

6.3 Theoretical Background and Analysis

6.3.1 Optical Pulse Chirp

A pulse is chirped if its carrier frequency changes with time. The frequency change relates to the phase derivative. Parameter C can be introduced to describe the linear frequency chirp imposed on the pulse. It depends on whether the instantaneous frequency of optical pulse is increasing or decreasing with time [148]. In the normal dispersion region, the GVD parameter β_2 is positive and the chirp is also positive, $C > 0$. At this condition, the higher frequency components' speed towards the pulse's leading edge is lower than the lower frequency components' speed at the trailing edge. On the other hand, in the anomalous dispersion region, the GVD parameter β_2 is negative and the chirp is also negative, $C < 0$. The higher frequency components' speed towards the pulse's leading edge is faster than the lower frequency components' speed at the trailing edge. If the optical pulses generated by Tx (at point-1) have a positive chirp then after propagation through a normal dispersion region ($\beta_2 > 0$), the positive chirp will become more positive (i.e., higher frequency components speed towards the leading edge will be even slower) and as a result, the pulse will be broadened. On the other hand, if these optical pulses will pass through a region with an anomalous dispersion ($\beta_2 < 0$), then the positive chirp can be brought to zero. This will happen after traveling a distance known as L_D. This leads to the compensation of GVD effect. Further propagation in the fibre (when distance L exceeds length L_D) will lead to the pulse broadening as the effect of GVD becomes positive [77]. To summarize, an initial pulse narrowing happens if the product $C\beta_2 < 0$, and the travel distance $L < L_D$, then if $L > L_D$, the pulse broadens

(until the end of the fibre link). The scenario described will also occur for optical pulses at the Tx output having a negative value of C ($C < 0$) where they would propagate in the optical fibre with normal dispersion ($\beta_2 > 0$ and $D_{CD} < 0$), also leading to $C\beta_2 < 0$.

6.3.2 Effect of Code Carriers Chirp on OCDMA Autocorrelation Temporal Envelope and Its Width

A temporal Gaussian shape of an optical pulse affected by chirp C is represented as [149]:

$$P_L(t) = P_0 \exp[-2.77(1 + iC) \left(\frac{t}{\tau}\right)^2] \quad (6.2)$$

where t is time, P_0 is a peak power and coefficient 2.77 indicates a pulse width τ measured at FWHM.

In the investigation, four multi-wavelength picosecond pulses as 2D-WH/TS OCDMA code carriers, each of linewidth $\Delta\lambda$j and spectrally separated by $\Delta\Lambda$j where j = 1, 2, 3, 4, respectively are used. In light of Eq. (6.2), by following [12], for the OCDMA autocorrelation temporal envelope recovered by the Rx receiver (Fig. 6.1 point-4) an expression is written as:

$$S_{L(\lambda_1 - \lambda_4)}(t) = \sum_{k=0}^{w-1} P \exp[-2.77(1 + iC) \left(\frac{t - k\Delta\tau_0}{\tau - \Delta\tau_0}\right)^2] \quad (6.3)$$

In the above expression, $w = 4$ is a number of code carriers (wavelengths) also known as the code weight. The numerator ($t - k\Delta\tau_0$) represents time skewing

among wavelength carriers, the denominator $(\tau - \Delta\tau_0)$ reflects their spectral broadening due to dispersion effects and

$$\Delta\tau_0 = D_{CD} \times L \times \Delta\lambda_j \tag{6.4}$$

where D_{CD} = - 0.157 ps/(nm•km) represents the dispersion of the partially compensated fibre testbed, L = 16 km is the testbed length, and $\Delta\lambda_j = \Delta\Lambda_j$ = 0.8 nm.

By following [149], from Fig. 6.3, one can obtain the value of chirp C affecting the resulting OCDMA autocorrelation S_L as:

$$C = [(\Delta\Omega \times a_0)^2 - 1]^{½} = [(\Delta\Omega \times \frac{\tau}{1.665})^2 - 1]^{½} = + 2.36 \tag{6.5}$$

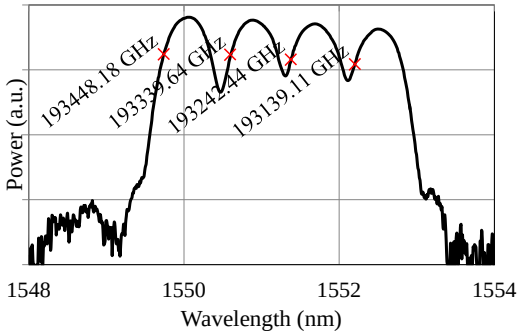

Fig. 6.3: Spectrum recorded during Back-to-Back measurements at point-1.

Here $\Delta\Omega$ = 3.42 nm (see Fig. 6.3) is the spectral width of the OCDMA autocorrelation found from the measurements at point-1 by the OSA (Agilent 86146B), and $a_0 = \tau$ /1.665 reflects the use of the 'back-to-back' FWHM value of τ = 10 ps (see Fig. 6.2(a)).

The frequency domain representation of the OCDMA autocorrelation envelope after L = 16 km of propagation in the optical fibre can be obtained from Eq. (6.3) as follows [150]:

$$S_{L(\lambda_1-\lambda_4)}(f) = \text{fft}\{S_{L(\lambda_1-\lambda_4)}(t)\} \times \{\exp(-i\,\omega_j^2 \times \beta_2 / 2) \times L\} \quad (6.6)$$

where β_2 = 0.2 ps^2/km is the fibre link group velocity dispersion coefficient; ω_j is an angular frequency of a particular code carrier j; and $\{\exp(-i\,\omega_j^2 \times \beta_2 / 2) \times L\}$ factors in the GVD effects imposed by the propagation in the fibre.

In order to obtain the OCDMA autocorrelation function at the fibre end in the time domain, an inverse Fourier transform on Eq. (6.6) was performed:

$$S_{L(\lambda_1-\lambda_4)}(t) = \text{ifft}\{S_{L(\lambda_1-\lambda_4)}(f)\} \quad (6.7)$$

Now, using C = +2.36 found from Eq. (6.5) and substituting Eq. (6.3) and (6.6) into Eq. (6.7), it is possible to calculate the 2D-WH/TS OCDMA autocorrelation envelope S_L recovered by the matched OCDMA receiver Rx at point-4 after L = 16 km long transmission (Fig. 6.4(b)) and the related FWHM width is 14.2 ps. The corresponding experimental measurement shows the FWHM value of 14 ps (Fig. 6.4(a)). For a comparison, the '*back-to-back*' measured and calculated FWHM widths for the OCDMA envelope are also shown in Fig. 6.4(a) and 6.4(b), respectively each having the same value of 10 ps.

Based on [77] it is seen that, the larger $C > 0$ code carriers have at Tx output, the more broadening they will experience during their fibre propagation. However, if

the *C* value can be reduced, the OCDMA autocorrelation widths observed at the fibre output will be also reduced. This will be explored next.

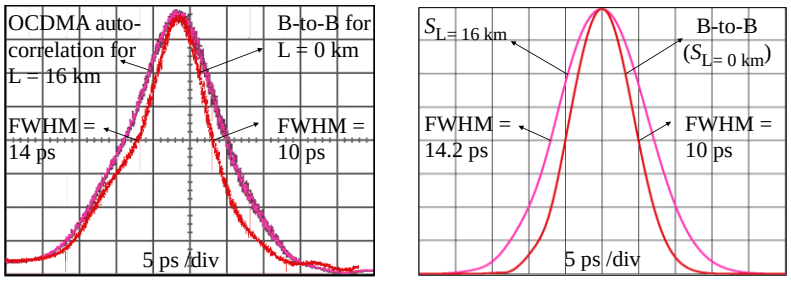

(a) Experiment (b) Calculations

Fig. 6.4: (a) Measured 2D-WH/TS OCDMA autocorrelation recovered by a matched OCDMA decoder Rx for back-to-back (L = 0) and after L = 16 km propagation; (b) Calculations for the same.

6.3.3 Chirp variation by SOA

To explore the possibility of reducing the *C* value, an SOA has been added after the Tx in between the points 1 and 2 (see Fig. 6.1). This allows to vary the SOA's gain dynamics through a change in bias current *I* (carrier density), which results in refractive index changes thus causing a phase shift [77, 149]. Before going any further, the optical spectrum of 2D-WH/TS code immediately after passing the SOA biased at I = 7 mA was taken. The measured result is shown in Fig. 6.5. Now

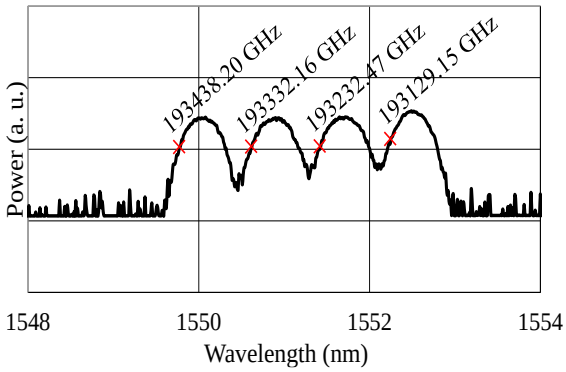

Fig. 6.5: Spectrum recorded at SOA output (point-2) at bias current I = 7 mA.

recall, Fig. 6.3 shows the code optical spectrum at the SOA input. By comparing it with Fig. 6.5 the respective spectral frequency shifts $\Delta\nu(\lambda_4)$ = 9.98 GHz for λ_4, $\Delta\nu(\lambda_2)$ = 7.48 GHz for λ_2, $\Delta\nu(\lambda_1)$ = 9.97 GHz for λ_1 and $\Delta\nu(\lambda_3)$ = 9.96 GHz for λ_3 imposed by the SOA biased at I = 7 mA resulting in a frequency chirp of $\Delta\nu$ = 9.34 GHz was obtained. In order to find the related chirp parameter C_{out} induced by SOA, the following expression is used [151]:

$$C_{out} = \Delta\nu\ (\text{GHz}) \times 2\pi\sigma = 0.25 \tag{6.8}$$

where $\sigma = \tau$ /2.35 and τ = 10 ps are the measured FWHM value of code carriers entering the SOA. The coefficient 2.35 is a result of conversion between the FWHM width τ of a Gaussian shape pulse and standard deviation σ. Now, after substituting $C = C_{out}$ = 0.25 into Eq. (6.3) and following steps as before, from Eq. (6.7) it is possible to calculate the 2D-WH/TS OCDMA autocorrelation envelope S_L recovered by the OCDMA decoder Rx after an L = 16 km long fibre transmission at point-4 and the related FWHM width value. The result of this calculation is shown in Fig. 6.6(b) as curve C = 0.25. Its calculated FWHM width is 10.6 ps. In contrast, the curve marked I = 7 mA in Fig. 6.6(a) is the experimentally recovered OCDMA autocorrelation at point-4 for SOA current I = 7 mA. The corresponding FWHM value is 11 ps. Results of measurements for different I values are also included in Fig. 6.6(a) together with results of OCDMA autocorrelation envelope calculations for different chirp values C in Fig. 6.6(b). Then OCDMA autocorrelation FWHM values as a function of SOA current I were extracted from Fig. 6.6(a).

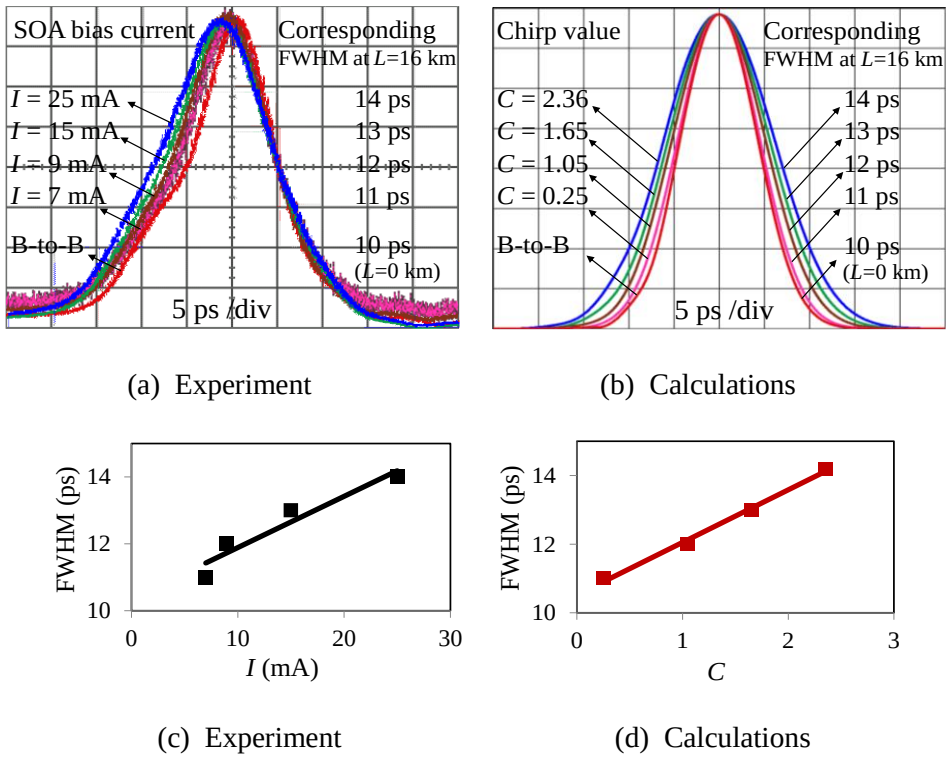

Fig. 6.6: (a) Measured 2D-WH/TS OCDMA autocorrelation envelope for different SOA bias currents I after L = 16 km fibre propagation; (b) Calculated 2D-WH/TS OCDMA autocorrelation envelope after 16 km fibre propagation for different values of chirp C; (c) OCDMA autocorrelation FWHM width vs SOA bias current I; (d) OCDMA autocorrelation FWHM width vs chirp C.

These results were shown in Fig. 6.6(c). Similarly, the OCDMA autocorrelation FWHM values as a function of chirp C were extracted from Fig. 6.6(b) and results were plotted in Fig. 6.6(d). Looking at the calculated results, it was seen that for a 16 km long propagation in the fibre testbed, C = 0.25 delivered the maximal autocorrelation width reduction, from 14 ps to 11 ps. This was then confirmed experimentally where for the SOA bias current I = 7 mA, the FWHM value 11 ps was also minimal. Any further decreases of I with attempts to achieve a '*back-to-back*' τ = 10 ps value of the OCDMA autocorrelation width also for L = 16 km led to an impractically low SOA gain. To overcome this, a continuous wave (CW) holding beam technique (CWHB) was used [152]. The CW source (see Fig. 6.7(a))

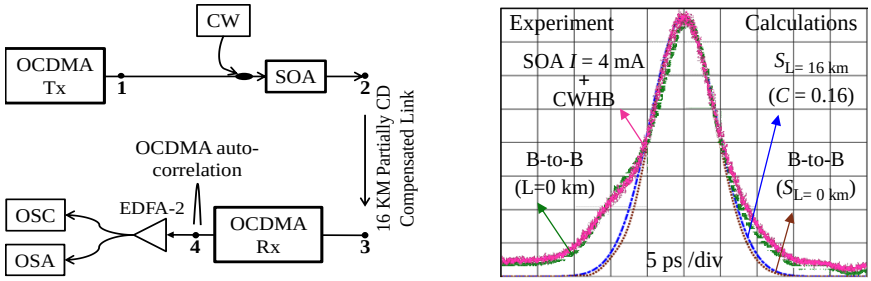

(a) (b)

Fig. 6.7: (a) Testbed setup after adding CW source as CWHB. (b) Corrected OCDMA autocorrelation envelope: red line - measurement after L = 16 km propagation (point-4) for the SOA bias current I = 4 mA in the presence of CW and blue dot-dashed line - calculation when SOA induced chirp parameter is C = 0.16. Brown dotted (green dashed) line is the $S_{L=0km}$ calculation (back-to-back measurement at point-1), respectively.

was an SOA (Kamelian OPA-20-N-C) with its gain set to one. A collinearly added CW enhanced the stimulated emission in the SOA [153], and thus the SOA gain dynamics. In this configuration and with an SOA bias current of I = 4 mA, it was possible to experimentally achieve the OCDMA FWHM value of 10 ps (see Fig. 6.7(b) red line) which was in an agreement with '*back-to-back*' measurements (green dashed line). Using the steps described earlier, it was found that the resulting value of the chirp at point-2 was C = 0.16. By using Eq. (6.7), the 'corrected' OCDMA autocorrelation envelope $S_{L=16\ km}$ was found as shown in Fig. 6.7(b) by the blue dot-dashed line. It was seen that its OCDMA FWHM value was also 10 ps and matched well with back-to-back measurements (green dashed line) and the related calculations $S_{L=\ 0\ km}$ (brown dotted line). The misalignments observed at the pulses base are due to a minor FBG encoder/decoder miss-match resulted from manufacturing imperfections.

6.4 Comparative Study of Using SOA at Tx Site or at Rx Site

In this investigation, a comparative study has been conducted using an OCDMA transmission system seen in Fig. 6.8 where the SOA was located at its transmission (Option-1) or receiving (Option-2) site, respectively. It has been investigated, to what extent a placement of a single SOA would play a role in mitigating the CD impairments i.e., the spreading and time skewing which are affecting the recovered OCDMA auto-correlation at the receiving site.

The setup for investigating a chirp control by the single SOA is shown in Fig. 6.8. The experimental setup has already been described before. The only difference was that, the single SOA was located alternatively at the Tx site in Option-1 and

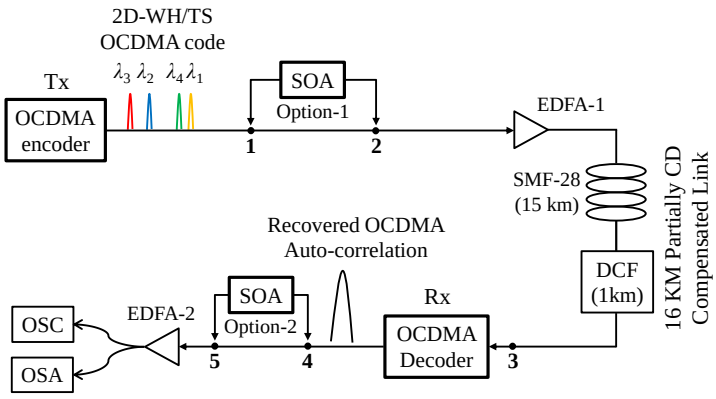

Fig. 6.8. Experimental setup. Tx – OCDMA Transmitter/Encoder, SOA – Semiconductor Optical Amplifier, EDFA – Erbium Doped Fibre Amplifier, DCF – Dispersion Compensating Fibre, SMF – Single Mode Fibre, Rx – OCDMA Receiver/Decoder, OSC – oscilloscope, OSA – Optical Spectrum Analyser.

the OCDMA autocorrelation widths were measured for varied SOA drive current controls and this SOA was again placed at the Rx site in Option-2 and the measurements were repeated.

First, a back-to-back measurement was performed at Point-1. The obtained OCDMA auto-correlation FWHM was found to be 10 ps. Then the measurement was repeated after 16 km of propagation in a CD affected transmission link (Point-5). In this case, the recovered OCDMA auto-correlation width was found to be 14 ps. Both measurements were performed by a digital oscilloscope DCA-J 86100C with a 64 GHz optical sampling head, OSC. Next, it was investigated how using the SOA placement either in position Option-1 or Option-2, would be effective in CD link compensation via controlling the chirp.

6.4.1 CD Management by a Single SOA on *Tx* Site

First, the SOA was placed in the testbed as indicated by Option-1 (See Fig. 6.8). The value *R* was defined as a ratio of a measured OCDMA auto-correlation FWHM value at Point-5 and its back-to-back value of 10 ps found at Point-1. The

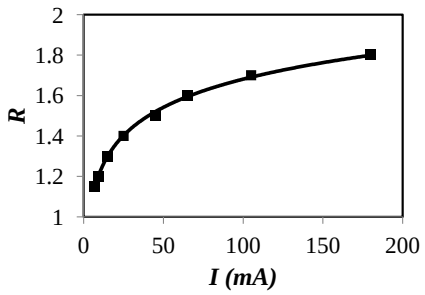

Fig. 6.9. *R* as a function of the SOA bias current *I*. SOA is placed at the Tx site.

obtained values of *R* as a function of SOA bias current *I* were plotted in Fig. 6.9. It was seen that the SOA by controlling the OCDMA code carriers chirp was very effective in restoring the distorted FWHM value of the 2D-WH/TS OCDMA autocorrelation (note $R \rightarrow 1$). A detailed explanation can be found in Section-6.3. In short, the positive chirp of the OCDMA code carriers generated by OCDMA *Tx* and

propagated in the testbed makes the speed of the longer wavelength code carriers propagate faster than of those with a shorter wavelength. By reducing the carriers chirp through the SOA bias current adjustments will reduce the speed of the longer wavelengths and increase the speed of the shorter wavelengths code carriers. This way, the individual code carrier's temporal width narrows aided further by the GDV induced anomalous propagation through the SMF-28 fibre [77].

6.4.2 CD Management by a Single SOA on *Rx* Site

Now, the SOA was placed right after the OCDMA receiver/decoder (Option-2) as indicated in Fig. 6.8. The experiment was repeated and the obtained values of *R* as function of the SOA bias current *I* are plotted in Fig. 6.10. In this configuration, the SOA has the opposite effect on the values of *R* when compared to pre-chirping by the SOA described in Section-6.4.1. It is seen that *R* increases with an increasing SOA bias current, i.e. the FWHM of the OCDMA auto-correlation recovered at Point-5 is becoming wider with the larger values of *I*. Because the SOA at the output of the OCDMA *Rx* decoder is facing four times more optical peak power compare to its Option-1 position, SOA becomes gain saturated which leads to an SPM induced broadening [134].

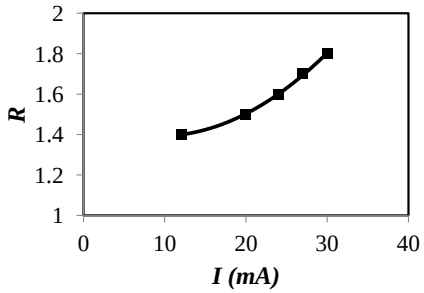

Fig. 6.10. *R* as a function of the SOA bias current *I*. SOA is placed at the Rx site.

6.4.3 Investigation of Using SOA to Manage Impact of GVD on OCDMA Auto-correlation

Here the effect of a varying value of transmission link average residual group velocity dispersion, GVD (parameter β_2) on the OCDMA auto-correlation FWHM as a function of changing chirp C has been investigated. The obtained results are shown in Fig. 6.11. The investigation was done for β_2 between (0.10 – 0.20) ps^2/nm. It is seen that for varying the values of chirp C and β_2 the values $R \in (0.93 – 1.41)$.

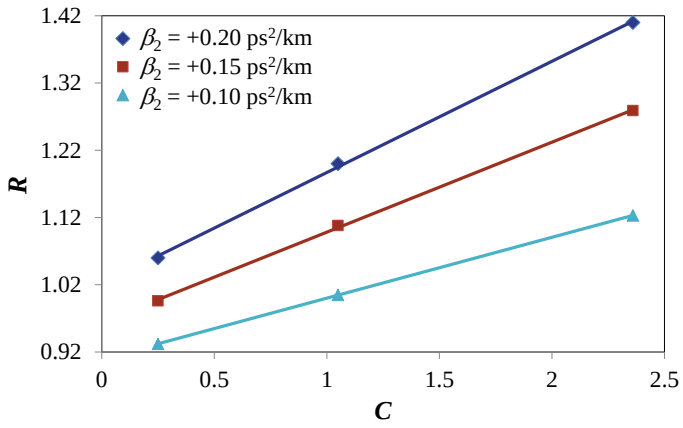

Fig. 6.11. R as a function of chirp C for different values of β_2. SOA is placed at the Tx site.

6.5 Discussion

It has been shown for the first time both experimentally and by calculation, that an SOA at the transmission side can be used to control a recovered 2D-WH/TS OCDMA autocorrelation function and its width at the receiver end by controlling the chirp of picosecond multi-wavelength OCDMA code carriers at the transmitter end. The experiments and calculations were conducted for a 16 km long fibre transmission in a partially CD compensated fibre testbed. It is found that OCDMA autocorrelation and its 14 ps width when CD distorted by a fibre transmission can be

restored back to its 10 ps '*back-to-back*' value by controlling the code carriers' chirp by varying the SOA bias current. Using CW/HB does not offer the same CD tuning range as OP/HB [152], however using CW/HB eliminates the need for synchronization and simplifies system implementation. Because the SOA faces code carriers having low power and equal amplitude, no bandwidth limitations are noted which is contrary to [152] where the SOA is implemented on the receiving end. A comparative study was also conducted to investigation the effect of OCDMA code carriers' chirp on the OCDMA auto-correlation and its width by placing the SOA either at the OCDMA transmitter (*Tx*) or at the receiver (*Rx*) site. The OCDMA code carriers' chirp was controlled by varying the SOA gain dynamics through its bias current changes. It was observed that controlling the chirp of multi-wavelength code carriers by a single SOA located at the *Tx* site could effectively compensate for the observed OCDMA auto-correlation broadening resulted from the fibre link CD as well as for the transmission link's residual GVD changes. With a single SOA located at the *Rx* site after the OCDMA decoder, it was observed that additional OCDMA auto-correlation broadening could be imposed by increasing the SOA bias current.

Chapter 7

Conclusions

7.1 Summary of The Thesis

Chromatic and temperature induced dispersion can severely affect incoherent high data rate communication in optical fibre. This is also true for incoherent OCDMA system with multi-wavelength picosecond code carriers. Even a relatively small deviation from a fully dispersion compensated transmission link can strongly impact the overall system performance, the number of simultaneous users, and the system cardinality due to the recovered OCDMA autocorrelation being strongly distorted, time-skewed, and having its FWHM value changed [11, 12, 102, 103, 122, 123]. Hence, to preserve the integrity of fibre transmission in incoherent systems using picosecond code carriers, the CD must be controlled with high accuracy. This can be a very challenging task, particularly in a multi-wavelength environment under varying conditions. It is therefore of utmost importance to have a simple tuneable means for controlling fibre chromatic or temperature induced dispersion with high sub-picosecond accuracy. Tune-ability of dispersion control in an incoherent picosecond multi-colour OCDMA system was the main interest of this research work. To establish the tuneable dispersion compensation of this system, at first, the incoherent OCDMA system was discussed and attention was focused on 2D-WH/TS with ps code carriers in Chapter-2. Chapter-3 discussed the basic dispersion phenomena in optical fibre and the reason of pulse broadening and time skewing due

to GVD effects. Chaper-4 investigated the use of SOA for the tuneable dispersion control for OCDMA system using 2D-WH/TS code based on multi-wavelengths ps pulses. The SOA was first used on the receiver site for a continuous manipulation of the broadened OCDMA autocorrelation due to fibre link CD (CD coefficient $D_{CD} > 0$ in SMF-28). The SOA compensation was applied directly on the distorted OCDMA autocorrelation composed of four multi-wavelength code carriers. In this configuration, the use of a picosecond optical pulse called an OP/HB synchronized with the OCDMA autocorrelation at the SOA input was investigated. It has been demonstrated that the OCDMA autocorrelation that was broadened by the fibre CD can be continuously 'compressed'. The OCDMA autocorrelation FWHM width could be compressed even below its original back-to-back width. In Chapter-5, the temperature affected OCDMA autocorrelation broadening for a fully CD compensated fibre link was experimentally investigated. It was reported for the first time the use of the SOA on the receiver site to continuously compensate for the broadening of the OCDMA autocorrelation due to the changing temperature induced dispersion in the optical fibre (the temperature induced dispersion coefficient $D_T < 0$ in SMF-28). The compensation by the SOA was applied directly on the recovered distorted OCDMA autocorrelation. It was shown that the broadening of the OCDMA autocorrelation width could be mitigated using the twin SOA, by controlling its chirp through bias current adjustments. Chapter-6 was devoted to show that, by controlling the chirp of the individual multi-wavelength OCDMA code carriers spread over a bit period before the code is launched into a fibre link, the OCDMA autocorrelation broadening due to the fibre CD ($D_{CD} > 0$) observed on the OCDMA receiver site, could be compensated. The mathematical formula was developed incorporating the

chirp parameter and calculated the OCDMA autocorrelation envelope and its width changes with the calculated chirp changes by SOA.

In conclusion, it was shown that SOA could be successfully used for tuneable dispersion compensation of an incoherent OCDMA autocorrelation (based on picosecond multi-wavelength carriers) broadening affected with chromatic or temperature induced dispersion as depicted in various chapters of this thesis.

7.2 Future Works

This thesis primarily focused on all-optical tuneable dispersion management using the SOA control implemented on 2D-WH/TS OCDMA based on multi-wavelength picosecond code carriers to overcome the dispersion related impairments. Further research may be continued in line with the following directions:

In Chapter-4, a locally generated OP/HB was used to achieve the highest compression of the recovered OCDMA autocorrelation width. To make the system more robust against the effects of timing jitter, future investigation should be focussed on how to generate OP/HB using an all-optical clock recovery technique.

In case of multiuser incoherent 2D-WH/TS OCDMA systems, different techniques of SOA based tuneable dispersion compensation as described and depicted in the thesis can also be investigated into to reduce MAI, thereby help to increase the system scalability.

The OP/HB approach can also be investigated while using the SOA at the transmitter site with the goal to achieve more compression of the OCDMA autocorrelation widths at the receiving site.

The future research can also investigate the effects of SOA recovery time on the developed compensation techniques.

Finally, the all-optical tuneable dispersion management using the SOA control can also be investigated on 2-D wavelength-time codes, such as the carrier-hopping prime codes (CHPCs).

References

[1] R. S. Tucker, G. Eisenstein, and S. K Korotky, "Optical time-division multiplexing for very high bit-rate transmission," *J. Lightwave Technol*., vol. 6, no. 11, pp. 1737-1749, Nov. 1998.

[2] P. R. Prucnal. Optical code division multiple access: fundamentals and applications. CRC press, 2005.

[3] I. Glesk, I. Andonovic, and P. R. Prucnal, "Design and demonstration of OCDMA system with superior scalability". In Photonics, Devices, and Systems IV (Vol. 7138, p. 71381P). International Society for Optics and Photonics, Nov. 2008.

[4] A. B. Dar, and R. K. Jha, "Opt Quant Electron (2017) 49:108", [Online] Available at:https://doi.org/10.1007/s11082-017-0944-4.

[5] H. Toda, I. Akiyoshi, N. Yamaguchi, and A. Liang, "On the dispersion slope compensation in dense dispersion managed solitons," in *Proc. 5th Optoelectronics and communications conference*, July 2000, 13A1-3, pp. 338-339.

[6] Z. Pan, et al., "Tunable chromatic dispersion compensation in 40-Gb/s systems using nonlinearly chirped fibre Bragg gratings," *J. Lightwave Technol*., vol. 20. no. 12, pp. 2239-2246, Dec. 2002.

[7] K. Takiguchi, K. Okamoto, and K. Moriwaki, "Planar lightwave circuit dispersion equalizer," *J. Lightwave Technol*., vol. 14, no. 9, pp. 2003-2011, Sep. 1996.

[8] G. H. Lee, S. Xiao, and A. M. Weiner, "Optical dispersion compensator with > 4000-ps/nm tuning range using (VIPA) and spatial light modulator (SLM)," *IEEE Photonics Tech. Letters*, vol. 18, no. 17, pp. 1819-1829, Sep. 2006.

[9] F. Kerbstadt, and K. Petermann, "Analysis of adaptive dispersion compensators with double-AWG structures," *J. Lightwave Technol*., vol. 23, no. 3, pp. 1468-1477, Mar. 2005.

[10] Z. Pan, C. Yu, and A. E. Willner, "Optical performance monitoring for the next generation optical communication networks," *Optical Fibre Technology*, vol. 16, pp. 20-45, 2010.

[11] A. Sahin and A. E. Willner, "System limitations due to chromatic dispersion and receiver bandwidth for 2-D time-wavelength OCDMA systems," in Proc. *Lasers and Electro-Optics Society (LEOS 2003)*, vol. 2. IEEE, 2003.

[12] T. B. Osadola, et al., "Effect of variations in environmental temperature on 2D-WH/TS OCDMA code performance," *J. Opt. Commun. Netw*., vol. 5, pp. 68–73, 2013.

[13] H. Ghafouri-Shiraz, and M. M. Karbassian, "Optical CDMA networks: principles, analysis and applications, vol. 38", John Wiley & Sons, 2012.

[14] Z. Gao, “Advanced optical modulation and fast reconfigurable en/decoding techniques for OCDMA application” Doctoral dissertation, Heriot-Watt University, 2011.

[15] A. Stok and E. H. Sargent, “The role of optical CDMA in access networks,” *IEEE Commun. Mag.*, vol. 40, no. 9, pp. 83–87, 2002.

[16] J. Ratnam, “Optical CDMA in broadband communication–scope and applications”, *Journal of optical communications*, no. 23, no. 1, pp. 11-21, 2002.

[17] Z. Jiang, D. Seo, S. Yang, D. E. Leaird, R. V. Roussev, C. Langrock, M. M. Fejer, and A. M. Weiner, “Four-user 10-Gb/s spectrally phase-coded O-CDMA system operating at ~ 30 fJ/bit,” *IEEE Photon. Technol. Lett*., no. 17, pp. 705-707, 2005.

[18] X. Wang and N. Wada, “Spectral phase encoding of ultra-short optical pulse in time domain for OCDMA application,” Opt. Express, vol. 15, no. 12, pp. 7319–7326, 2007.

[19] J. Ratnam, “Optical CDMA in broadband communication–scope and applications,” *Journal of optical communications*, vol. 23, no. 1, pp. 11-21, 2002.

[20] https://msnucleus.org/membership/html/k-6/as/technology/5/ast5_1a.html

[21] http://www.physlink.com/Education/AskExperts/ae372.cfm

[22] J. Hui, “Pattern code modulation and optical decoding-A novel code-division multiplexing technique for multifibre networks,” *IEEE Journal on Selected Areas in Communications*, vol. 3, no. 6, pp. 916-927. 1985.

[23] P. R. Prucnal, M. A. Santoro, and T. R. Fan, “Spread spectrum fibre optic local area network using optical processing,” *J. Lightw. Technol*., vol. LT-4, no. 5, pp. 547–554, May 1986.

[24] P. Prucnal, M. Santoro, and S. Sehgal, “ Ultrafast all-optical synchronous multiple access fibre networks,” *IEEE Journal on Selected Areas in Communications*, vol. 4, no. 9, pp. 1484-1493, 1986.

[25] A.S. Holmes and R.R Syms, “All optical CDMA using ‘quasi-prime’ codes,” *IEEE/OSA Journal of Light Wave Technology*, vol. 10, no. 2, pp. 279-286, Feb 1992.

[26] S. V. Maric, Z. I. Kostic, and E. I. Titlebaum, “A new family of optical code sequence for use in spread-spectrum fibre-optic local area network,” *IEEE Trans. on Communication*, vol. 41, no. 8, pp. 1217-1221, Aug. 1993.

[27] G. -C. Yang and W. C. Kwong, “Performance analysis of optical CDMA with prime codes,” *IEEE Electronic Letters*, vol. 31, no. 7, pp. 569 570, Mar. 1995.

[28] W. C. Kwong, P. A. Perrier, and P. R. Pruncal, “Performance comparison of asynchronous and synchronous code division multiple-access technique for fibre-optic local area network,” *IEEE Trans. on Communication*, vol. 39, no. 11, pp. 1625-1634, Nov. 1991.

[29] A. J. Mendez, R. M. Gagliardi, V. J. Hernandez, C. V. Bennett, and W. J. Lennon, "Design and Performance Analysis of Wavelength/Time (W/T) Matrix Codes for Optical CDMA," *IEEE J. of Lightwave Technol.*, vol. 21, pp. 2524-2533, Nov. 2003.

[30] J. A. Salehi, "Emerging OCDMA communication systems and data networks [Invited]," *J. Opt. Netw.*, vol. 6, no. 9, pp. 1138, 2007.

[31] F. R. Chung, J. A. Salehi, and V. K. Wei, "Optical orthogonal codes: design, analysis and applications," *IEEE Transactions on Information theory*, vol. 35, no. 3, pp. 595-604, May. 1989.

[32] L. Tancevski and I. Andonovic, "Wavelength hopping/time spreading code division multiple access systems," *Electron. Lett.*, vol. 30, pp. 1388–1390, 1994.

[33] J. A. Salehi, "Code division multiple-access techniques in optical fiber networks. I. Fundamental principles," *IEEE Trans. on Communications*, vol. 37, no. 8, pp. 824–833, 1989.

[34] Y. K. Huang et al., "Novel multicode-processing platform for wavelength-hopping time-spreading optical CDMA: A path to device miniaturization and enhanced network functionality," IEEE J. Sel. Top. Quantum Electron., vol. 13, no. 5, pp. 1471–1479, 2007.

[35] G. -C. Yang and W. C. Kwong, Prime Codes With Applications to CDMA Optical and Wireless Networks. Artech House, Boston 2002.

[36] X. Wang, and K. I. Kitayama, "Analysis of beat noise in coherent and incoherent time-spreading OCDMA", *Journal of Lightwave Technology*, vol. 22, no. 10, pp. 2226, 2004.

[37] T. Bazan, D. Harle, and I. Andonovic, "Interferometric noise in optical code division multiple access systems", In Transparent Optical Networks, 2006 International Conference on (Vol. 3, pp. 97-100). IEEE, 2006.

[38] C. Michie, R. Atkinson, I. Andonovic, I. Glesk, P. Prucnal, K. Sasaki, and G. Gupta, "Interferometric noise characterisation of a 2-D time spreading wavelength hopping OCDMA networks using FBG encoding/decoding," In Transparent Optical Networks, 2007. ICTON'07. 9th International Conference on (Vol. 1, pp. 114-117). IEEE, July 2007.

[39] T. B. Osadola, "Investigating the scalability of incoherent OCDMA systems based on ultrashort optical pulses", Doctoral dissertation, University of Strathclyde, 2015.

[40] S. K. Idris, "The impact of WH/TS codes in implementing incoherent OCDMA system" Doctoral dissertation, University of Strathclyde, 2014.

[41] V. Baby, D. Rand, C.-S. Brès, L. Xu, I. Glesk, and P. R. Prucnal, "Incoherent Optical CDMA Systems," in optical code division multiple access : fundamental and applications, Boca Raton, 2006, pp. 199–240.

[42] S. Yegnanarayanan, A. S. Bhushan, and B. Jalali, “Fast wavelength-hopping time-spreading encoding/decoding for optical CDMA,” *IEEE Photon. Technol. Lett.*, vol. 12, no. 5, pp. 573-575, May. 2000.

[43] X. Wang, K. T. Chan, Y. Liu, L. Zhang, and I. Bennion, “Novel temporal/ spectral coding technique based on fiber Bragg gratings for fiber optic CDMA application,” In Dig. OFC/ IOOC’99, paper WM50, pp. 341–343. 1999.

[44] N. Wada, H. Sotobayashi, and K. Kitayama, “2.5Gbit/s timespread/ wavelength-hop optical code division multiplexing using fiber Bragg grating with supercontinuum light source,” *Electron. Lett*., vol. 36, pp. 815–817, 2000.

[45] S. Yegnanarayanan, A. S. Bhushan, and B. Jalali, “Fast wavelength hopping time-spreading encoding/decoding for optical CDMA,” *IEEE Photon. Technol. Lett*., vol. 12, pp. 573–575, May 2000.

[46] D. D. Sampson, G. J. Pendock, and R. A. Griffin, “Photonic code-division multiple-access communications,” Fiber Integr. Opt., vol. 16, pp. 126–157, 1997.

[47] I. Fsaifes, C. Lepers, M. Lourdiane, R. Gabet, and P. Gallion, “Pulsed laser source coherence time impairments in a direct detection DS-OCDMA system,” In Lasers and Electro-Optics, 2006 and 2006 Quantum Electronics and Laser Science Conference. CLEO/QELS 2006. Conference on (pp. 1-2). IEEE, May, 2006.

[48] A. Farhat, M. Menif, C. Lepers, H. Rezig, and P. Gallion, “Performance comparison of coherent versus incoherent direct sequence optical code division multiple access system”, In Photonics North 2008, vol. 7099, p. 70991N, International Society for Optics and Photonics, 2008.

[49] T. Okuno, M. Onishi, and M. Nishimura, “Generation of ultra-broad-band supercontinuum by dispersion-flattened and decreasing fiber,” *IEEE Photon. Technol. Lett.*, vol. 10, no. 1, pp. 72-74, Jan. 1998.

[50] L. Adam, E. Simova, and M. Kavehrad, “Experimental optical CDMA system based on spectral amplitude encoding of non-coherent broadband sources,” Proc. SPIE., vol. 2614, pp. 122–132, 1995.

[51] https://www.nktphotonics.com/wp-content/uploads/sites/3/2015/02/Application_note_-_Supercontinuum-SC-5.0-10401.pdf

[52] N. Bloembergen, “The influence of electron plasma formation on superbroadening in light filaments,” *Optics Communications*, vol. 8, no. 4, pp. 285-288, Aug. 1973.

[53] D. Schumacher, “Controlling continuum generation,” *Optics letters*, vol. 27, no. 6, pp. 451-453, Mar 2002.

[54] T. Morioka, S. Kawanishi, K. Mori, M. Saruwatari, “Nearly penalty-free,< 4 ps supercontinuum Gbit/s pulse generation over 1535-1560 nm,” *Electronics Letters*, vol. 30, no. 10, pp. 790-791, 1994.

[55] T. Morioka, K. Uchiyama, S. Kawanishi, S. Suzuki, and M. Saruwatari, "Multiwavelength picosecond pulse source with low jitter and high optical frequency stability based on 200 nm supercontinuum filtering," *Electronics Letters*, vol. 31, no.13, pp. 1064-1066. 1995.

[56] K.-L. Deng, I. Glesk, K. I. Kang, and P. R. Prucnal, "A 1024-channel fast tunable delay line for ultrafast all-optical TDM networks," *IEEE Photon. Technol. Lett*., vol. 9, no. 11, pp. 1496–1498, Nov. 1997.

[57] V. Baby, R. J. Runser, I. Glesk, and P. R. Prucnal, "Analysis of a rapidly reconfigurable multicast capable photonic switched interconnect," *Opt. Commun*., vol. 253, no. 1–3, pp. 76–86, 2005.

[58] S. Yegnanarayanan, P. D. Trinh, and B. Jalali, "Recirculating photonic filter: A wavelength selective time-delay filter for optically-controlled phased-array antennas and wavelength CDMA," *Opt. Lett*., vol. 21, no. 10, pp. 740–742, May. 1996.

[59] J. F. Huang, C. C. Yang, "Reductions of multiple-access interference in fibre-grating-based optical CDMA network," *IEEE Trans. Commun*., vol. 50, no. 10, pp. 1680–1687, Oct. 2002.

[60] A. R. Goodwin, "Semiconductor laser sources for optical communications," in IEE Colloquium on Optical Sources, 1990.

[61] A. Yarib, "Optical Electronics, 4th Edition," Saunders college publishing, 1971.

[62] J. A. Leegwater, "Theory of Mode-locked Semiconductor Lasers," IEEE J. Quantum Electron., vol. 32, pp. 1782-1790, 1996.

[63] M. Suzuki, H. Tanaka, N. Edagawa, K. Utaka and Y. Matsushima, "Transform-Limited Optical Pulse Generation up to 20 GHz Repetition Rate by a Sinusoidally Driven InGaAsP Electroabsorption Modulator," *IEEE J. of Lightwave Technol*., vol. 11, pp. 468-473, 1993.

[64] P. Paulus, R. Langenhorst, and D. Jager, "Generation and Optimum Control of Picosecond Optical Pulses from gain Switched Semiconductor Lasers," *IEEE J. Quantum Electron.*, vol. 24, pp. 1519-1523, 1988.

[65] A. M. Clarke, "Optical pulse processing towards Tb/s high-speed photonic systems," Doctoral dissertation, Dublin City University, 2007.

[66] E. A. Avrutin, J. H. Marsh, and E. L. Portnoi, "Monolithic and Multi-Gigahertz Mode-Locked Semiconductor Lasers: Constructions, Experiments, Models and Applications," IEE Proc. Optoelectronics, vol. 147, pp. 251-278, Aug. 2000.

[67] P.W. Smith, "Mode-locking of Lasers," Proc. of the IEEE, vol. 58, pp. 1342-1363, Sept. 1970.

[68] P. Vasil'eV, "Ultrafast Diode Lasers; Fundamentals and Applications," Artech House, Boston, pp. 95-149, 1995.

[69] M. Rochette, and L. A. Rusch, "Spectral Efficiency of OCDMA Systems With Coherent Pulsed Sources", *J. Lightw. Technol*., vol. 23, no. 3, pp. 1033-1038, Mar. 2005.

[70] A. Farhat, M. Menif, and H. Rezig, "Spectral efficiency of optical CDMA systems," In Transparent Optical Networks (ICTON), 2011 13th International Conference on (pp. 1-4). IEEE, June. 2011.

[71] S. Galli, R. Menendez, E. Narimanov, and P. R. Prucnal, "A novel method for increasing the spectral efficiency of optical CDMA," *IEEE Transactions on Communications*, vol. 56, no. 12, Dec. 2008.

[72] V. Arbab, "Advanced Modulation, Detection, and Monitoring Techniques for Optical Communication Systems," Doctoral dissertation, University of Southern California, 2012.

[73] D. V. Sarwate, and M. B. Pursley, "Crosscorrelation properties of pseudorandom and related sequences". *Proceedings of the IEEE,* vol. 68, no. 5, pp. 593-619, 1980.

[74] W. Huang, M. H. Nizam, I. Andonovic, and M. Tur, "Coherent optical CDMA (OCDMA) systems used for high-capacity optical fibre networks-system description, OTDMA comparison, and OCDMA/WDMA networking," *J. Lightwave Technol*., vol. 18, no. 6, pp. 765, 2000.

[75] C. S. Brès, and P. R. Prucnal, "Code-empowered lightwave networks," *J. Lightwave Technol.*, vol. 25, no. 10, pp. 2911-2921, 2007.

[76] I. Glesk, P. R. Prucnal, I. Andonovic, "Incoherent ultrafast OCDMA receiver design with 2 ps all-optical time gate to suppress multiple-access interference," *IEEE J. Sel. Top. Quantum Electron*. vol. 14, no. 3, pp. 861–867, May. 2008.

[77] H. Abramczyk, "Dispersion phenomena in optical fibres," Technical University of Lodz, Laboratory of Laser Molecular Spectroscopy, 27-28, 2005.

[78] N. Massa, "Fibre optic telecommunication. Fundamentals of Photonics," University of Conneticut, 2000.

[79] Thefoa.org. (2018). "The FOA Reference For Fibre Optics - Testing - Chromatic Dispersion and Polarization Mode Dispersion", [online] Available at: http://www.thefoa.org/tech/ref/testing/test/CD_PMD.html [Accessed 13 Feb. 2018].

[80] N. R. Teja, M. A. Babu, T. R. S. Prasad, and T. Ravi, "Different types of dispersions in an optical fibre," *International Journal of Scientific and Research Publications*, vol. 2, no. 12, pp. 2, Dec. 2012.

[81] B. Collings, Fred Heismann, and Gregory Lietaert (2010), "Reference Guide to Fibre Optic Testing- Volume-2", [online] Available at: https://www.c3comunicaciones.es/Documentacion/fiberguide2_bk_fop_tm_ae.pdf

[82] K. R. Lefebvre, "Environmental Effects on Chromatic and Polarization Mode Dispersion." (2001).

[83] G. Ghosh, M. Endo, and T. Iwasaki, “Temperature-dependent Sellmeier coefficients and chromatic dispersions for some optical fibre glasses,” *J. Lightw. Technol*., vol. 12, no. 8, pp. 1338-1342, Aug. 1994.

[84] M. S. Wartak, “Computational photonics: an introduction with MATLAB,” Cambridge University Press, 2013.

[85] R. J. Nuyts, Y. K. Park, and P. Gallion, “Dispersion equalization of a 10 Gb/s repeatered transmission system using dispersion compensating fibres,” *J. Lightw. Technol*., vol. 15, no. 1, pp. 31-42, 1997.

[86] Intelligence, In-Fibre. “Dispersion Management.”

[87] Štěpánek, Ladislav. “Chromatic dispersion in optical communications,” *International Journal of Modern Communication Technologies & Research 7*, 2012.

[88] http://www.datacenterjournal.com/chromatic-dispersion-compensation-extending-reach/

[89] J. Vojtech, M. Karasek, and J. Radil, “Comparison of an Unconventional All-Optical Chromatic Dispersion Compensation Techniques in Nothing in Line Scenarios with Emphasis to Tunability.” In *Proc. Transparent Optical Networks, 2007. ICTON'07. 9th International Conference on*, vol. 4, pp. 71-75. IEEE, 2007.

[90] M. Singh, “Different Dispersion Compensation Techniques in Fibre Optic Communication System: A Survey,” *International Journal of Advanced Research in Electronics and Communication Engineering (IJARECE)* Volume, 4, 2015.

[91] A. S. Karar, et al., “Electronic Pre-Compensation for a 10.7-Gb/s System Employing a Directly Modulated Laser”, *J. Lightw. Technol*., vol. 29, no. 13, pp.2069-2076, 2011.

[92] S. K. Idris, T. B. Osadola, I. Glesk. “Investigation of all-optical switching OCDMA testbed under the influence of chromatic dispersion and timing jitter,” *J. Eng. Technol*., vol. 4, no.1, pp. 51-65. 2013.

[93] B. J. Eggleton, A. Ahuja, P. S. Westbrook, J. A. Rogers, P. Kuo, T. N. Nielsen, and B. Mikkelsen, “Integrated tunable fibre gratings for dispersion management in high-bit rate systems,” *J. Lightw. Technol*., vol. 18, no. 10, pp. 1418–1432, Oct. 2000.

[94] K. Tanizawa, and A. Hirose, “Adaptive control of tunable dispersion compensator that minimizes time-domain waveform error by steepest descent method.” *IEEE photon. Technol. Lett.*, vol. 18, no. 13, pp. 1466-1468. 2006.

[95] A. Sano, T. Kataoka, M. Tomizawa, K. Hagimoto, K. Sato, K. Wakita, and K. Kato, “Automatic dispersion equalization by monitoring extracted-clock power level in a 40-

Gbit/s, 200-km transmission line," in *Proc. 22nd Eur. Conf. Optical Communication (ECOC'96), Oslo, Norway*, 1996, vol. 2, pp. 207–210, Paper TuD.3.5.

[96] H. Ooi, K. Nakamura, Y. Akiyama, T. Takahara, T. Terahara, Y. Kawahata, H. Isono, and G. Ishikawa, "40-Gb/s WDM transmission with virtually imaged phased array (VIPA) variable dispersion compensators," *J. Lightw. Technol*., vol. 20, no. 12, pp. 2196–2203, Dec. 2002.

[97] D. T. Neilson, "Advanced MEMS devices for channelized dispersion compensation," in *Proc. Tech. Dig. Optical Fibre Communications Conf. (OFC2004), Los Angeles, CA*, 2004, vol. 1, Paper WK4.

[98] B. J. Vakoc, W. V. Sorin, and B. Y. Kim, A tunable dispersion compensator comprised ofcascaded singlecavity etalons, *IEEE Phot. Technol. Lett*., vol. 17, p. 1043-1045, 2005.

[99] S. Doucet, R. Slavik, and S. LaRochelle, "Tunable dispersion and dispersion slope compensator using novel Gires-Toumois Bragg grating coupled-cavities," *IEEE Phot. Technol. Lett*., vol. 16, pp. 2529-2531, 2004.

[100] I. Glesk et al., "Evaluation of OCDMA system deployed over commercial network infrastructure," in Proc. *ICTON, 13th International Conference on* (pp. 1-4). IEEE. Jun. 2011.

[101] F. B. Mezger and M. Brandt-Pearce, "Dispersion limited fiber-optic CDMA systems with overlapped signature sequences," in Conference Proceedings EOS'96 9th Annual Meeting IEEE asers and Electro-Optics Society, 1996, vol. 2, pp. 408–409.

[102] E. K. H. Ng, G. E. Weichenberg, and E. H. Sargent, "Dispersion in multiwavelength optical code-division multiple-access systems: impact and remedies," *IEEE Trans. Commun*., vol. 50, no. 11, pp. 1811–1816, Nov. 2002.

[103] S. P. Majumder, A. Azhari, and F. M. Abbou, "Impact of fibre chromatic dispersion on the BER performance of an optical CDMA IM/DD transmission system," *IEEE Photon. Technol. Lett*., vol. 17, no. 6, pp. 1340-1342, Jun. 2005.

[104] Y. Igarashi and H. Yashima, "Dispersion Compensation for Ultrashort Light Pulse CDMA Communication Systems.," EICE Trans Commun (Inst Electron Inf Commun Eng), vol. E85-B, no. 12, pp. 2776–2784, 2002.

[105] N. T. Dang, A. T. Pham, and Z. Cheng, "Impact of GVD on the performance of 2-D WH/TS OCDMA systems using heterodyne detection receiver," IEICE transactions on fundamentals of electronics, communications and computer sciences, vol. 92, no. 4, pp. 1182-1191, Apr. 2009.

[106] M. J. Islam, K. K. Halder, M. R. Islam, "Effect of optical pulse shape on the performance of OCDMA in presence of GVD and pulse linear chirp," *Int. J. Comput. Sci. Eng*. Vol. 2, pp. 1041–1046, 2010.

[107] What is frequency chirp in an optical Pulse? (VIDEO), Accessed: Apr. 5, 2018, [Online], Available:https://www.fiberoptics4sale.com/blogs/wave-optics/what-is-frequency-chirp-in-an-optical-pulse-video.

[108] A. H. Gnauck et al., "Dispersion penalty reduction using an optical modulator with adjustable chirp," *IEEE Photon. Technol. Lett*., vol. 3, pp. 916-918, Oct. 1991.

[109] T. Watanabe, et al., "Transmission performance of chirp-controlled signal by using semiconductor optical amplifier," *J. Lightwave Technol*., vol. 18. No. 8, pp. 1069-1077, Aug. 2000.

[110] G. P. Agrawal, and N. A. Olsson, "Amplification and compression of weak picosecond optical pulses by using semiconductor-laser amplifiers," *Opt. Lett*., vol. 14, no. 10, pp. 500-502, May. 1989.

[111] R. Bonk, T. Vallaitis, W. Freude, J. Leuthold, R. Penty, A. Borghesani, and I. F. Lealman, "Linear semiconductor optical amplifiers," In Fibre Optic Communication, Springer, Berlin, Heidelberg, pp. 511-571, 2012.

[112] C. H. Henry, R. A. Logan, and K. A. Bertness, "Spectral dependence of the change in refractive index due to carrier injection in GaAs lasers," *Journal of Applied Physics*, vol. 52, no. 7, pp. 4457-4461, 1981.

[113] J. Wang, A. Maitra, C. G. Poulton, W. Freude, and J. Leuthold, "Temporal dynamics of the alpha factor in semiconductor optical amplifiers," *J. Lightwave Technol*., vol. 25, no. 3, pp. 891-900, 2007.

[114] "Application Notes for Kamelian SOA," [Online] Available at: http://www.kamelian.com/products.html

[115] P. A. Yazaki, K. Komori, S Arai, A. Endo, and Y. Suematsu, "Chirping compensation using a two-section semiconductor laser amplifier," *J. Lightwave Technol.*, vol. 10, no. 9, pp. 1247-1255, Sep. 1992.

[116] N. C. Frateschi, J. Zhang, W. J. Choi, H. Gebretsadik, R. Jambunathan, and A. E. Bond, "High performance uncooled C-band, 10 Gbit/s InGaAlAs MQW electroabsorption modulator integrated to semiconductor amplifier in laser-integrated modules," Electron. Lett.,vol. 40, no. 2, pp. 140–141, Jan. 2004.

[117] X. S. Yao, J. Feinberg, R. Logan, and L. Maleki, "Limitations on peak pulse power, pulse width, and coding mask misalignment in a fibre-optic code-division multiple-access system," *J. Lightwave Technol*., vol. 11, no. 56, pp. 836-846, May. 1993.

[118] N. T. Dang, A. T. Pham, and Z. Cheng, "Impact of GVD on the performance of 2-D WH/TS OCDMA systems using heterodyne detection receiver," *IEICE transactions on fundamentals of electronics, communications and computer sciences*, vol. 92, no. 4, pp. 1182-1191, Apr. 2009.

[119] C. R. Doerr, et al., "Simple multichannel optical equalizer mitigating intersymbol interference for 40-Gb/s nonreturn-to-zero signals," *J. Lightwave Technol*., vol. 22. pp. 249, 2004.

[120] A. E. Willner, B. Hoanca, "Fixed and tunable management of fibre chromatic dispersion." Opt. Fibre Telecom., vol. IVB, pp. 642-724, 2002.

[121] X. S. Yao, J. Feinberg, R. Logan, and L. Maleki, "Limitations on peak pulse power, pulse width, and coding mask misalignment in a fibre-optic code-division multiple-access system," J. Lightwave Technol., vol. 11, pp. 836-846, 1993.

[122] X. S. Yao, J. Feinberg, R. Logan, and L. Maleki, "Limitations on peak pulse power, pulse width, and coding mask misalignment in a fibre-optic code-division multiple-access system," *J. Lightwave Technol*., vol. 11, no. 5, pp. 836-846, May. 1993.

[123] S. K. Idris, T. B. Osadola, and I. Glesk, "Investigation of all-optical switching OCDMA testbed under the influence of chromatic dispersion and timing jitter," *J. Eng. Technol*., vol. 4, no. 1, pp. 51-65, Jun. 2013.

[124] M. S. Ahmed, and I. Glesk, "Recent advances in all-optical signal processing for performance enhancement enhancement of interconnects," in *Proc. 18th International Conference on Transparent Optical Networks ICTON*, 2016, Trento, Italy. Invited.

[125] M. S. Ahmed, and I. Glesk, "Tunable chromatic dispersion management of optical fibre communication link using SOA," in *Proc. 11th International conference Electro* 2016, Strbske Pleso, Slovakia. Invited.

[126] D. H. Jeon, H. D. Jung, and S. K. Han, "Mitigation of dispersion-induced effects using SOA in analog optical transmission," *IEEE Photonics Tech. Letters*, vol. 14, pp. 1166-1168, Aug. 2002.

[127] B. Han, et al., "Tunable chromatic dispersion compensation using chirp control based on XPM in a SOA," in *Proc. Asia Pacific Optical Communications, International Society for Optics and Photonics*, Nov. 2008, pp. 71362A-71362A.

[128] C. H. Henry, R. A. Logan, and K. A. Bertness, "Spectral dependence of the change in refractive index due to carrier injection in GaAs lasers," *J. Appl. Phys*., vol. 52, no. 7, pp. 4457-4461, Jul. 1981.

[129] E. P. Ippen, and C. V. Shank, "Ultrashort Light Pulses – Picosecond Techniques and Applications," Springer-Verlag, Berlin, 1977.

[130] K. A. Dala, G. A. Kenny-Wallace, and G. E. Hall, "CW Autocorrelation Measurements of Picosecond Laser Pulses," J. Quantum Electron., vol. QE-16, pp. 990-996, Sept. 1980.

[131] H. N. Tan, M. Matsuura, and N. Kishi, "Enhancement of input power dynamic range for multiwavelength amplification and optical signal processing in a semiconductor optical amplifier using holding beam effect," *Journal of Lightwave Technology*, vol. 28, no. 17, pp. 2593-2602, Sep. 2010.

[132] O. Liboiron-Ladouceur, K. Bergman, M. Boroditsky, and M. Brodsky, "Polarization-dependent gain in SOA-based optical multistage interconnection networks," *Journal of lightwave technology*, vol. 24, no. 11, pp. 3959-3967, 2006.

[133] P. P. Baveja, D. N. Maywar, A. M. Kaplan, and G. P. Agrawal, "Self-phase modulation in semiconductor optical amplifiers: impact of amplified spontaneous emission," *IEEE J. Quantum Electron.*, vol. 46, no. 9, pp. 1396-1403, Sep. 2010.

[134] G. P. Agrawal and N. A. Olson, "Self-phase modulation and spectral broadening of optical pulses in semiconductor laser amplifiers," *IEEE J. Quantum Electron.*, vol. 25, no. 11, pp. 2297-2306, Nov. 1989.

[135] M. P. Fok, Y. Deng, and P. R. Prucnal, "Asynchronous detection of optical code division multiple access signals using a bandwidth-efficient and wavelength-aware receiver," *Opt. Lett.*, vol. 35, no. 7, pp. 1097-1099, Apr. 2010.

[136] S. K. Idris, T. B. Osadola, and I. Glesk, "OCDMA receiver with built-in all-optical clock recovery," *Electron. Lett*, vol. 49, no. 2, pp. 143-144, Jan. 2013.

[137] H. C. Ji, J. H. Lee, and Y. C. Chung, "System outage probability due to dispersion variation caused by seasonal and regional temperature variations," in Proc. *OFC/NFOEC 2005. OSA*, 2005. OME79.

[138] W. H. Hatton and M. Nishimura, "Temperature dependence of chromatic dispersion in single mode fibres," *J. Lightwave Technol.*, vol. LT-4, pp. 1552–1555, Oct. 1986.

[139] P. S. André and A. N. Pinto, "Implications of temperature in the chromatic dispersion: Consequences on high speed optical networks performance," in *Proc. Lasers and Electro-Optics Society, 2003. LEOS 2003. The 16th Annual Meeting of the IEEE*, vol. 1, pp. 175-176. IEEE, 2003.

[140] H. C. Ji, J. H. Lee, and Y. C. Chung, "System outage probability due to dispersion variation caused by seasonal and regional temperature variations," in *Proc. Optical Fibre Communication Conf. and the Nat. Fibre Optic Engineers Conf. (OFC/NFOEC)*, 2005, OME79.

[141] T. B. Osadola, S. K. Idris, I. Glesk, and W. C. Kwong, "Investigating the influence of thermal coefficients on 2-D WH/TS OCDMA code propagation in optical fibre," in *Proc. The European Conference on Lasers and Electro-Optics, p. CI_P_15. Optical Society of America*, 2013.

[142] J. Laferrière, G. Lietaert, R. Taws, and S. Wolszczok, "Reference guide to fibre optic testing," *JDS Uniphase Corporation.*, 2007.

[143] B. J. Eggleton, et al., "Integrated tunable fibre gratings for dispersion management in high-bit rate systems," *J. Lightwave Technol.*, vol. 18, pp. 1418–1432, Oct. 2000.

[144] G. Ishikawa and H. Ooi, “Demonstration of automatic dispersion equalization in 40 Gbit/s OTDM transmission,” in Proc. *Optical Communication, 1998. 24th European Conference on*, vol. 1, pp. 519-520. IEEE, 1998.

[145] T. Kato, Y. Koyano, and M. Nishimura, “Temperature dependence of chromatic dispersion in various types of optical fibre,” *Optics Lett*., vol. 25, no. 16, pp. 1156-1158, Aug. 2000.

[146] G. P. Agrawal, “Carrier-induced group-velocity dispersion and pulse compression in semiconductor laser amplifiers,” *Electron. Lett*., vol. 27, no. 8, pp. 620-621, Apr. 1991.

[147] S. T. Cundiff, B. C. Collings, L. Boivin, M. C. Nuss, K. Bergman, W. H. Knox, and S. G. Evangelides, “Propagation of highly chirped pulses in fibre-optic communications systems”, *J. Lightwave Technol*., vol. 17, no. 5, pp. 811-816, May. 1999.

[148] M. N. Ngo, H. T. Nguyen, C. Gosset, D. Erasme, Q. Deniel, and N. Genay, “Transmission performance of chirp-controlled signal emitted by electroabsorption modulator laser integrated with a semiconductor optical amplifier,” in *Proc. Optical Fibre Communication Conference*, Optical Society of America, pp. OW4F-6, March. 2012.

[149] G. P. Agrawal. Nonlinear fibre optics. Academic press, 2007.

[150] E. M. Wright, “Module 3–Numerical Pulse Propagation in Fibres,” [Online] Available at: http://data.cianerc.org/supercourse/Graduatelevel/module_3/3_SC_GRAD_LEVEL_Module3_wright.pdf

[151] G. P. Agrawal, and M. J. Potasek, “Effect of frequency chirping on the performance of optical communication systems,” *Optics Lett*., vol. 11, no. 5, pp. 318-320, May. 1986.

[152] M. S. Ahmed, M. S. K. Abuhelala, and I. Glesk, “Managing dispersion-affected OCDMA autocorrelation based on PS multiwavelength code carriers using SOA,” *IEEE/OSA J. Opt. Commun. Net*., vol. 9, no. 8, pp. 693-698, Aug. 2017.

[153] H. N. Tan, M. Matsuura, and N. Kishi, “Enhancement of input power dynamic range for multiwavelength amplification and optical signal processing in a semiconductor optical amplifier using holding beam effect,” *J. Lightwave Technol*., vol. 28, no. 17, pp. 2593-2602, Sep. 2010.